NEW HYBRID AND IONIC POLYMER ELECTROLYTES FOR LITHIUM METAL SOLID STATE BATTERIES

MARINE LECHARTIER

PhD thesis 2021

Thesis advisor:

Prof. David Mecerreyes

Table of contents

CHAPTER 1. Introduction

CHAPTER 2. Methodology: ASSB set-up and study of dendrites formation

CHAPTER 3. Lithium single ion hybrid solid electrolytes (HSIPEs) based on PEG network and LLZO particles.

CHAPTER 4. Lithium single ion hybrid and polymer electrolytes based on crosslinked PEO blends.

CHAPTER 5. Hybrid and polymer electrolytes based on pseudo-zwitterionic interpenetrated networks.

Appendix

Los capítulos 1 y 2 están sujetos a confidencialidad por la autora

CHAPTER 3.

Lithium single-ion hybrid solid electrolytes (HSIPEs) based on PEG network and LLZO particles.

3.1. Introduction

Crosslinked polymer electrolytes swollen with liquid plasticizer (organic solvent, glymes, etc), also known as “gel polymer electrolytes” (GPEs), received increased attention due to their superior ionic conductivity compared to “dry” polymers solid electrolytes (SPEs). By introducing a large amount of plasticizer (up to 50 wt.%), Li ions preferably move in the liquid phase, the polymer maintaining only the solid integrity of the gel. Common polymers such as PEO, PVDF or even poly(ionic liquids) PILs have been used as polymer host and can achieve up to 10^{-3} S/cm at room temperature[1]. Besides, in situ gelification of liquid monomers on electrode surface enables excellent interfacial compability, which greatly improves the ASSB performance [2]. Nevertheless, generally soft solids can be obtained for this type of material, especially when liquid content exceeds 50 wt.%[3].

Dispersing inorganic particles within a crosslinked matrix has been widely employed to improve the mechanical stability and the ionic dissociation of Li salts [4]. Usually, inert fillers are elected such as SiO_2, Al_2O_3 or TiO_2. However, hybrid crosslinked polymers with Li inorganic conductors (LLZO, LAGP etc) arouse a growing interest thanks to their superior performance compared to inert particles, as explained previously in Chapter 1[5,6]. In addition, single-ion crosslinked hybrids with active fillers have been recently investigated and show interesting properties in term of dendrites protection thanks to their near single ion lithium conduction and improved ionic dissociation[7,8]. Single ion electrolytes, where only Li^+ ions are mobile, demonstrated to have beneficial effects on Li cycling stability [9]. For this reason, this type of polymer is a matrix of choice to develop high performance HSE. Furthermore, the ionic charges within the polymer matrix are thought to homogenise the dispersion of inorganic particles. Therefore, highly uniform and reproducible HSE can be synthesized without the need to use particle surface modifier or surfactants.

In this chapter, we report a new hybrid solid electrolyte (HSIPE) formed by a PEG single ion polymer network, Al doped $Li_{7-3x}Al_xLa_3Zr_2O_{12}$ (LLZO) garnet nanoparticles and propylene carbonate as plasticizer. The matrix of this hybrid is based on recently reported single ion crosslinked polymer formulation (SIPE) which showed near unity lithium transference number and enabled room temperature battery operation [10]. UV polymerization was elected as fast and green method to synthesise these hybrid electrolytes. Flexible and free-standing HSIPE films were prepared by varying the composition of polymer phase versus the LLZO content. To our knowledge, only a few studies related the use of LLZO particles with single-ion and UV crosslinked polymer matrix [7,11]. High conductivity and efficient Li stripping/plating can be expected from this electrolyte, thanks to its single ion Li sources (LLZO particles and single ion polymer matrix) and the plasticizer. LLZO ionic conductor is also known to form steady interphase in contact with Li metal and is predicted to interact with the tethered anionic moieties of the polymer matrix.

Morphological, electrochemical, thermal and mechanical properties of these new hybrid electrolytes have been investigated. Understanding of Li ion transport within the HSE is elucidated by solid state Nuclear Magnetic Resonance Spectroscopy (NMR). A special focus has been done on the stripping/plating performance of Li metal anode coupled with the designed solid electrolyte.

3.2. Experimental part

All the experimental methods (electrolyte characterization, battery set up) are fully described in the Appendix section.

3.2.1. Materials

Potassium 3-(methacryloyloxy)propane-1-sulfonate (98%), thionyl chloride (>99%), triethylamine (>99.5%), lithium hydride (LiH, 97%), poly(ethylene glycol) methyl ether methacrylate (500 g/mol) (PEGM), Poly(ethylene glycol) dimethacrylate (550 g/mol) (PEGDM), 2-Hydroxy-2-methylpropiophenone (DAROCUR, UV initiator, 97% purity), Phenylbis(2,4,6-trimethylbenzoyl)phosphine oxide (BAPO, UV initiator, 97% purity), anhydrous propylene carbonate (PC, 99.8% purity, H2O<10 ppm) and fluoroethylene carbonate (FEC, 99%) were purchased from Sigma Aldrich. PEGM and PEGDM were further dried with molecular sieves before use (4 Å, activated under vacuum for 24h at 300°C).

Anhydrous tetrahydrofuran (THF), anhydrous dimethylformamide (DMF), dichloromethane (DCM) and hexane were supplied from Acros. Trifluoromethanesulfonamide (97%) was purchased from ABCR.

LiTFSI salt was provided by TCI (98% purity). Before use, LiTFSI was dried under vacuum at 130°C for 24h and stored in Argon glovebox.

Cubic Al doped $Li_{7-3x}Al_xLa_3\ Zr_2O_{12}$ (LLZO) particles were received from MSE under argon atmosphere and were used as received (99.9% purity, 400-600 nm particles size).

Li foils (120 µm thickness) were purchased from Rockwood Lithium (USA).

3.2.2. Synthesis of single ion monomer lithium 1-[3-(methacryloyloxy)propylsulfonyl]-1- (trifluoromethanesulfonyl)imide (LiMTFSI)

LiMTFSI was synthesized according to the method described by Shaplov and al[12] (Figure 1). The different reaction steps are illustrated as follows:

Step 1: Synthesis of 3-(Chlorosulfonyl)propyl methacrylate (Product **2**)

Starting reactant potassium 3-(methacryloyloxy)propane-1-sulfonate **1** (30 g, 0.122 mol) is dissolved in anhydrous THF(50 mL) under nitrogen atmosphere. 3.4 mL DMF (catalyst)

is injected. The reaction flask is cooled down to 0°C before adding dropwise thionyl chloride in excess (50 mL). The reaction was let 1h in the ice bath, then proceeded at room temperature overnight. Obtained oily solution was neutralized by pouring it carefully into 400 mL of iced water. The lower organic oily phase was separated by decantation after its dilution in dichloromethane (180 mL). Then the solution was washed with Brine (6x80 mL) and dried over magnesium sulfate for 1h. After filtration of $MgSO_4$, the obtained slightly yellow oil was finally dried under vacuum overnight before Step 2.

Step 2: Synthesis of Triethyl ammonium 1-[3-(methacryloyloxy)propylsulfonyl]-1-(trifluoromethanesulfonyl)imide (Product **3**)

Trifluoromethanesulfonamide (14.6 g, 0.098 mol) was dissolved in triethylamine (30 mL, 0.214 mol) while purging with nitrogen. The reactants were then dissolved in anhydrous THF (80 mL) and cooled to 0°C. Product **2** was dissolved separately in 30 mL of anhydrous THF and the obtained solution was added dropwise to the reaction flask under inert atmosphere. The reaction was let 1h in the ice bath, then proceeded 2h at room temperature. The resulted precipitated was remove and the filtrate was concentrated at room temperature. Then the residual oil was dissolved in dichloromethane (180 mL) for the washing step with Brine (4x70 mL) and dried over $MgSO_4$ for 1h. After $MgSO_4$ filtration, CH_2Cl_2 was evaporated under reduced pressure and Product 3 was dried under vacuum overnight before final Step 3.

Step 3: Lithium 1-[3-(methacryloyloxy)propylsulfonyl]-1-(trifluoromethanesulfonyl)imide LiMTFSI (Product **4**)

Product **3** was dissolved in 45 mL of anhydrous THF and purged with nitrogen. Lithium hydride LiH (1.3 g, 0.17 mol) was added dropwise under stirring. The reaction flask was let 3h at room temperature and then the unreacted LiH was filtered. The obtained filtrate was concentrated under reduced pressure and washed with hexane (3x40 mL). The resulted product **4** is yellowish viscous oil which can be further crystallized in dichloromethane.

The crystallization of LiMTFSI was realized as follow: the oil was dissolved in minimum amount of CH_2Cl_2. Then, the solution was slowly added dropwise a cold CH_2Cl_2 solution. White powder crystals precipitated and were recovered by filtration. The crystalline powder was then carefully dried under vacuum at 60°C and stored in Argon glovebox.

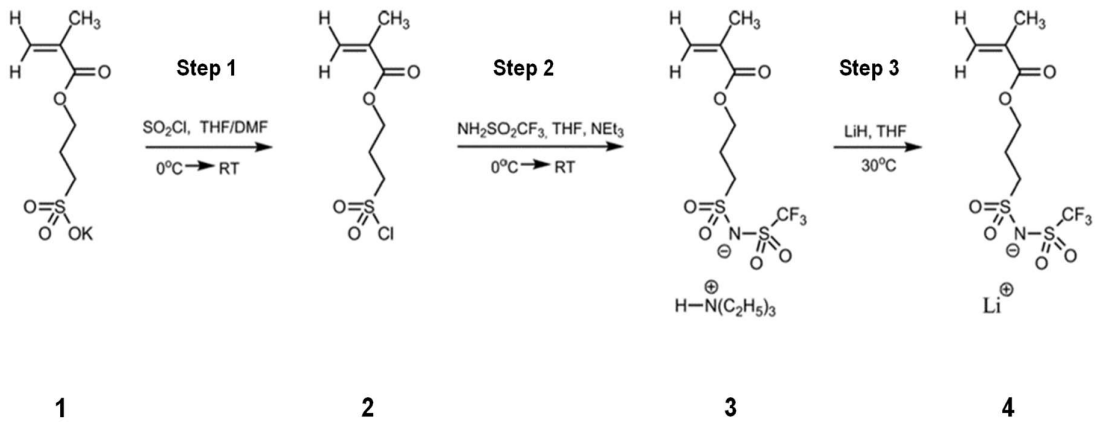

Figure 1: Synthesis of single ion monomer LiMTFSI

LiMTFSI monomer was successfully prepared by the method previously described. The resulted powder was further characterized by IR spectroscopy and ^{1}H NMR (Figure 2), confirming its structure and purity (Experimental method: Appendix A1).

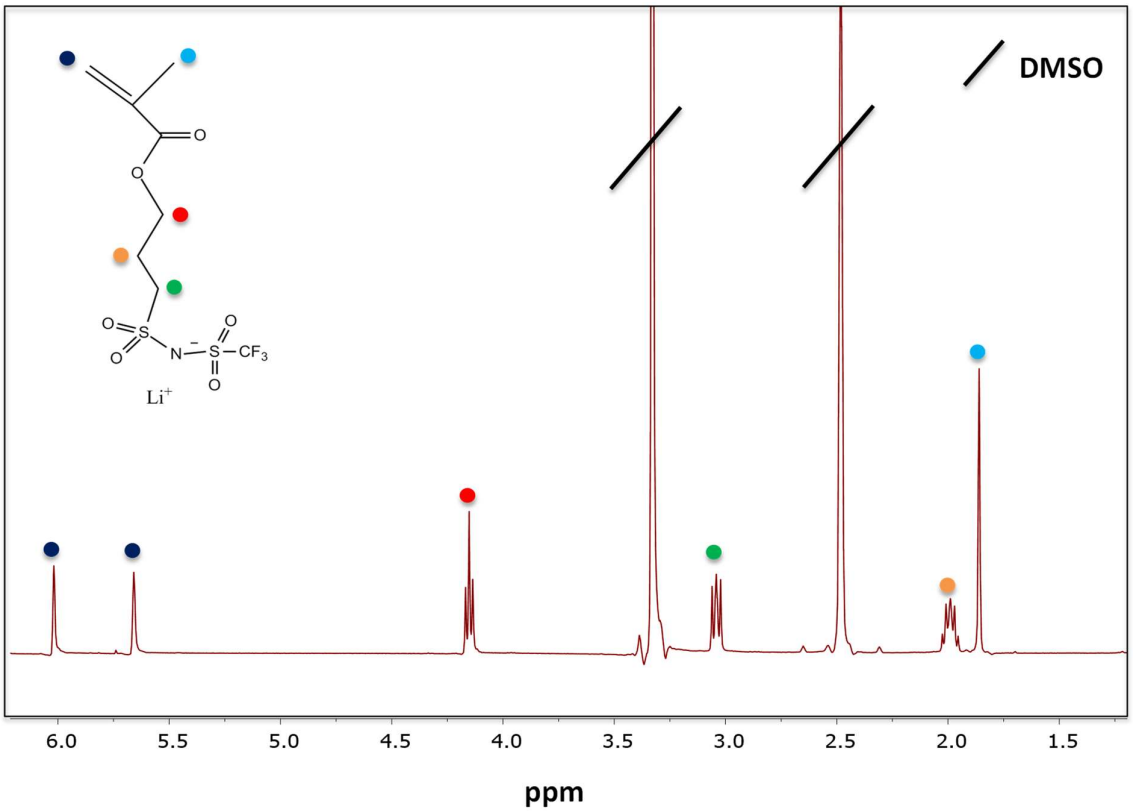

Figure 2: ^{1}H NMR of Lithium 1-[3-(methacryloyloxy)propylsulfonyl]-1-(trifluoromethanesulfonyl)imide LiMTFSI recorded in DMSO-d_6.

3.2.3. UV curing of hybrid and pristine PEG based network.

The synthesis of the crosslinked HSE membranes was carried out by fast UV curing, in order to avoid the sedimentation with time of LLZO particles. Figure 3 depicts the reaction mechanism for pristine and hybrid SSE. These Hybrid Single Ion Polymer Electrolytes, later on named HSIPE-X (X: LLZO content in weight), were obtained in three steps. Firstly, monomers (PEGM, PEGDM, LiMTFSI), chosen plasticizer and UV initiator were mixed by magnetic stirring (450 rpm, 1h). Secondly, appropriate amount of LLZO particles (shown in Table 1) was added from 5 to 50 wt.% and the reactants mixture was left under stirring for 24h. Finally, the mixture was poured into a silicon mould (thickness~ 1mm) and exposed to the UV light for 15 min to obtain the different HSIPEs. Same method was used for the synthesis of dual ion pristine and hybrid membranes. In the dual ion case, the monomer LiMTFSI was replaced by a lithium salt LiTFSI (equimolar content) in the compositions.

A Lightningcurve TM LC-L1-V5 UV curing lamp (λ= 365 nm) from Hamamastsu was used for UV polymerization. The distance between the sample and the lamp was set up at 10 cm; the corresponding irradiance was measured to be 58 $mW.cm^{-2}$. The optimal duration of UV exposure was determined before thanks to photo-rheology experiments. The synthesis of the crosslinked membranes was carried out inside an Argon filled glovebox with H_2O and O_2 levels below 10 ppm. After curing, self-standing hybrid crosslinked electrolytes were obtained, with thicknesses comprised between 0.7-1 mm. Unfortunately, thinner membranes were too brittle to be used as solid-state electrolyte.

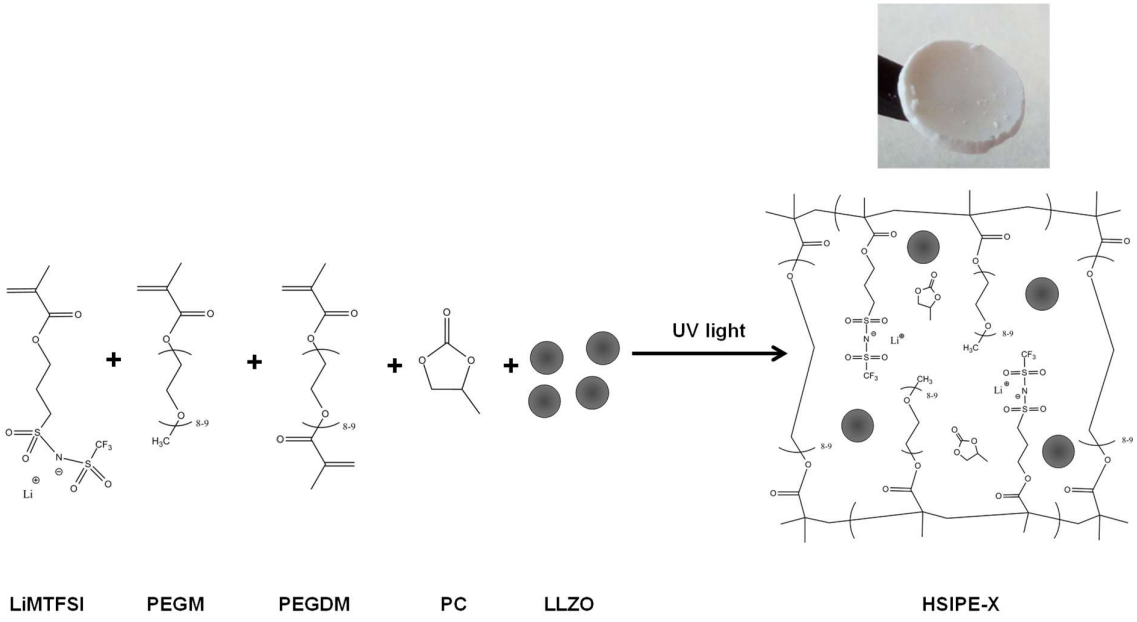

Figure 3: Reaction mechanism of Hybrid Single ion Crosslinked Polymer Electrolytes

Table 1. Compositions in weight for pristine and hybrid crosslinked polymer electrolytes

Compositions	PEGDM [w/w]	PEGM [w/w]	PC [w/w]	LiMTFSI [w/w]	LiTFSI [w/w]	LLZO [w/w]
SIPE	5	36	50	9	-	0
HSIPE-5	4,7	34,2	47,6	8,5	-	5
HSIPE-9	4,6	32,7	45,5	8,2	-	9
HSIPE-26	3,7	26,6	37	6,7	-	26
HSIPE-40	3	21,6	30	5,4	-	40
HSIPE-50	2,5	18	25	4,5	-	50
HPE	3,7	33,3	37	-	-	26
DIPE	5	36,6	50,8	-	7,6	-
HDIPE-26	3,7	27	37,5	-	5,8	26

UV initiator 3% w/w of the monomers

3.3. Results and discussion

3.3.1. In situ photopolymerization kinetic study

In situ rheological study during photopolymerization (Photo-rheology) was performed to determine the gel point of the polymer composition SIPE thanks to a rotational rheometer equipped with a UV lamp (Experimental method: Appendix A4). Measuring storage G' and loss G'' moduli evolution provides accurate information about the formation of a 3D polymer network during irradiation[13,14]. The intersection between G' and G'' gives the gel point of the crosslinked network, which is the transition between liquid state of unreacted monomers to solid state crosslinked polymer. As shown in Figure 4, the gel point equals 2 min, which shows a fast polymerization kinetic and should limit LLZO particles to agglomerate or sediment. Nonetheless, mechanical properties were still evolving under irradiation after the gel point. Up to 8 min, G' and G" finally reached a plateau. After 13 min, G' and G'' remain stable. To ascertain high conversion of monomers by UV polymerization, irradiation time was set up to 15 min for the synthesis of pristine and hybrid crosslinked polymer electrolytes.

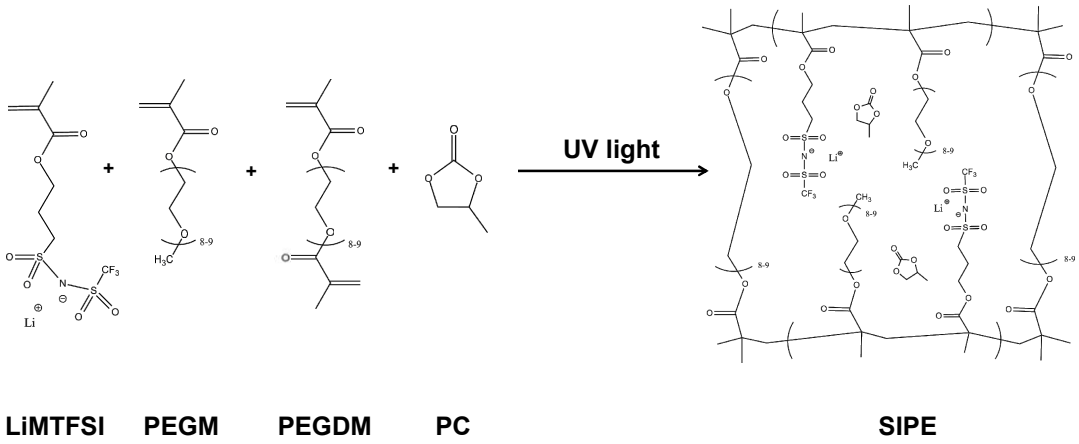

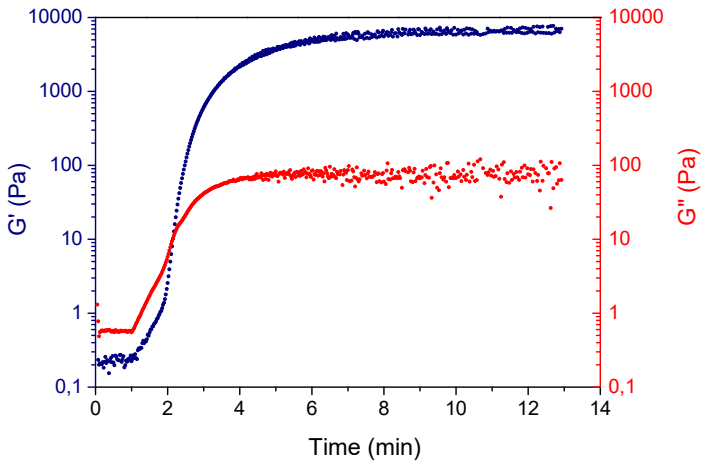

Figure 4: Storage and loss moduli G' and G'' evolutions depending on UV irradiation time.

Complete polymerization of the pristine polymer electrolyte was further confirmed by ATR-FTIR before and after UV curing as displayed in Figure 5 (Experimental method: Appendix A1). The "polymerizable" group from the methacrylate monomers is the vinyl bonds C=C. The related band can be observed at 1635 cm^{-1} in the case of the monomer mixture before irradiation. This latter disappeared completely after 20 min of UV curing indicating a high conversion.

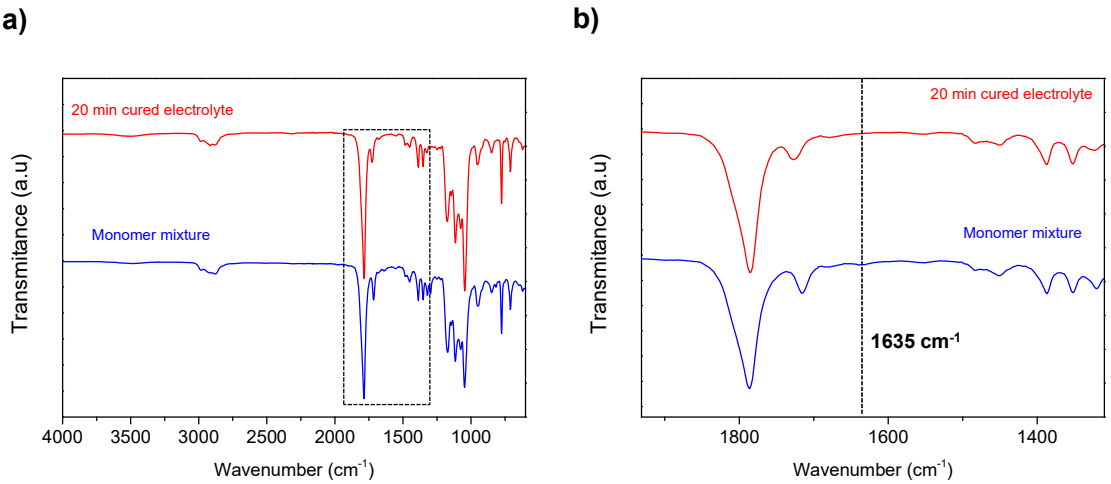

Figure 5: a) ATR-FTIR spectra of monomer mixture before and after UV exposure, b) Zoom in the 1900-1300 cm^{-1} region to observe the disappearance of 1635 cm^{-1} band.

3.3.2. Morphological and mechanical characterization

To investigate the dispersion of particles within the polymer matrix, environmental Scanning Electron Microscopy (ESEM, experimental method in Appendix A5) was performed on three hybrid electrolytes, containing 5, 26 and 50 wt.% LLZO (namely HSIPE-5, HSIPE-26 and HSIPE-50). Observations were done at three different locations: in the bottom, the middle and the top part of the cross-section of the electrolyte. Up to a loading of 26 wt.%, very homogeneous dispersion of LLZO particles is achieved through the entire cross-sections of the HSE, as highlighted in Figure 6.a and Figure 6.b.

We can thus conclude that there are no particles sediments for these compositions and the inorganic particles are very well dispersed within the polymer matrix. On the other hand, some agglomeration of particles is noticed in HSIPE-50, especially at the bottom part (Figure 6.c.i). Such observations show that the particles are very well dispersed in the ionic polymer network except at high particle content. It is worth to note that only magnetic stirring was used in this work. Other methods such as sonication or faster polymerization kinetics may be needed in conjunction with traditional mechanical stirring to achieve homogeneous dispersion of the LLZO particles at high loading.

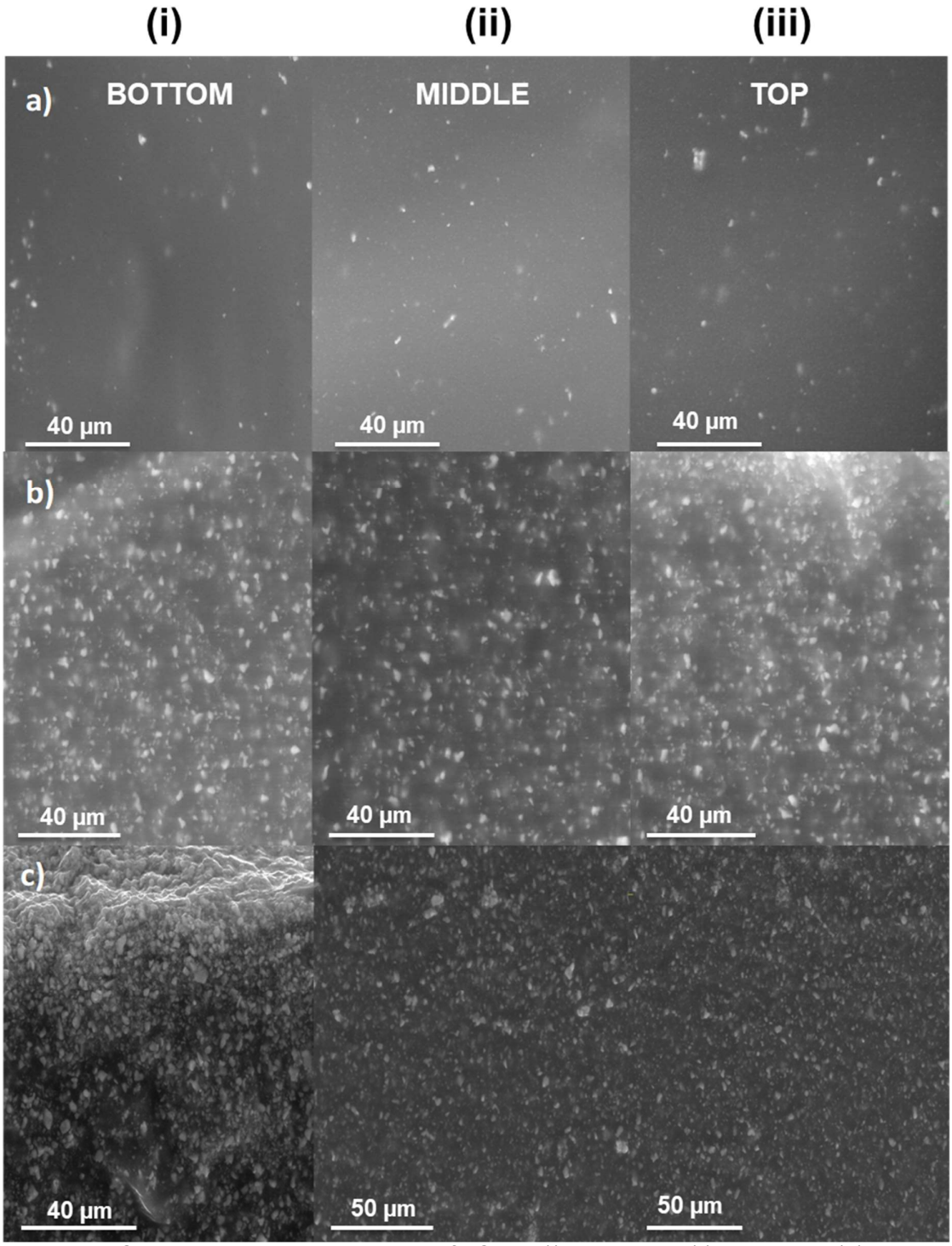

Figure 6: ESEM images at the cross-section of HSIPEs:(i) Bottom part, (ii) Middle part, (iii) Top part; (a) HSIPE-5, (b) HSIPE-26, (c) HSIPE-50

Mechanical proprieties of the pristine and hybrid crosslinked polymers (HSIPE-26 and HSIPE-40) were assessed by dynamic mechanical analysis over a temperature range of -100 °C to 80°C (Experimental method in Appendix A6). Figure 7.a shows the storage modulus G' as a function of temperature. Two distinct regimes are observed over the temperature range studied. A clear glass transition, from a glassy state to a rubbery state, is observed around -60 °C for all compositions. In the glassy state, storage modulus G' of pristine and hybrids electrolytes are quite similar (100 MPa). On the opposite, mechanical properties of HSIPEs are dramatically improved compared to pristine SIPE despite the viscoelastic state. The storage modulus increases from 73 kPa for the pristine SIPE to 0,58 and 3,7 MPa for hybrids HSIPE-26 and HSIPE-40 respectively.

Tan (δ), in others words the ratio of the storage and the loss moduli, is depicted in Figure 7.b. The maximal value of Tan (δ) gives us information about the value of the glass transition temperature T_g. In polymer electrolytes, the ionic conductivity is strongly dependent on T_g, as Li ion conduction is closely related to ion hopping mechanisms between polymer chains [15]. Thus, it has been widely recognized in the literature that low T_g leads to high ionic conductivity for polymer electrolytes. From DMTA experiments, T_g was determined to be -58,9°C for SIPE. After adding 26 wt.% LLZO, the T_g decreased to -64,75°C. Different tendency was observed for HSIPE-40 composition. The T_g slightly rises to -55°C. This data indicates that up to a certain composition, LLZO particles look to slow down the segmental motion of polymer phase.

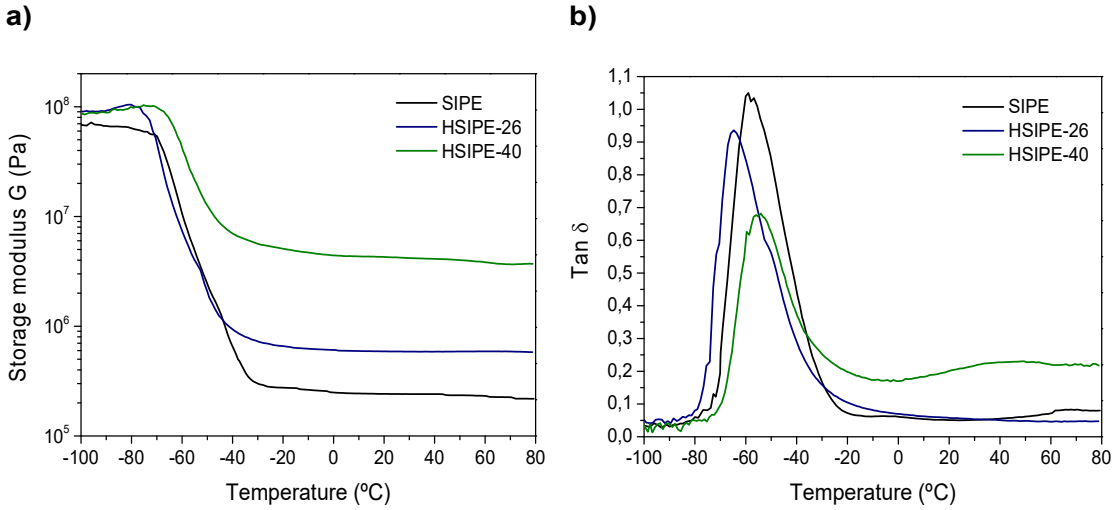

Figure 7: a) DMTA analysis in compression from -100 to 100°C b) Resulted Tan δ evolution.

3.3.3. Study of ionic conduction mechanisms by EIS and solid NMR

Electrochemical Impedance Spectroscopy (EIS) was used to determine the ionic conductivity of the hybrid electrolytes (Experimental method in Appendix B1). Figure 8 shows the ionic conductivity as a function of temperature for the different hybrid compositions. While increasing the particles loading, the ionic conductivity rises and reaches surprisingly a maximum for the HSIPE-40 composition. The ionic conductivity achieves $1{,}4.10^{-4}$ S.cm^{-1} at room temperature, which is 3,3-fold higher than the one measured for the pristine SIPE ($4{,}8.10^{-5}$ S.cm^{-1}).

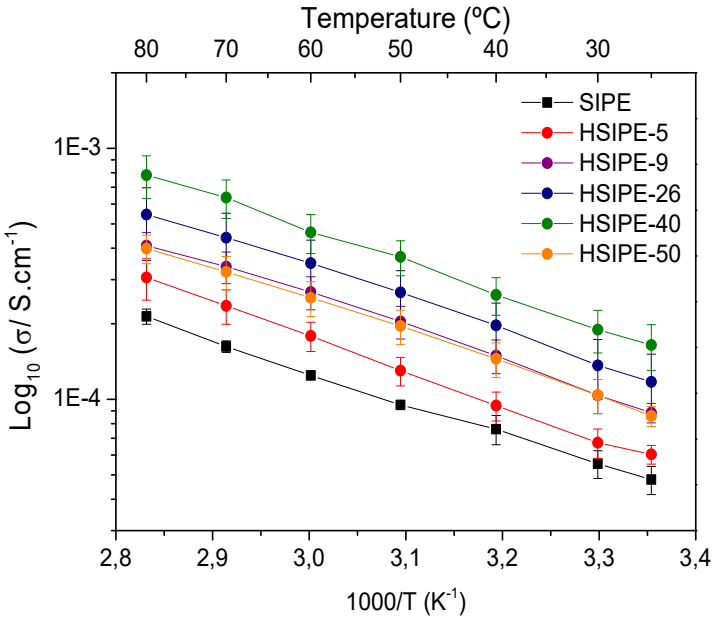

Figure 8: Arrhenius plot for SIPE and HSIPEs

This result is in agreement with previous studies on hybrid single ion polymer electrolytes with conductive inorganic particles reported in the literature. The inorganic particles can interact with tethered anionic moieties, enhancing the dissociation of Li ions [7,8]. For HSIPE-50, the ionic conductivity starts to decrease. According to ESEM observations (Figure 6.c), it can be hypothesized that the ionic conductivity drop at 50 wt.% may be explained by the poor dispersion of LLZO. To further confirm the beneficial effect of LLZO particles on the single ion matrix, dual ion membranes were synthesized to compare their ionic conductivity. DIPE refers to the pristine dual ion crosslinked polymer composed of LiTFSI salt. DIPE-26 is the related hybrid reinforced with 26 wt.% of particles. In addition, an inert hybrid membrane (without salt) composed of 26 wt.% of particles (HPE-26) was studied in order to clarify if LLZO can participate to the Li ion conduction. Their compositions are summarized in Table 1. Table 2 presents their ionic conductivity at room, mild and high temperatures.

Table 2. Ionic conductivities and activation energies E_a for SIPE, HPE, HSIPEs, DIPE and HDIPE compositions

Compositions	$\sigma_{25°C}$ (10^{-4} S.cm^{-1})	$\sigma_{50°C}$ (10^{-4} S.cm^{-1})	$\sigma_{70°C}$ (10^{-4} S.cm^{-1})	E_a (kJ/mol)
SIPE	0,48	0,95	1,62	11,2
HPE-26	0,11	0,22	0,34	8,9
HSIPE-26	1,17	2,67	4,41	10,8
HSIPE-9	0,88	2,04	3,38	10,7
DIPE	21	42	106	9,6
HDIPE-26	14,2	28,9	48,4	11,8

As demonstrated previously, the ionic conductivity of HSIPE-X is increased by the addition of LLZO particles (X=9 and 26 wt.% LLZO). Besides, the activation energy E_a appears to be lower for the hybrids. This result indicates that the presence of LLZO generates a beneficial ionic environment for Li^+ conduction. HPE-26, containing LLZO as the unique Li ion source, achieves lower ionic conductivity than SIPE, up to 10^{-5} S/cm. This interesting result implies that Li ions from the LLZO phase can transfer to the polymer matrix and may participate to the ionic transport in HSIPE-X. Few studies reported that possible ionic exchange takes place between LLZO and PEO matrix [16,17]. Nonetheless, the interface between Li ion conductive ceramic and polymer had been formerly investigated, revealing high interfacial resistance between the two phases [18]. Therefore, this characteristic can explain the lower ionic conductivity obtained for HPE-26. On the opposite, this hybrid has unexpectedly the lowest E_a. DIPE displays higher ionic conduction than SIPE. This difference can be explained by the substitution of single ion monomer LiMTFSI by the dual ion LiTFSI. In DIPE, both the anions and the cations are mobile, which results in larger ionic conductivity. Additional surprising information is the opposite ionic conductivity trend for the dual ion hybrid electrolyte. Once 26 wt.% LLZO is added to dual ion crosslinked polymer matrix (HDIPE-26), the conductivity drops fiercely. The activation energy rises from 9,6 to 11,8 kJ/mol once DIPE is reinforced with the ISE. This result implies that LLZO particles affect distinctively dual and single ion polymer matrices.

^{7}Li MAS NMR was used to better understand the ionic conduction in HSIPE-X (Experimental method in Appendix A7). Firstly, SIPE and HPE are compared (Figure 9). Spectra of SIPE and HPE allow to experimentally differentiate the distinct Li ion environments. The difference between these two electrolytes is the Li ion source: in SIPE, LiMTFSI monomer is the only source of Li whereas it is solely LLZO particles for HPE-26. For both electrolytes, one signal is observed with different line width and resonance. For SIPE, one narrow signal is detected at -6,13 ppm. On the opposite, one broad signal at -4,01 ppm is distinguished for HPE-26. Solid NMR confirms that distinct Li ion environments can be identified in these two materials. In addition, narrow signal is strongly related to fast Li ion motion [19]. It can be concluded that the narrow line width indicates fast lithium transport in the polymer phase (SIPE), the broad one slow lithium transport in the LLZO phase (HPE-26). These spectra will be used as references to determine Li ion environments in the hybrid electrolytes.

HSIPEs were examined to see the effect of LLZO particles on the Li ion environment of the single ion polymer matrix (Figure 9). HSIPE-26 presents two resonances: a narrow signal at -6,01 ppm and a broad one at -4,89 ppm. The first resonance is assigned to the Li in the polymer phase, the second one to the Li contained in LLZO particles. These results are in contrast from the ones reported by Zhang and co-workers, who studied LLZO-TEGDME-

PEO($LiClO_4$) system [20]. After mixing the particles with the plasticized polymer TEGDME-PEO, they could observe two additional signals. They identified them as the Li at the LLZO/TEGDME interface and decomposed LLZO diluted in TEGDME. Extra signals are not detected in our study. This discrepancy can be explained by the analysis of different LLZO compositions and their experimental method. Indeed, Li from the interface and decomposed LLZO phases was clearly distinguished up to 40 wt.% LLZO [20,21]. In addition, Zhang and co-workers used ^{6}Li solid NMR, enabling higher resolution of Li ion environments within the materials [19].

Besides, ^{7}Li resonances are strongly distinctive in term of chemical shifts, once LLZO is added in SIPE matrix. Signal at -6,13 broadens and shifts to lower fields. This indicates that Li ion environment in the polymer phase is strongly modified by LLZO particles. Additionally, Li from LLZO inorganic phase is also affected as its corresponding Li resonance greatly shifted to upper fields compared to SIPE. These chemical shifts evidence significant structural changes for both Li ion environments, in the polymer and the LLZO phases. HSIPE-9 only presents one narrow signal at -6,05 ppm. This resonance is attributed to the polymer phase. Signal from LLZO is not discernible for this composition. It can be explained by the lower concentration of particles. Nevertheless, low content of LLZO looks to affect Li ion environment in the polymer phase, as the peak shifts and broadens.

SIPE and DIPE were also compared to apprehend the impact of free anions on Li environment (Figure 9). For DIPE, LiMTFSI single ion monomer is replaced by LiTFSI salt (eq. %.mol). One signal can be observed at -6,15 ppm, corresponding to the polymer phase. When 26 wt.% LLZO is added in the dual ion pristine electrolyte (HDIPE-26), ^{7}Li resonance displays two Li environments, as a narrow and broad signals are observed at -6,05 and -4,47 ppm. They are assigned to the Li in the polymer and LLZO respectively. As observed previously for HSIPEs compositions, LLZO particles affect Li ion environment in the polymer matrix, as ^{7}Li narrow resonance is shifted to lower fields. On the opposite, Li from LLZO inorganic phase seems to be less affected by free $TFSI^-$ anions as its corresponding ^{7}Li resonance slightly shifts to upper fields compared to HSIPE-26.

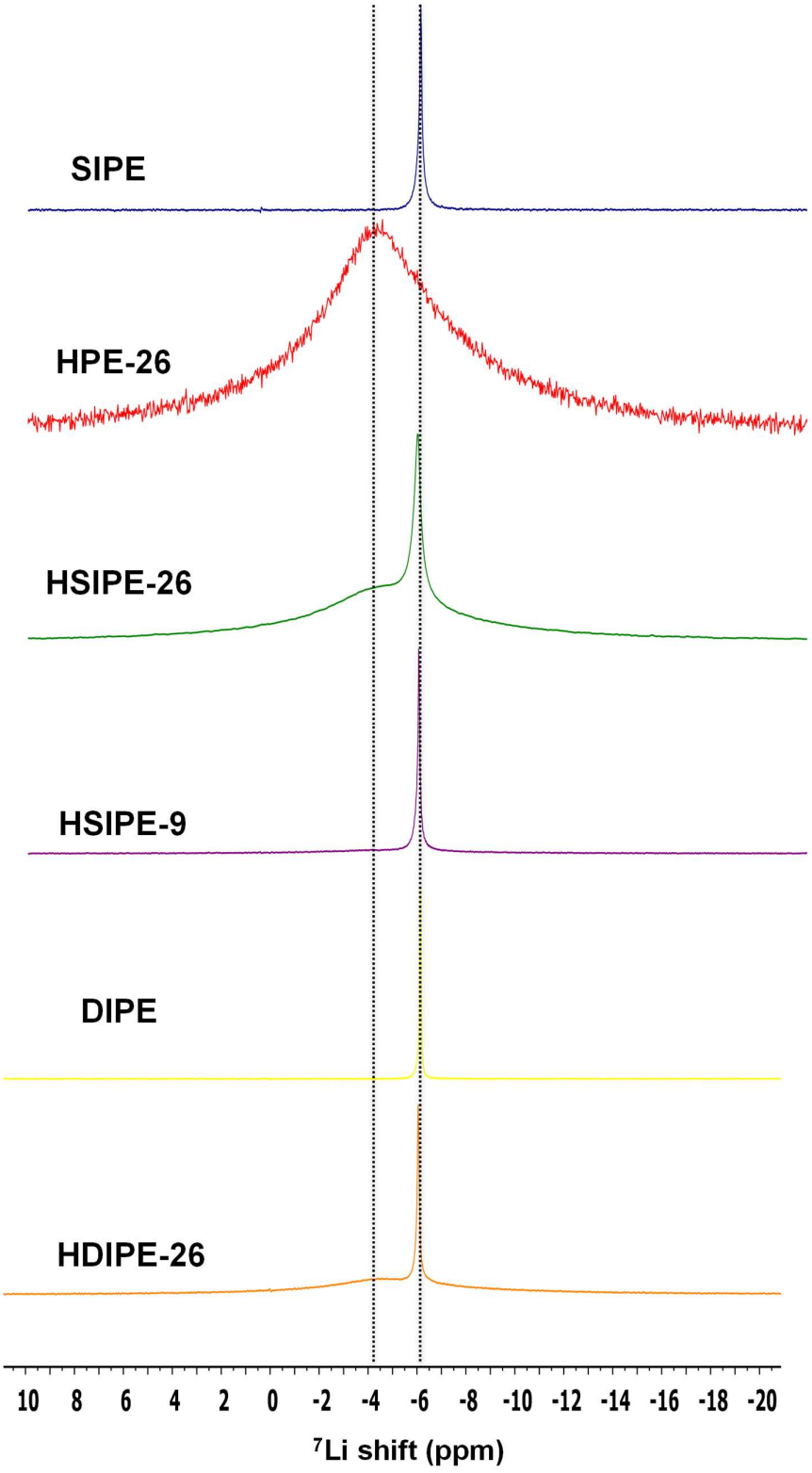

Figure 9: ^{7}Li MAS solid NMR on single and dual ion hybrid crosslinked polymer electrolytes

To deepen our analysis, ^{19}F MAS NMR was carried out on the same compositions to figure if LLZO particles can also affect fluorinated anions environment (Experimental method in Appendix A7).. Single ion compositions are firstly compared SIPE and HSIPE-X (Figure 10). In SIPE, a unique signal is observed at -85,84 ppm and is assigned to anchored $TFSI^-$ anion. In HSIPEs, additional "shoulder" component is detected at -85,90 and -85,95 ppm for HSIPE-26 and HSIPE-9 respectively. As LLZO does not contain fluorine atoms in its crystallographic structure, these resonances are assigned to two distinct $TFSI^-$ environments in the polymer phase. Once LLZO was added to the single ion matrix, major peaks become narrower and shift to lower fields, to -85,78 and to -85,83 ppm for HSIPE-26 and HSIPE-9 respectively. This implies that the addition of LLZO particles changes $TFSI^-$ environment in the polymer matrix. The "shoulder" signal intensity is increasing when LLZO content rises. Then, this additional resonance is assigned to $TFSI^-$ moieties interacting with LLZO surface. Few ^{19}F solid NMR studies already reported the appearance of a shoulder signal for polymers electrolytes reinforced by inorganic fillers, indicating strong absorption of fluorinated anions on the inorganic filler surface [23,24].

DIPE and HDIPE-26 are also examined by ^{19}F MAS NMR (Figure 10). For both, one peak is observed, assigned to fluorine environment in the polymer matrix. When single ion LiMTFSI monomer is replaced by LiTFSI salt (DIPE), ^7Li resonance becomes narrower and shifts to upper fields at -86,97 ppm, indicating higher mobilities of fluorinated anions. This result was expected as $TFSI^-$ anions are not covalently immobilized into the polymer backbone compared to SIPE [25]. Once 26 wt.% LLZO is added to the dual ion crosslinked polymer (HDIPE-26,Figure 10.b), the peak broadens and shifts to lower fields at -86,92 ppm, meaning lower mobilities for TFSI- anions.

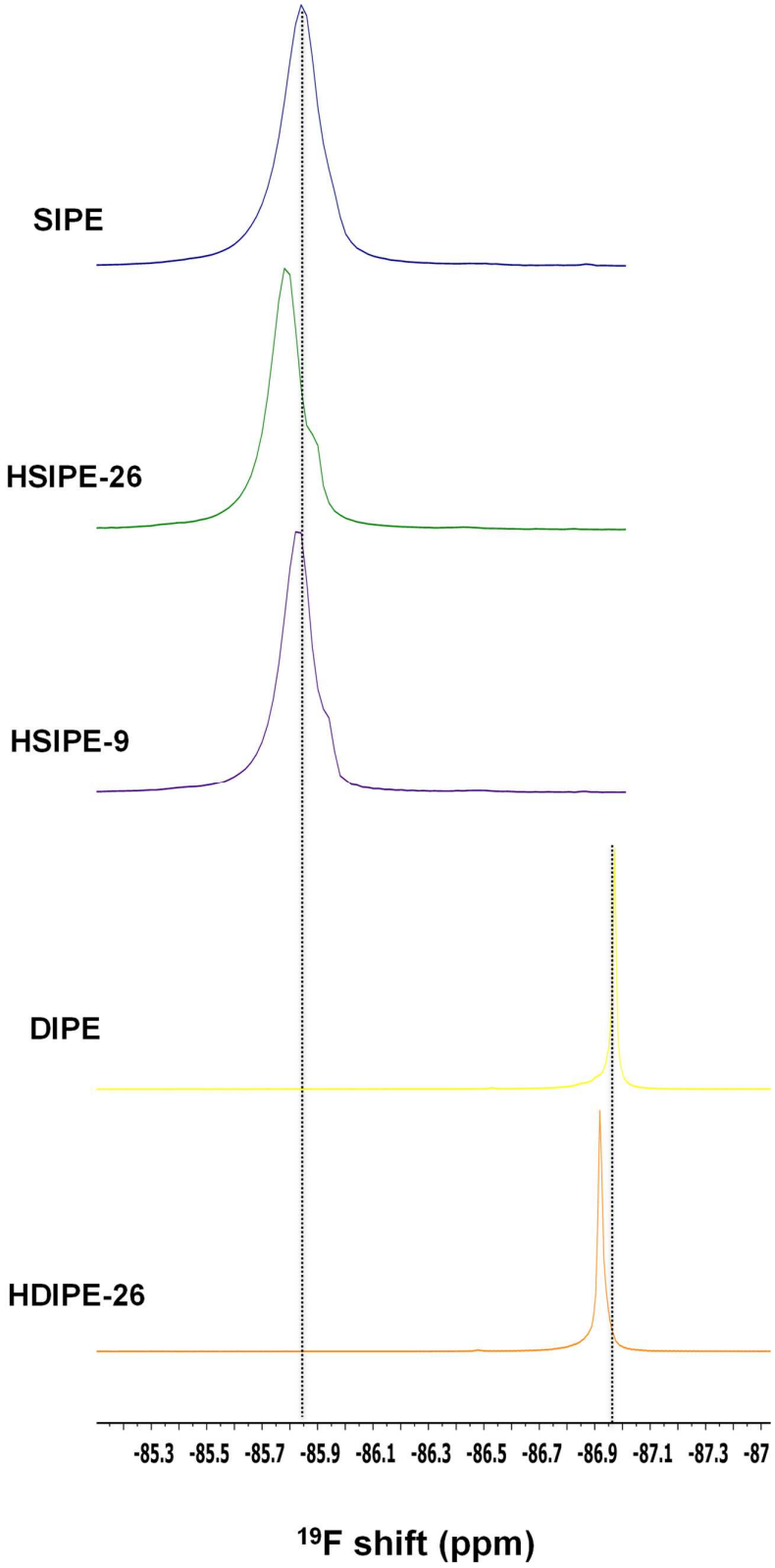

Figure 10: ^{19}F MAS solid NMR on single and dual ion hybrid crosslinked polymer electrolytes a) SIPE and HSIPEs; b) DIPE and HDIPE-26.

To get more insights on ionic conductivity mechanisms, static ^{7}Li solid NMR is used to determine Li ion mobilities. T_1 relaxation times can be calculated for polymer and hybrid compositions as shown in Table 3. Narrow and broad components represent the Li in the polymer and LLZO phase respectively. T_1 relaxations of narrow components become larger after addition of LLZO particles, in both single and dual ion crosslinked electrolytes. This result signifies that LLZO helps to increase Li ion mobility in the polymer phase. Opposite tendency was reported in the work of Zheng & co-workers on LLZO-PEO (LiTFSI) system [21]. ^{7}Li T_1 relaxation times became smaller while increasing LLZO content, indicating a slowdown of Li ion motion in the PEO phase. After addition of plasticizer (20 wt.% TEGDME), similar trend to our results was observed, Li ion mobility was improved dramatically despite high content of LLZO. This information emphasizes the beneficial effect of propylene carbonate on Li ion motion in the hybrid crosslinked polymer electrolytes. Nevertheless, LLZO phase exhibits very long ^{7}Li T_1 relaxation times. Similar values were communicated by Zhang and co-workers for decomposed LLZO[20]. They figured that this latter broke down due to ball milling process and its reaction with TEGDME. It can be hypothesized that propylene carbonate may alter LLZO phase, as T_1 relaxation of bulk LLZO is reported to be close to ~ 1s.

Table 3. ^{7}Li T_1 relaxations times (s) obtained by saturation recovery at 22°C.

Signal components	SIPE	HSIPE-26	HSIPE-9	DIPE	HDIPE-26
Narrow	0,23	1,6	0,25	0,26	1,03
Broad	-	15,8	6,9		15,0

Diffusion coefficients of Li^+ and $TFSI^-$ were also determined at different temperatures. Table 4 and Table 5. summarize the obtained ^{7}Li and ^{19}F diffusion coefficients for the previous compositions. SIPE and HSIPEs are first compared (Table 4.): ^{7}Li diffusion coefficients increase slightly in the whole range of temperature thanks to LLZO addition in the polymer matrix. Opposite trend is observed for DIPE and HDIPE-26: ^{7}Li diffusion coefficient is lightly higher at low temperatures for the hybrid. Nonetheless, increasing the temperature has the adverse impact on Li diffusion, becoming lower in the presence of LLZO particles. These opposite tendencies between single and dual ion electrolytes may reveal the different nature of interactions between LLZO and immobilized/free $TFSI^-$ anions.

^{19}F diffusion coefficients are also determined for DIPE and HDIPE-26 (Table 5). Anion diffusion drops significantly, especially at low temperatures where it is divided by two. These results confirm the presence of ionic interactions between LLZO and LiTFSI salt, which play an important role on the final ionic transport in the dual ion electrolytes.

Table 4. ^{7}Li diffusion coefficients at various temperatures

Composition	$D_{70°C}$ (10^{-12} m².s^{-1})	$D_{50°C}$ (10^{-12} m².s^{-1})	$D_{22°C}$ (10^{-12} m².s^{-1})
SIPE	13,1	6,77	2,05
HSIPE-26	17,1	7,03	2,94
HSIPE-9	15,3	8,68	2,78
DIPE	27,7	15,5	5,44
HDIPE-26	23,8	15,2	5,81

Table 5. ^{19}F diffusion coefficients at various temperatures

Composition	$D_{70°C}$ (10^{-11} m².s^{-1})	$D_{50°C}$ (10^{-11} m².s^{-1})	$D_{22°C}$ (10^{-11} m².s^{-1})
DIPE	16,4	10	3,91
HDIPE-26	10,3	5,65	1,98

To conclude, Li ion transport in single and dual ion hybrid polymer electrolytes is strongly distinct. The appearance of an additional peak in ^{19}F MAS spectrum in HSIPE-X implies that LiMTFSI monomer is strongly absorbed on the particles' surface. As a result, Li ions can better dissociate from the anions and the ionic conductivity is improved in the whole range of temperature. As confirmation, ^{7}Li ion diffusion coefficients are bigger in HSIPE-X, which increase with larger LLZO content. ^{7}Li mobility is enhanced in dual ion hybrid electrolytes at room temperature, but reversed tendency is observed at higher temperatures. Physical interactions between $TFSI^-$ anions and LLZO particles must occur. These distinct interactions between LLZO particles and free/immobilized $TFSI^-$ moieties can explain the different ionic conductivity trend in single and dual ion hybrid electrolytes.

3.3.4. Electrochemical application in Li/Li symmetrical cells

Firstly, lithium transference numbers t_{Li+} were determined at 60ºC (Experimental method in Appendix B4). As the membranes were extremely brittle, low tightening pressure was adjusted for pristine and hybrid electrolytes (2,6 and 2,8 N.m). To extract the resistances from the impedance spectra, the equivalent circuit model (ECM) from Bouchet and co-workers study was used [26]. The spectra are composed of two semi-circles, the first one at high frequencies is related to the bulk resistance of the electrolyte, the second one corresponds to the SEI. Typical EIS spectra fitted with this ECM for SIPE and HSIPEs are presented in Figure 11.a and Figure 11.c.

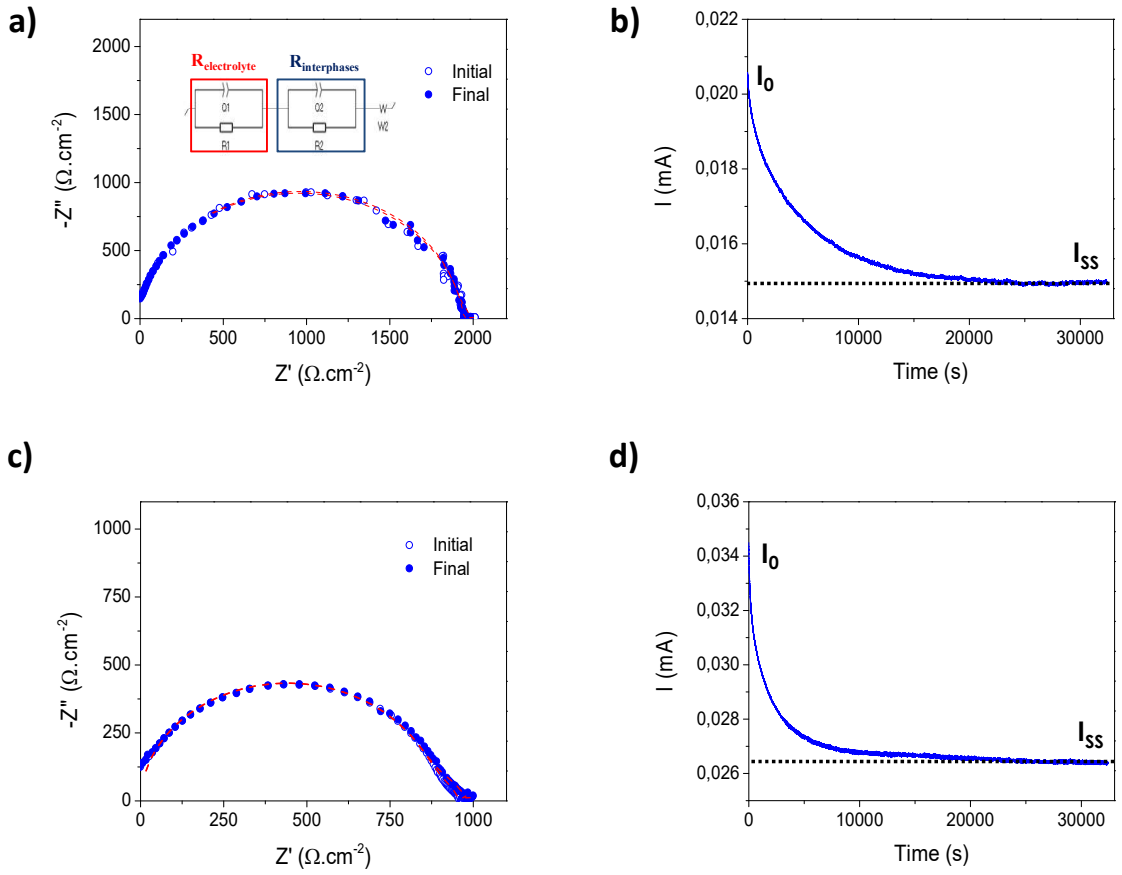

Figure 11: Transference number determination at 60°C for SIPE and HSIPE-9 SIPE: a) EIS spectra and ECM fit; b) Intensity decay after polarization HSIPE-9: c) EIS spectra and ECM fit; d) HSIPE-9 Intensity decay after polarization

Obtained t_{Li+} for SIPE, HSIPE-9 and HSIPE-26 are summarized in Table 6. SIPE and HSIPEs have higher transference numbers than most of HPE in the literature. Nonetheless, t_{Li+} tends to go down while increasing LLZO content. This tendency may be related to the poor efficiency of the UV initiator in presence of particles (DAROCUR), leaving unreacted monomer.

The addition of a co-initiator for the composite formulations and the optimization of the photopolymerization process may be needed.

Table 6. t_{Li+} determination for SIPE and HSIPEs

Composition	t_{Li+}
SIPE	0,73
HSIPE-9	0,63
HSIPE-26	0,57

The cycling performance of SIPE and HSIPE-26 were further assessed by galvanostatic cycling. This hybrid was chosen for its high ionic conductivity and easier reproducibly than HSIPE-40 composition. Figure 12.a.i displays the galvanostatic cycling of SIPE. Two voltage profiles are observed at low and high current densities. At 0,1 mA.cm^{-2}, the voltage remains flat, meaning that Li stripping/plating processes are homogeneous. Between 0,25 to 0,4 mA.cm^{-2}, overpotential starts to rise extensively. This type of voltage profile was reported to correlate to a quasi-homogeneous Li needle morphology. New SEI is forming to accommodate the expansion of Li metal anode, increasing the overall resistance of the cell. Starting from 0,5 mA.cm^{-2}, voltage response transits to a “neck” shape which is a strong indication of formation of mossy dendritic Li. These deposits tend to be detached from the anode surface during cycling, forming a thick layer of dead Li (inactive Li). It can be concluded that the CCD reached for SIPE is 1 mA.cm^{-2}. Nevertheless, dramatic rise of resistance can be observed during cycling (Figure 12.a.ii). Thanks to ECM fitting, R_{bulk} and R_{SEI} were estimated to rise from 236 Ω and 25 Ω to 1290 Ω and 960 Ω respectively. This increase can be explained by the formation of a “bad” SEI, leading gradually to the deterioration of the electrolyte and the lithium.

Galvanostatic cycling of HSIPE-26 is presented in Figure 12.b.i. Three voltages profiles can be seen at low and high current densities. Between 0,1 to 0,25 mA.cm^{-2}, Li needles growth is taking place. Starting from 0,4 to 1 mA.cm^{-2}, mossy like Li is deposited as it is indicated by the “neck” shape of the voltage profile. From 2 to 4 mA.cm^{-2}, voltage spikes are detected. It was shown in Chapter 2 that erratic voltage is a sign of dendrites growth. Besides, EIS spectrum in Figure 12.b.ii presents a drop of the overall resistance, which is also related to dendrites propagation within the electrolyte. From ECM fitting, R_{bulk} was observed to slightly increase (from 272 to 326 Ω) whereas R_{SEI} is sharply reduced from 115 Ω to a few ohms. It is important to note that these characteristics (Voltage spikes, impedance drop) are only observed when the crosslinked polymer electrolyte is reinforced with LLZO particles. Based on these results, it can be concluded that addition of LLZO particles does not help Li stripping/plating processes.

Post-mortem optical microscope observations are carried out on SIPE and HSIPE-26 (Experimental method in Appendix B6). Image presented in Figure 13.a displays cross-section HSIPE-26 which was short-circuited after the test. Lithium filaments crossing the electrolyte can be clearly noticed when the cross-section is examined. On the top view of SIPE (Figure 13.b), when the Li foil was removed, a thick dead Li layer is discerned, explaining the dramatic rise of resistance over cycling. This layer is also observed for cycled HSIPEs. A better design of the SEI (with fluorinated additives for example) should be beneficial for the cycling efficiency.

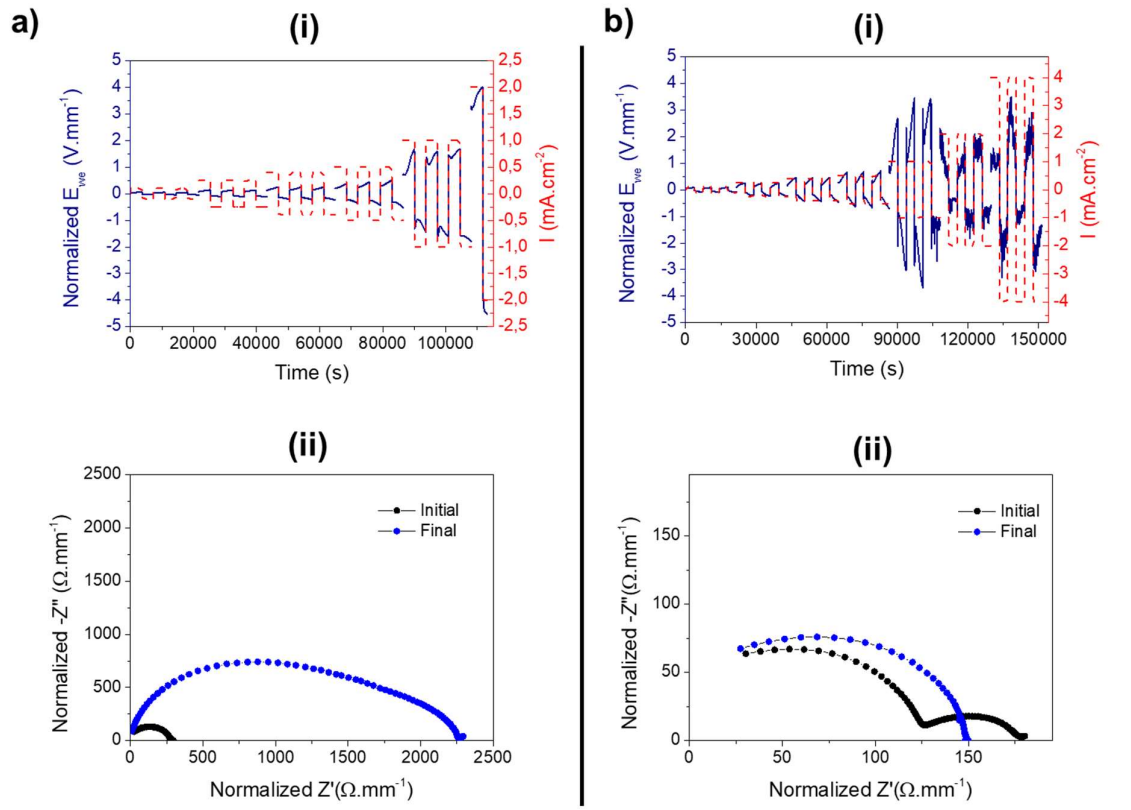

Figure 12: Galvanostatic cycling with increased current densities at 60°C for a) Li|SIPE|Li; b) Li|HSIPE-26|Li

i) Voltage profiles; ii) EIS spectra before and after GEIS

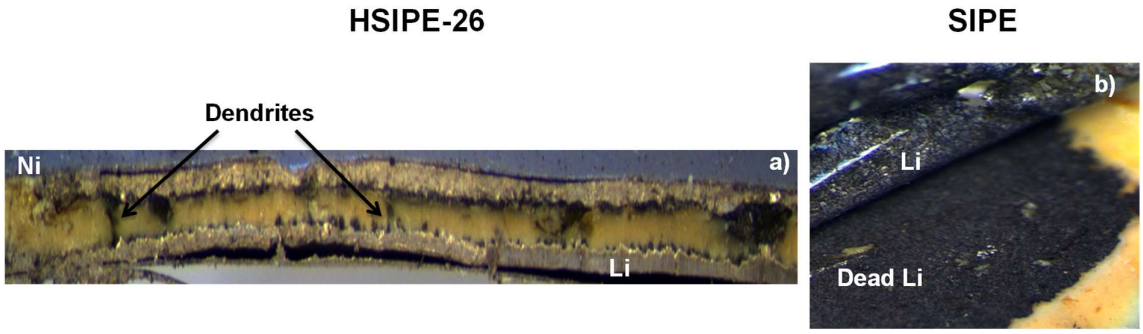

Figure 13: Optical images of a) cross section of cycled HSIPE-26; b) Top view of cycled SIPE

Dendrite formation appears to come from the use of LLZO particles, as dendritic growth characteristics are not observable for the cycled SIPE battery. To our knowledge, it is the first time that polymer electrolyte reinforced with LLZO particles is reported to form dendrites. LLZO is usually used as ideal active inorganic filler for polymer hybrid electrolytes. However, most of the studies do not focus on Li stripping and plating processes or use smaller current densities ($\leq$ 1 mA. cm^{-2}), which are less aggressive conditions to form dendrites. CCD study similar to

our work was carried out by Keller & al [27]. The current density was progressively increased from 0,005 mA.cm^{-2} to 0,1 mA.cm^{-2} but was too small to investigate fractal dendrite growth. Voltage instabilities had been recorded by Zagórski and co-workers for 30 wt.% LLZO-PEO(LiTFSI) at the beginning of cycling (0,1 mA.cm^{-2}) [17]. According to them, this erratic voltage comes from the direct contact of LLZO particles with Li metal, increasing the interfacial resistance. Then, voltage instabilities observed during the first cycles may originate from the structural reorganization at the interface Li/electrolyte.

In our case, three hypotheses can be considered:

- Different Li ion environments are present in HSIPE-X, comprising polymer and LLZO phases, which have distinct Li diffusion. This discrepancy may favour some areas rather than others for Li plating/stripping, leading to dendrites formation.

- Recently, it was demonstrated that densified LLZO can form dendrites within itself, due to its high electronic conductivity[28]. This feature can maybe explain why dendrites form in HSIPEs up to 1 mA.cm^{-2}. Nevertheless, the CCD for LLZO single crystal was established around 0,3 mA.cm^{-2} [29]. Then, the CCD obtained for the hybrid is surprisingly high.

- Chemical stability of LLZO in SIPE: Chemical deterioration of LLZO may be the cause of dendrites formation. Solid NMR proved that LLZO particles were altered in contact of the plasticizer. This degradation may worsen the already unstable SEI formed by the propylene carbonate. This may explain why HSIPEs can form dendrites whereas SIPE does not.

To ascertain this last hypothesis, resistance evolutions of Li/Li symmetrical cells with SIPE and HSIPE-26 electrolytes were monitored (Experimental method in Appendix B2). Figure 14 shows the resulted chemical stabilities of the polymer and the hybrid electrolytes towards the lithium. SIPE bulk resistance R_{bulk} (first semi-circle) decreases after 6h stabilization, then is kept constant up to 70h. From R_{bulk}=620 Ω, the resistance stabilized around 500 Ω. On the opposite, the resistance R_{SEI} related to the SEI formation (second semi-circle) keeps increasing over the time, especially after 50h. From 130 Ω, R_{SEI} increases to 480 Ω. The rise of R_{SEI} over time confirms that this latter is unstable. Some studies already reported that PC does not form stable SEI despite its interesting features as liquid electrolyte[30]. Addition of additives in cyclic carbonates have been under investigation to improve their performance when coupled to Li anode [31,32]. In Figure 14.b, HSIPE-26 shows both a dramatic increase of R_{bulk} and R_{SEI} over time. From 240 and 120 Ω, the resistances rise to 360 and 237 Ω respectively. This indicates that this hybrid composition is not chemically stable and the resulted SEI is much more unsteady compared to SIPE. To conclude, LLZO must degrade gradually and must react with one of the components of the SIPE matrix. Then, a focus on LLZO stability towards PC and LiMTFSI has been undertaken to better understand HSIPE's performance.

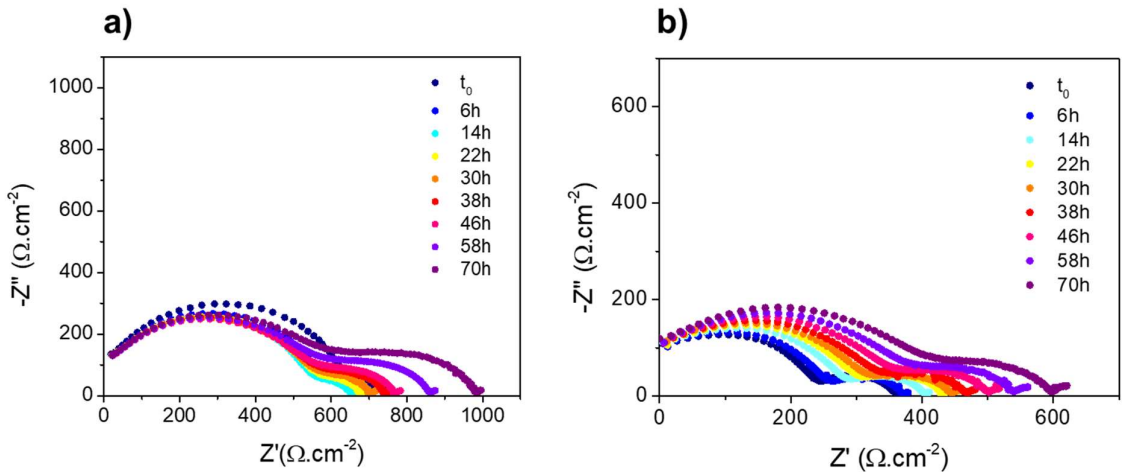

Figure 14: Resistance evolution in Li | Li symmetrical cells at 60°C for a) SIPE; b) HSIPE-26

3.3.5. LLZO stability with propylene carbonate and LiMTFSI

Neat and "treated" LLZO particles were compared by XRD (Experimental method in Appendix C1). "Treated" particles were immersed one month in PC, filtered and then dried for a couple of days in the glovebox. The PC filtrate was cloudy, indicating potential particles deterioration in the solvent. The diffractograms for neat and "treated" particles are presented in Figure 15.a. After immersion in the liquid, LLZO crystalline structure is strongly affected. Structural disordering of the cubic phase is observed as all the peaks become smaller and wider. This is quite surprising as it was reported recently that garnet stability can be protected while using aprotic organic solvents[33]. Water impurities (< 10ppm) in PC can maybe explain the deterioration of LLZO. As a matter of fact, this ceramic is highly reactive towards H_2O [34]. This reaction produces LiOH, which can further react with CO_2 to form Li_2CO_3. This latter can be easily observed by FTIR (1508-1451 cm^{-1}). Unfortunately, high concentration of PC and overlaps of its vibration bands in this desired observation zone makes it difficult to conclude about LLZO contamination. Then, determination of pH of the liquid monomer mixtures of SIPE and HSIPE-26 was carried out (Figure 15.b). SIPE liquid formulation shows neutral pH. On the opposite, basic pH can be detected for the hybrid composition (up to 9-10). This clearly proves that LiOH have been formed by LLZO contamination with water traces. LiOH formation within HSIPEs can explain its poor chemical stability towards the Li. On addition, probable formation of Li_2CO_3 on LLZO surface sheds light on increased R_{bulk} and R_{SEI} over time and low T_1 relaxation times calculated by solid NMR.

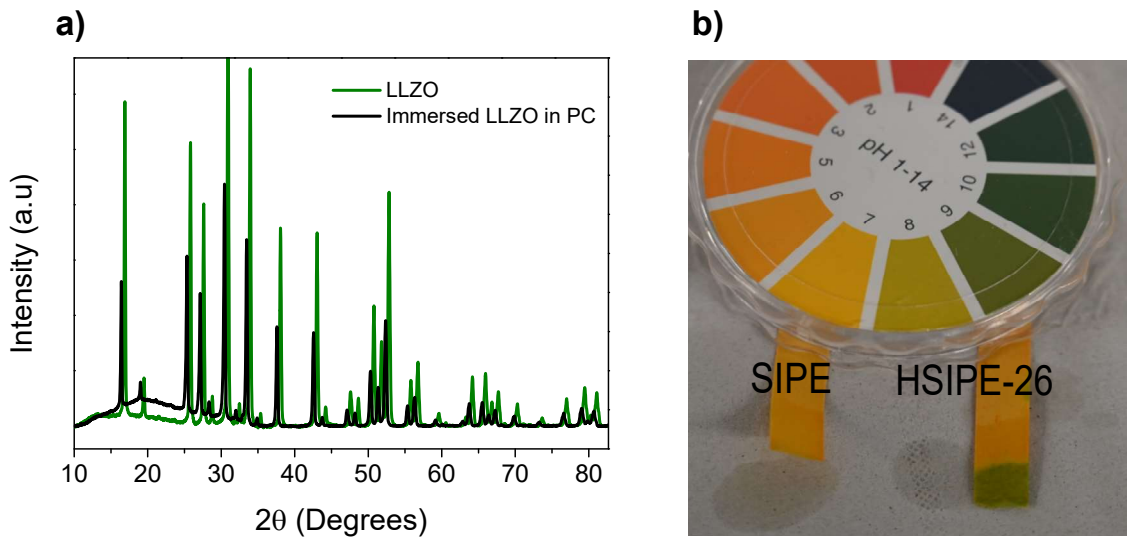

Figure 15: Study of LLZO stability towards the solvent: a) XRD of neat and "treated" LLZO particles in PC; b) pH determination of SIPE and HSIPE-26 liquid monomer mixtures.

Additional concern about LLZO stability in HSIPEs aroused from the observation of a colour change of the membranes, especially at low content of LLZO. HSIPE-26 and HSIPE-9 become respectively yellowish and brown (Figure 16.a). This alteration has been previously witnessed in HPE, especially in PVDF membranes[35,36]. According to Nan and co-authors[35], this colour comes from the structural modification of the polymer, which is triggered by the alkaline environment formed by the reaction of LLZO and the solvent (in this case, dimethylformamide DMF). A colour change was also notified for hybrids made with lithiated Nafion with NMP[7], PTFE with succionitrile[37] or PAN with DMF[38]. Different reaction mechanisms depending on the polymer or the solvent were described, which complicates the whole understanding of LLZO effect on this phenomenon. To summarize, most of the studies pointed out that LLZO does not react directly with the polymer, but its reaction with the solvent is the triggering factor for the matrix modification. However, it was reported that functionalized LLZO by in situ polymerized dopamine on its surface experiences a colour change [39].This change of colour is therefore directly related to the presence of a polymerized dopamine layer on the particles surface. This last study underlines that a colour alteration of the hybrid can be related to a structural modification of LLZO by its functionalization with a polymer. In our case, solid NMR revealed the presence of an additional environment for tethered TFSI moieties. This appearance of a shoulder in ^{19}F spectrum was already reported for anionic species strongly absorbed at the surface of inorganic particles. We can imagine similar phenomenon in the HSIPE-X, where LiMTFSI monomer is able to cover LLZO surface before being polymerized.

We attempted to demonstrate the possibility of LLZO to be functionalized by LiMTFSI monomer. For this purpose, LiMTFSI and LLZO were immersed and mixed in PC, with the same amounts used for HSIPE-9 and HSIPE-26 compositions. After some minutes, the liquid mixtures solidified. Hard and soft gels were obtained respectively for HSIPE-9 and HSIPE-26 compositions (Figure 16.b and Figure 16.c). Vinyl groups of LiMTFSI remain unchanged after gelation (ATR-FTIR) which means than the monomer did not react. This strongly suggests the formation of LiMTFSI layers on LLZO surface. Discrepancies of the mechanical properties

come from LLZO content: in HSIPE-26, LLZO concentration is superior to LiMTFSI. Then, some of the particles do not complex with the single ion monomer, which is result in a loose gel. These latter can further react with LiOH to form Li_2CO_3. We can imagine that UV polymerization of LiMTFSI/LLZO/PC mixtures with PEG based monomers will lead to the colour change noticed for aged HSIPEs: brown for HSIPE-9 and yellow for HSIPE-26.

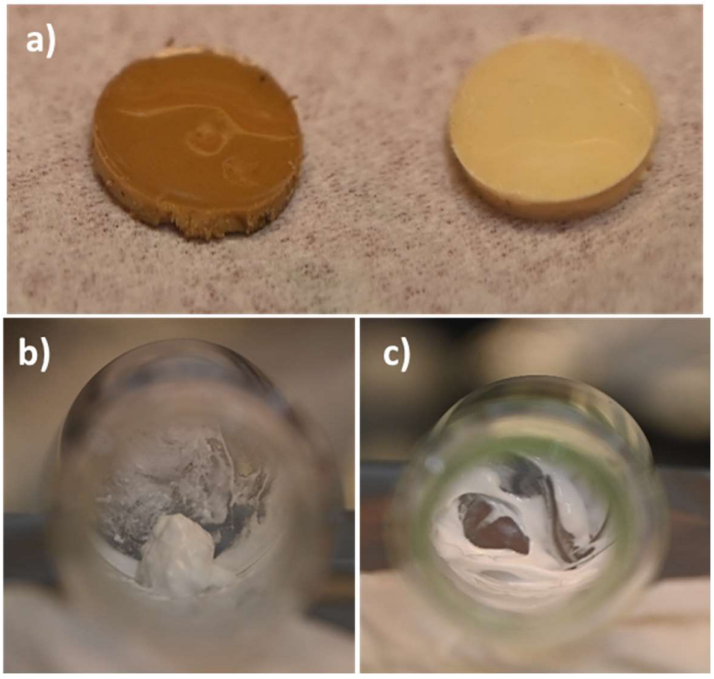

Figure 16: Pictures of HSIPEs and LiMTFSI/LLZO/PC mixtures: a) aged HSIPE-9 (brown) and aged HSIPE-26 (yellow); b) Gelation of LiMTFSI/LLZO/PC (HSIPE-9); c) Gelation of LiMTFSI/LLZO/PC (HSIPE-26)

High CCD reached for HSIPE-26 further tends to confirm the formation of “an interphase” formed by LiMTFSI and LLZO. This promising result emphasizes the beneficial effect of LiMTFSI/LLZO complex; nevertheless, additional characterization techniques (XPS, Raman) will be necessary to fully understand the role of LLZO in HSIPEs’ properties.

3.3.6. Upgraded Li/Li symmetrical cells by in situ polymerization and SEI additives.

We decide to upgrade SIPE composition as it shows the most promising cycling performance towards the lithium. Li|SIPE|Li battery can further be improved thanks to in situ polymerization, in other words, by directly forming SIPE electrolyte on the top of the Li foil. It was reported that enhanced electrolyte/electrode contact was possible by firstly wetting the anode by liquid monomers which are then polymerized thermally or by UV [40,41]. This results to a homogeneous interface between the Li and the electrolyte, with lower resistance. In addition,

the use of SEI additives in the liquid precursors may allow to form directly a stable SEI. It is well known that solid batteries made by in situ processes generally outstand their “ex situ” counterparts in term of cycling thanks to their better interfacial compatibility and SEI interphase[42]. Furthermore, this one pot synthesis is achievable for large scale manufacturing, which is a strong asset for the widespread implementation of ASSBs.

To form a thin polymer layer on the Li, it was necessary to improve the robustness of the crosslinked network. Previously, DAROCUR (D) was used as sole UV initiator to launch the UV polymerization, which led to brittle membranes and inefficient monomer conversion (SIPE transference number equals to 0,63). Then, it was decided to use UV co-initiator (BAPO=B) in presence of DAROCUR to achieve the desired mechanical properties. BAPO is widely used as UV co-initiator to cure pigmented polymer solutions. A ratio D/B was set up to 20, D still fixed to 3wt.% towards the total weight of monomers. Liquid monomer mixture (SIPE composition) was then spread off on the Li foil thanks to an adhesive mould (thickness: 300 µm). UV irradiation was let to 20 min and the coated Li was then punched out from the foil. Thin layers were successfully obtained between 200 and 350 µm. The cell pressure was set up to 2,4 N.m. Transference number (TN) was then determined for this optimized composition to ascertain the complete UV polymerization. EIS spectra and intensity decay after polarization are displayed in Figure 17. Extremely low resistance, especially R_{SEI}, can be noticed from Figure 17.a compared to previous SIPE impedance (Figure 11.a). Improvement of the interfacial compatibility of Li|SIPE|Li battery has been successfully undertaken by in situ polymerization. TN was determined to be 0,88, which is a greater value compared to the initial SIPE composition.

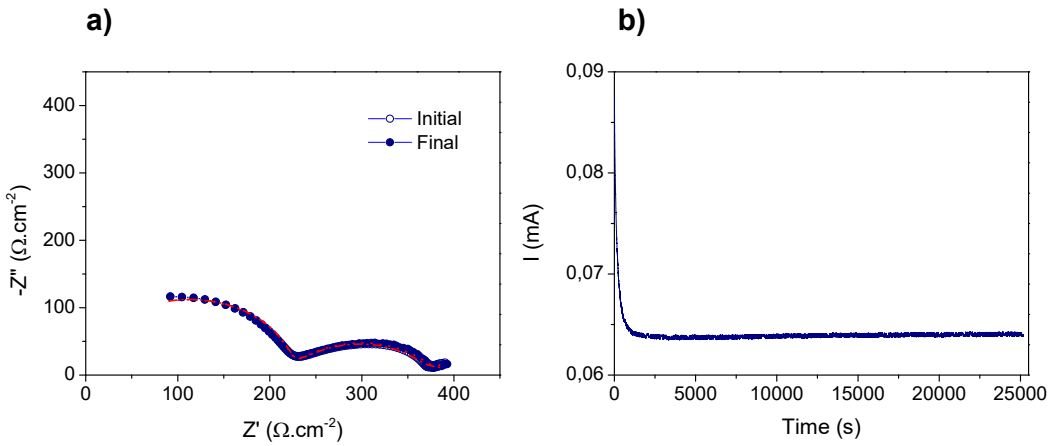

Figure 17: Transference number determination at 60°C for SIPE/BAPO

a) EIS spectrum and ECM fit; b) Intensity decay after polarization

Fluoroethylene carbonate (FEC) was elected as SEI additive as it previously shows promising effect on SEI formation in PC electrolyte[43]. 5wt.% FEC was enough to stabilize the Li. Decomposition of FEC on Li leads to an enriched LIF SEI, which is reported to be extremely stable[32]. Then, in situ polymerization of modified SIPE composition (BAPO+5 wt.% FEC) was carried out on Li and galvanostatic test was applied again to investigate how SEI additives

affect the cycling performance. The results are displayed in Figure 18. Addition of FEC leads to extremely stable voltage profiles at high current densities (Figure 18.a). Up to 1 mA.cm^{-2}, overpotential remains exceptionally flat, which indicates a homogeneous Li plating/stripping. Starting from 2 mA.cm^{-2}, Li mossy deposition/dissolution can be evidenced by the "neck" type voltage. The in-situ gel layer can further be cycled up to 4 mA.cm^{-2} but voltages spikes look to appear at the end of the test. The CCD was then established to 2 mA.cm^{-2}. EIS spectra (Figure 18.b) before and after the galvanostatic cycling test are strictly distinct. Cycling up to 4 mA.cm^{-2} deteriorates tremendously SIPE as both R_{bulk} and R_{SEI} rise enormously after the test. R_{bulk} rises from 590 Ω to 890 Ω whereas R_{SEI} skyrockets from 90 Ω to 1480 Ω. Despite the high current densities reached, the electrolyte does not form dendrites and further be cycled up to 2 mA.cm^{-2} once galvanostatic cycling was repeated.

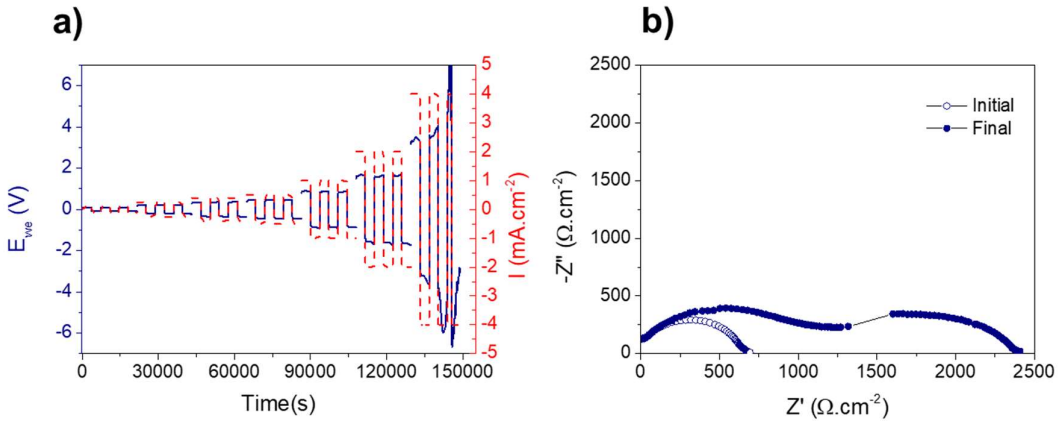

Figure 18: CCD determination SIPE-BAPO-FEC by galvanostatic cycling, a) Voltage profiles, b) EIS spectra before and after cycling

To conclude, optimized UV polymerization thanks to the use of a UV co-initiator allows the in-situ formation of a robust and thin PEG reticulated network with single ion conduction on the Li. Formation of a stable SEI was possible by the use of only 5wt.% FEC in the liquid precursors solution. This new composition enables to cycle the Li symmetrical cell up to 2 mA.cm^{-2}.

3.4. Conclusions

In this chapter, new HSIPEs were synthesized by fast UV polymerization combining a methacrylic lithium-single ion gel polymer formulation and LLZO particles. First the UV exposure and fast photo-polymerization kinetics were studied by photo-rheology and FTIR-ATR analysis. Homogeneous LLZO dispersion in the polymer matrix was easily achieved by simple magnetic stirring. High loading of inorganic particles (up to 40 wt.%) can be achieved without observing agglomerates or sediments. The obtained hybrids present enhanced properties, as higher ionic conductivity and better mechanical stability. An optimal ionic conductivity ($1{,}4.10^{-4}$ S/cm) was obtained for HSIPE-40 composition.

Solid NMR helps us to better understand the Li ion conduction mechanisms taking place in these HSE. For this purpose, HSIPEs were compared to hybrid gel compositions where the single ion monomer LiMTFSI is replaced by the salt LiTFSI (HDIPE). In both cases, two Li environments were detected, from the polymer and the inorganic LLZO phases. However, the Li ions preferably move in the organic phase. ^{19}F Solid NMR was then applied to explain the discrepancies between single and dual ion hybrid polymers. This revealed that two environments were observed for fluorinated anions in HSIPEs whereas HDIPE presents a unique peak. It was then hypothesized that, in the HSIPEs compositions, immobilized $TFSI^-$ moieties are strongly absorbed on the particles surface. This interaction explains the improvement of Li^+ mobility within these electrolytes, which increases the ionic conductivity.

Thanks to its promising properties, HSIPEs were thought to be interesting anolytes for dendrites protection. In addition to their superior ionic conductivity, these hybrids have high transference number (0,6-0,57), which can generate homogenous Li stripping/plating processes on Li metal anode. However, LLZO does not have a beneficial impact on the cycling performance of the polymer matrix. The CCD remains unchanged and dendrites can form in presence of LLZO particles. Chemical instability towards Li reveals the possible LLZO contamination by water traces, leading to the formation of Li_2CO_3 on particles' surface. Nonetheless, the hybrid can reach high current density (1 $mA.cm^{-2}$), which leads us to hypothesize about a possible formation of an interphase between the polymer and LLZO. Additional investigations (XPS, Raman) are necessary to rightfully decide about LLZO effect on SIPE matrix.

The optimization of the polymer Li symmetrical cells and the enhancement of its performance were realized by carrying out in situ UV photo-polymerization (on top of lithium) and the use of the fluoroethylene carbonate (FEC) additive within the HSE formulation . The use of co-initiator (BAPO) improves the polymerization conversion and allows to get robust and thinner electrolytes. By this method, thin polymer electrolyte layers (300 µm) were obtained on the surface on the lithium. The CCD was also extended to 2 $mA.cm^{-2}$ thanks to a stabler SEI generated by the fluorinated additive.

3.5. References.

1. Zhu, M. *et al.* Recent advances in gel polymer electrolyte for high-performance lithium batteries. *Journal of Energy Chemistry* vol. 37 126–142 (2019).

2. Liu, T. *et al.* Review — In Situ Polymerization for Integration and Interfacial Protection Towards Solid State Lithium Batteries Review — In Situ Polymerization for Integration and Interfacial Protection Towards Solid State Lithium Batteries. *J. Electrochem. Soc.* **167**, (2020).

3. Manuel Stephan, A. Review on gel polymer electrolytes for lithium batteries. *Eur. Polym. J.* **42**, 21–42 (2006).

4. Nunes-Pereira, J., Costa, C. M. & Lanceros-Méndez, S. Polymer composites and blends for battery separators: State of the art, challenges and future trends. *J. Power Sources* **281**, 378–398 (2015).

5. Lim, Y. J. *et al.* Ceramic-Based Composite Solid Electrolyte for Lithium-Ion Batteries. *Chempluschem* **80**, 1100–1103 (2015).

6. Yoshima, K., Harada, Y. & Takami, N. Thin hybrid electrolyte based on garnet-type lithium-ion conductor Li7La3Zr2O12 for 12 V-class bipolar batteries. *J. Power Sources* **302**, 283–290 (2016).

7. Gao, J., Shao, Q. & Chen, J. Lithiated Nafion-garnet ceramic composite electrolyte membrane for solid-state lithium metal battery. *J. Energy Chem.* **46**, 237–247 (2020).

8. Chen, Y. *et al.* Lithiated polyanion supported Li1.5Al0.5Ge1.5(PO4)3 composite membrane as single-ion conducting electrolyte for security and stability advancement in lithium metal batteries. *J. Memb. Sci.* **620**, 118926 (2021).

9. Diederichsen, K. M., McShane, E. J. & McCloskey, B. D. Promising Routes to a High Li+ Transference Number Electrolyte for Lithium Ion Batteries. *ACS Energy Lett.* **2**, 2563–2575 (2017).

10. Porcarelli, L. *et al.* Single-Ion Conducting Polymer Electrolytes for Lithium Metal Polymer Batteries that Operate at Ambient Temperature. *ACS Energy Lett.* **1**, 678–682 (2016).

11. Li, Z. *et al.* Ionic Conduction in Composite Polymer Electrolytes: Case of PEO:Ga-LLZO Composites. *ACS Appl. Mater. Interfaces* **11**, 784–791 (2019).

12. S. Shaplov, A. *et al.* Design and synthesis of new anionic “polymeric ionic liquids ” with high charge delocalization. *Polym. Chem.* **2**, 2609–2618 (2011).

13. Jung, K. I. *et al.* Effects of solvents on rheological and crosslinking properties of photo-polymerized poly(ethylene glycol) hydrogels. *Korean J. Chem. Eng.* **34**, 1517–1523 (2017).

14. Hwang, J. W., Noh, S. M., Kim, B. & Jung, H. W. Gelation and crosslinking characteristics of photopolymerized poly(ethylene glycol) hydrogels. *J. Appl. Polym. Sci.* **132**, (2015).

15. Marcinek, M. *et al.* Electrolytes for Li-ion transport – Review. *Solid State Ionics* **276**, 107–126 (2015).

16. Zhang, J. *et al.* Flexible and ion-conducting membrane electrolytes for solid-state lithium

batteries: Dispersion of garnet nanoparticles in insulating polyethylene oxide. *Nano Energy* **28**, 447–454 (2016).

17. Zagórski, J. *et al.* Garnet-Polymer Composite Electrolytes: New Insights on Local Li-Ion Dynamics and Electrodeposition Stability with Li Metal Anodes. *ACS Appl. Energy Mater.* **2**, 1734–1746 (2019).

18. Langer, F. *et al.* Impedance Spectroscopy Analysis of the Lithium Ion Transport through the Li 7 La 3 Zr 2 O 12 /P(EO) 20 Li Interface . *J. Electrochem. Soc.* **164**, A2298–A2303 (2017).

19. Vinod Chandran, C. & Heitjans, P. *Solid-State NMR Studies of Lithium Ion Dynamics Across Materials Classes*. *Annual Reports on NMR Spectroscopy* vol. 89 (Elsevier Ltd., 2016).

20. Zheng, J., Dang, H., Feng, X., Chien, P. H. & Hu, Y. Y. Li-ion transport in a representative ceramic-polymer-plasticizer composite electrolyte: Li7La3Zr2O12-polyethylene oxide-tetraethylene glycol dimethyl ether. *J. Mater. Chem. A* **5**, 18457–18463 (2017).

21. Zheng, J. & Hu, Y. Y. New Insights into the Compositional Dependence of Li-Ion Transport in Polymer-Ceramic Composite Electrolytes. *ACS Appl. Mater. Interfaces* **10**, 4113–4120 (2018).

22. Strauss, E., Menkin, S. & Golodnitsky, D. On the way to high-conductivity single lithium-ion conductors. *J. Solid State Electrochem.* **21**, 1879–1905 (2017).

23. van Wüllen, L. & Köster, T. K. J. The interaction between inorganic Li salts (LiTf, LiNTf2) and the surface of alumina particles as studied with solid state nuclear magnetic resonance. *Solid State Ionics* **180**, 141–147 (2009).

24. Mejía, A. *et al.* Scalable plasticized polymer electrolytes reinforced with surface-modified sepiolite fillers - A feasibility study in lithium metal polymer batteries. *J. Power Sources* **306**, 772–778 (2016).

25. Lago, N., Garcia-Calvo, O., del Amo, J. M., Rojo, T. & Armand, M. All Solid State Lithium Ion Batteries with Grafted Ceramic Nanoparticles Dispersed in Solid Polymer Electrolytes. *ChemSusChem* **8**, 3039–3043 (2015).

26. Bouchet, R., Lascaud, S. & Rosso, M. An EIS Study of the Anode Li/PEO-LiTFSI of a Li Polymer Battery. *J. Electrochem. Soc.* **150**, A1385 (2003).

27. Keller, M. *et al.* Electrochemical performance of a solvent-free hybrid ceramic-polymer electrolyte based on Li7La3Zr2O12 in P(EO)15LiTFSI. *J. Power Sources* **353**, 287–297 (2017).

28. Han, F. *et al.* High electronic conductivity as the origin of lithium dendrite formation within solid electrolytes. *Nat. Energy* **4**, 187–196 (2019).

29. Flatscher, F., Philipp, M., Ganschow, S., Wilkening, H. M. R. & Rettenwander, D. The natural critical current density limit for Li 7 La 3 Zr 2 O 12 garnets . *J. Mater. Chem. A* (2020) doi:10.1039/c9ta14177d.

30. Qian, J. *et al.* High rate and stable cycling of lithium metal anode. *Nat. Commun.* **6**, (2015).

31. Lin, D. *et al.* Solubility-mediated sustained release enabling nitrate additive in carbonate electrolytes for stable lithium metal anode. *Nat. Commun.* 1–10 doi:10.1038/s41467-

018-06077-5.

32. Brown, Z. L., Jurng, S., Nguyen, C. C. & Lucht, B. L. Effect of Fluoroethylene Carbonate Electrolytes on the Nanostructure of the Solid Electrolyte Interphase and Performance of Lithium Metal Anodes. *ACS Appl. Energy Mater.* **1**, 3057–3062 (2018).

33. Kun, R. *et al.* Structural and Computational Assessment of the Influence of Wet-Chemical Post-Processing of the Al-Substituted Cubic Li7La3Zr2O12. *ACS Appl. Mater. Interfaces* **10**, 37188–37197 (2018).

34. Huo, H. *et al.* Li2CO3: A Critical Issue for Developing Solid Garnet Batteries. *ACS Energy Lett.* **5**, 252–262 (2020).

35. Zhang, X. *et al.* Synergistic coupling between Li6.75La3Zr175Ta0.25O12 and poly(vinylidene fluoride) induces high ionic conductivity, mechanical strength, and thermal stability of solid composite electrolytes. *J. Am. Chem. Soc.* **139**, 13779–13785 (2017).

36. Yu, J. *et al.* A Ceramic-PVDF Composite Membrane with Modified Interfaces as an Ion-Conducting Electrolyte for Solid-State Lithium-Ion Batteries Operating at Room Temperature. *ChemElectroChem* **5**, 2873–2881 (2018).

37. Jiang, T. *et al.* Solvent-Free Synthesis of Thin , Flexible , Nonflammable Garnet-Based Composite Solid Electrolyte for All-Solid-State Lithium Batteries. **1903376**, 1–10 (2020).

38. Zhang, X. *et al.* Effects of Li 6.75 La 3 Zr 1.75 Ta 0.25 O 12 on chemical and electrochemical properties of polyacrylonitrile-based solid electrolytes. *Solid State Ionics* **327**, 32–38 (2018).

39. Jia, M., Bi, Z., Shi, C., Zhao, N. & Guo, X. Air-stable dopamine-treated garnet ceramic particles for high-performance composite electrolytes. *J. Power Sources* **486**, 229363 (2021).

40. Huang, S. *et al.* An in-situ polymerized solid polymer electrolyte enables excellent interfacial compatibility in lithium batteries. *Electrochim. Acta* **299**, 820–827 (2019).

41. Zuo, T. T. *et al.* Constructing a Stable Lithium Metal-Gel Electrolyte Interface for Quasi-Solid-State Lithium Batteries. *ACS Appl. Mater. Interfaces* **10**, 30065–30070 (2018).

42. Liu, T. *et al.* Review—In Situ Polymerization for Integration and Interfacial Protection Towards Solid State Lithium Batteries. *J. Electrochem. Soc.* **167**, 070527 (2020).

43. Mogi, R., Inaba, M., Jeong, S. & Iriyama, Y. Effects of Some Organic Additives on Lithium Deposition in Propylene Carbonate. 1578–1583 (2002) doi:10.1149/1.1516770.

CHAPTER 4.

Lithium single-ion hybrid and polymer electrolytes based on crosslinked PEO blends.

4.1. Introduction

Poly(ethylene oxide) (PEO) is the most investigated polymer electrolyte[1]. Nonetheless, PEO suffers from insufficient ionic conductivity at ambient temperature, low transference number and poor oxidation stability (4V). Several strategies have been developed over the years to improve its properties such as blending, crosslinking and addition of inorganic fillers[2]. Great success for PEO based composites with inorganic ionic conductors has been growing, thanks to their big improvement in term of ionic conductivity and mechanical stability[3].

Lithium single-ion anionic polymer electrolytes have been widely studied as a promising option to mitigate dendrites formation in Li metal batteries. These electrolytes have single ion conduction, as their anionic component is tethered in the polymer backbone; the current is only provided by Li ions. This property allows homogeneous Li stripping/plating processes on the anode. Nevertheless, single ion anionic homopolymers often present low ionic conductivity at room temperature due to their high glass transition (T_g). Therefore, they are often copolymerized or blended with polymers bearing soft or flexible segments to achieve acceptable ionic mobility.

The combination of PEO and single-ion anionic polymers by copolymerization has been commonly applied to obtain single ion and highly conductive SPE[4]. This process amorphize the PEO and lowers the T_g of the single-ion polymer, providing fast ionic pathways. Besides, the anionic polymer phase supplies the Li ions with single ion conduction. However, copolymerization synthesis of such materials requires additional chemical steps. Then, simple process method such as blending has been considered. Recently, some studies have reported the mixing strategy between PEO and different single ion conducting polymer electrolytes to increase its ionic conductivity while keeping the single ion property [5,6,7]. Among them, Olmedo-Martinez & al. prepared blends based on high molecular weight PEO and single ion polymer poly(LiMTFSI)[8]. Self-standing and single ion materials were obtained, which showed the highest conductivity value at room temperature reported for a single ion conducting polymer (up to 10^{-5} S/cm at room temperature). It was showed that p(LiMTFSI) interacts greatly with PEO, decreasing its crystallinity. However, the strong complexation of PEO with p(LiMTFSI) may also limit ultra-fast Li conduction in these materials. As explained before in this PhD thesis, inorganic ionic conductors may enhance ionic dissociation in single ion matrices and polymeric blends, as they can free up Li ions by interacting with tethered anions moieties[9]. This invited us to explore the combination of the successful blending strategy for PEO, poly(LiMTFSI) and LLZO particles as a second method in this thesis to obtain single ion conducting HSE.

Interestingly, the single ion block copolymer based on LiMTFSI and polyethylene glycol methyl ether methacrylate (PEGM) monomers showed bigger ionic conductivity at room temperature than the homopolymer p(LiMTFSI) and still presents a high transference

number[10]. LiMTFSI moieties provide the Li ions while PEGM improves chain mobility of the copolymer. This material can be an interesting candidate for single ion PEO based blend, as PEGM moieties can further lessen PEO-Li interactions. As PEGM and LiMTFSI monomers are both methacrylic with similar reactivity, free random copolymerization can be considered a facile and one pot synthesis when compared to RAFT technique[11]. In the first part of this chapter, various poly(LiMTFSI$_x$-co-PEGM$_{1-x}$) random copolymers were synthesized and evaluated to elect the best composition in term of ionic conductivity to mix with PEO.

Resulting PEO-poly(LiMTFSI$_x$-co-PEGM$_{1-x}$) blends were prepared and the effect of LiMTFSI concentration and copolymer content on the ionic conductivity of the blends was thoroughly investigated. Additional UV crosslinking of the optimized compositions was carried out to obtain true self-standing solid state polymer electrolytes[12]. LLZO was elected again as inorganic filler, thanks to its interesting properties as Li inorganic conductor and its affinity with LiMTFSI moieties (See Chapter 3). Finally, both pristine PEO- poly(LiMTFSI$_x$-co-PEGM$_{1-x}$) and its hybrid were assembled in Li symmetrical cells to examine their performance as potential solid electrolyte for Li metal batteries.

4.2. Experimental

All the experimental methods (electrolyte characterization, battery set up) are fully described in the Appendix section.

4.2.1. Materials

Poly(ethylene glycol) methyl ether methacrylate (500 g/mol) (PEGM), PEO (1.000 kg/mol), Azobis(2-methylpropionitrile) (AIBN thermal initiator, 98% purity), Benzophenone (BZ, UV initiator, 99% purity) and anhydrous acetonitrile were purchased from Sigma Aldrich. PEGM and PEGDM were further dried with 10 wt.% molecular sieves before use (4 Å, activated under vacuum for 24h at 300°C). Anhydrous acetonitrile was also dried with the same method to minimize the risk of LLZO contamination in presence of H_2O traces.

Diethyl ether (Et_2O) and methanol (MeOH) were supplied from Acros.

Lithium Bis(fluorosulfonyl)imide LiFSI salt was provided by TCI (98% purity). Before use, LiFSI was dried under vacuum at 130°C for 24h and stored in Argon glovebox. LiMTFSI single ion monomer was synthesized according to the reaction reported in Chapter 3.

Cubic Al doped $Li_{7-3x}Al_xLa_3\ Zr_2O_{12}$ (LLZO) particles were received from MSE under argon atmosphere and were used as received (99.9% purity, 400-600 nm particles size).

Li foils (120 µm thickness) were purchased from Rockwood Lithium (USA).

4.2.2. Free radical copolymerization of LiMTFSI and PEGM

A serie of poly($LiMTFSI_x$-co-$PEGM_{1-x}$) random copolymers were synthesized as illustrated in Figure 1. Desired LiMTFSI and PEGM amounts were diluted in methanol in a Schlenk tube. 2 wt.% (versus monomer weight) of thermal initiator (AIBN) was added in the reaction flask. Freeze-Vacuum-Thaw (FVT) degassing was carried out at least four times in order to remove as much as possible oxygen. Then, the reaction flask was immersed in a hot oil bath at 70°C and let for 6h. After reaction, the polymer was precipitated in cold diethyl ether. Finally, the polymer was thoroughly dried at 60 °C under high vacuum for 24 h and stored in the glovebox.

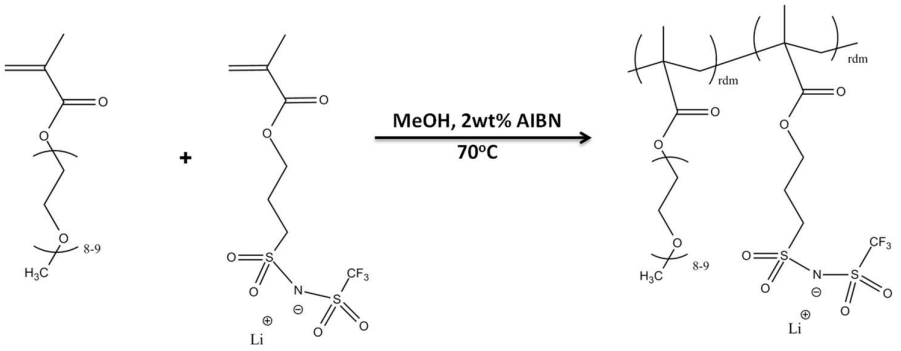

Figure 1: Synthesis of poly($LiMTFSI_x$-co-$PEGM_{1-x}$) copolymer

4.2.3. Process of pristine and hybrid PEO-poly(LiMTFSI$_x$-co-PEGM$_{1-x}$) blends

Blends were synthesized in Argon filled glovebox and polymers were carefully dried before using. Polymer blends were processed by a simple solvent casting method as reported by Olmedo-Martinez et al[8]. PEO and poly(LiMTFSI$_x$-co-PEGM$_{1-x}$) were dissolved in anhydrous acetonitrile at 10 wt.%, then mixed magnetically for 1 day to obtain a homogeneous mixture. After mixing, the solution was poured in a silicon mould et let to evaporate at room temperature in the glovebox. Additional drying under vacuum at 60°C overnight was carried out to remove traces of solvent. A serie of polymer blends with different compositions were prepared by varying the PEO/poly(LiMTFSI$_x$-co-PEGM$_{1-x}$) weight ratio such as 85/15, 70/30, 50/50, 30/70 and 25/75.

Hybrid blends were also synthesized by wet process. For preparing hybrid HSEs, appropriate amount of LLZO was added in the homogenous PEO-poly(LiMTFSI$_x$-co-PEGM$_{1-x}$) solution and the mixture was let stirring for a couple of hours. Then, the slurry was cast by tape casting or spray coating in a Teflon sheet to disperse harmoniously LLZO particles. Obtained films were dried at room temperature, followed by additional vacuum drying at 60°C.

4.2.4. UV crosslinking of pristine and hybrid PEO- poly(LiMTFSI$_x$-co-PEGM$_{1-x}$) blends

The blends were cured by UV in Argon filled glovebox. To perform UV polymerization, a UV initiator (Benzophenone) was added in PEO-poly(LiMTFSI$_x$-co-PEGM$_{1-x}$) solution. Polymer and hybrid films were prepared as explained previously. Once the films were dried, discs with a diameter of 11 mm were punched and melted on a Teflon sheet disposed on hot plate (80°C). The melted blends were then irradiated to UV light for 10 min. After UV curing, the reticulated films were hot pressed under two Teflon sheets for 5 min and let to cool down to room temperature.

4.3. Results and discussion

4.3.1. Characterization poly(LiMTFSI$_x$-co-PEGM$_{1-x}$) copolymers

Poly(LiMTFSI$_x$-co-PEGM$_{1-x}$) random copolymers were synthesized as depicted in Figure 2 by conventional free radical polymerization. By this method, statistical random copolymers are obtained when using monomers of similar reactivity as the two methacrylates involved here. Oily to gummy like materials have been obtained, which is strongly dependent on the composition (Figure 2). High LiMTFSI content in the copolymer formulation leads to gummy materials whereas high PEGM copolymers are oily as it can be seen in the pictures.

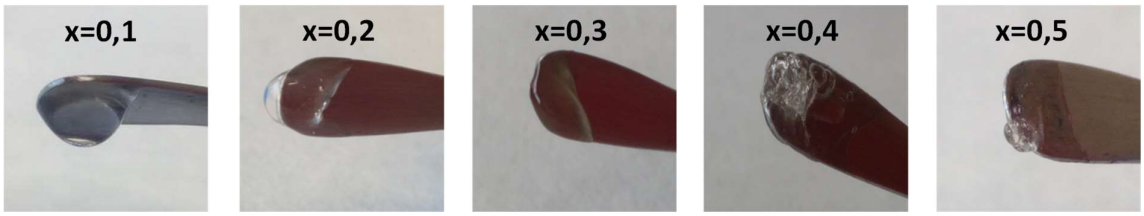

Figure 2: Pictures of poly(LiMTFSI$_x$-co-PEGM$_{1-x}$) copolymer in function of molar content x

The successful copolymer synthesis has been confirmed by ^{1}H NMR (Experimental method in Appendix A1). Figure 3 displays representative spectra before and after polymerization, associated with their chemical structures. The H signals associated with the methacrylic double bond of PEGM and LiMTFSI monomers, present at 6 and 5,8 ppm, totally disappeared after 6h. High monomer conversion (up to 98%) has been calculated for poly(LiMTFSI$_x$-co-PEGM$_{1-x}$) synthesis by integrating the remaining polymer signals. The characteristic signals of LiMTFSI and PEGM monomers can be observed in the final copolymer structure and the final composition is similar to the reaction feed due to the high reaction conversion.

Table 1 summarizes the molecular weights determined by SEC-GPC and the glass transition temperatures evaluated by DSC for the poly(LiMTFSI$_x$-co-PEGM$_{1-x}$) compositions (Experimental methods in Appendix A2 and A3). High molecular weights were obtained by free radical polymerization. It was not possible to obtain SEC-GPC results for the copolymers having higher LiMTFSI content, which is typical for ionic polymers that interact with the conventional EC-GPC columns. Large polydispersity is observed for both x=0,4 and x=0,5.

Glass transition temperature T_g is good indicator about the ionic mobility in a polymer electrolyte. Typically, lower the T_g is, faster the ionic conduction will be. Thus, DSC was then carried out to determine the glass transitions temperatures of the serie poly(LiMTFSI$_x$-co-PEGM$_{1-x}$). Figure 4 displays the DSC traces and Table 1 summarizes the results. The T_g shows a typical trend which follows Fox equation: in other words, the glass transition of random copolymers is an intermediate of the homopolymers. Due to this tendency, the copolymer with

the lowest ratio of LiMTFSI (x=0,1) shows the lowest glass transition (-57°C) whereas the one with the highest ratio (x=0,5) presents the highest T_g (-20°C).

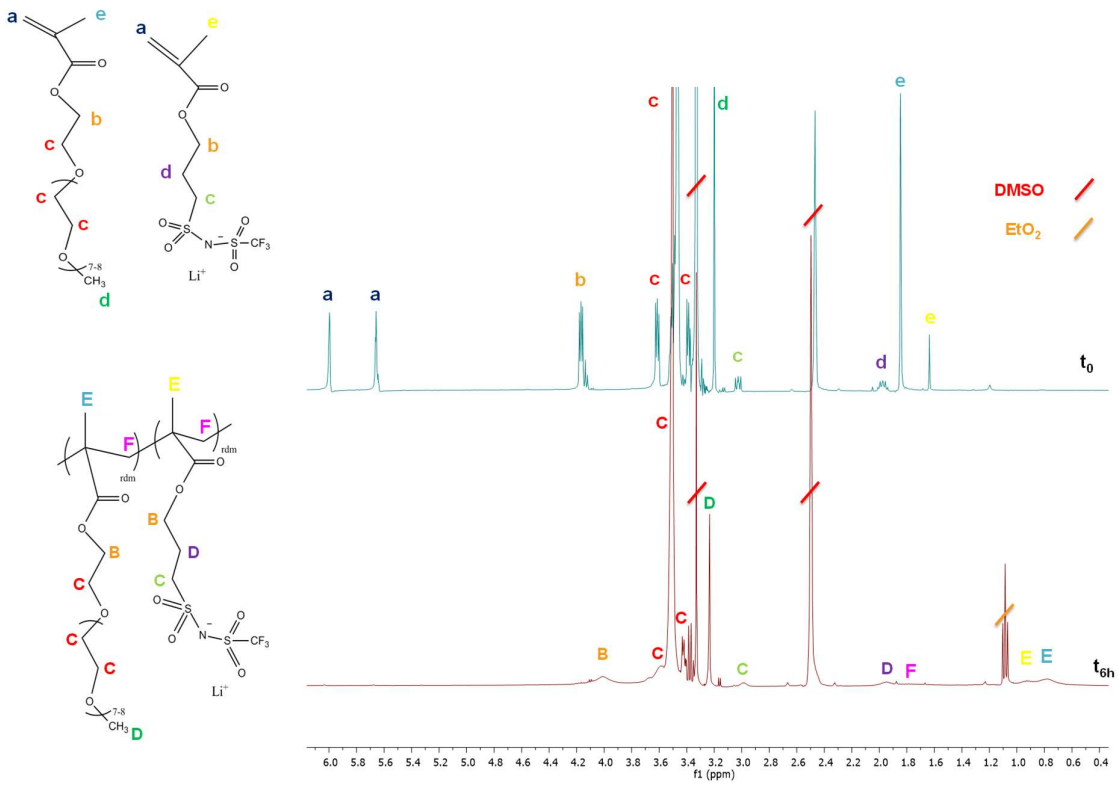

Figure 3: Representative ^{1}H NMR spectrum for poly(LiMTFSI$_{0,2}$-co-PEGM$_{0,8}$) electrolyte synthesized by free radical copolymerization.

Table 1. Molar masses and glass transition temperatures T_g of poly(LiMTFSI$_x$-co-PEGM$_{1-x}$) copolymers

LiMTFSI$_x$-PEGM$_{1-x}$	M_n (g.mol^{-1})	PDI	Tg (°C)
x=0,5	108 500	5,1	-20
x=0,4	287 100	3,6	-36,9
x=0,3	-	-	-40,7
x=0,2	-	-	-58,6
x=0,1	-	-	-57
poly(LiMTFSI)[10]	52 700	1,16	95
poly(PEGM)[10]	23 600	1,2-	-62

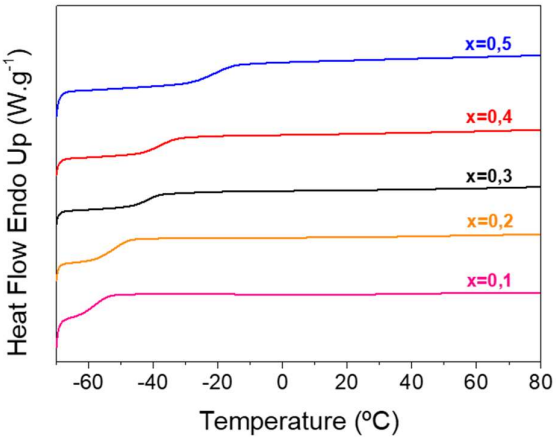

Figure 4: DSC traces of poly(LiMTFSI$_x$-co-PEGM$_{1-x}$) copolymers

Electrochemical Impedance Spectroscopy (EIS) was carried out in order to measure the ionic conductivity of the random copolymers (Experimental method in Appendix B1). Ionic conductivity follows an Arrhenius law as it is depicted in Figure 5, which confirms the amorphous nature of the single ion copolymers. As expected from its highest T_g value, poly(LiMTFSI$_{0,5}$-co-PEGM$_{0,5}$) composition has the lower ionic conductivity at room temperature (σ= 2,4.10^{-8} S/cm). The ionic conductivity keeps rising while LiMTFSI content is going down. A maximum is obtained for poly(LiMTFSI$_{0,2}$-co-PEGM$_{0,8}$), achieving up 6.10^{-6} S/cm at 25°C. This value is higher than block copolymers reported by Porcarelli and co-workers[10]. The ionic conductivity starts decreasing for the lowest LiMTFSI content (x=0,1), likely because of the low lithium concentration in the electrolyte. Thereby, poly(LiMTFSI$_{0,2}$-co-PEGM$_{0,8}$) copolymer was the first choice to prepare the blend with PEO. To better apprehend the effect of LiMTFSI composition on PEO's crystallinity, poly(LiMTFSI$_{0,5}$-co-PEGM$_{0,5}$) copolymer was also selected to prepare the blends.

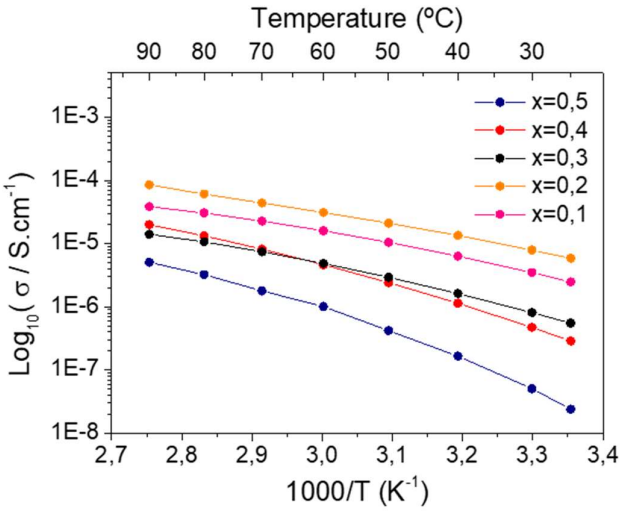

Figure 5: Arrhenius plot of poly(LiMTFSI$_x$-co-PEGM$_{1-x}$) compositions

4.3.2. Physicochemical characterization and ionic conductivity study of PEO-poly(LiMTFSI$_x$-co-PEGM$_{1-x}$) blends

Polymer blends based on the previously described copolymers and PEO with different ratios were prepared. Figure 6 displays the images of the blend electrolytes. Distinct aspects and mechanical properties can be noticed for the blends based on poly(LiMTFSI$_{0,2}$-co-PEGM$_{0,8}$) and poly(LiMTFSI$_{0,5}$-co-PEGM$_{0,5}$) copolymers. These blend series are going to be named later on as **Li$_x$BL**, x corresponding to the molar content of LiMTFSI in the copolymer formulation. Accordingly, **Li$_{0,2}$BL** and **Li$_{0,5}$BL** are the blend series based on poly(LiMTFSI$_{0,2}$-co-PEGM$_{0,8}$) and poly(LiMTFSI$_{0,5}$-co-PEGM$_{0,5}$) copolymers respectively. For each serie, PEO content was varied from 85, 70, 50, 30 and 25 wt.%. Regardless of Li$_x$BL, the film flexibility improves while decreasing PEO content. Rigid and opaque blends are achieved for highest compositions of PEO, whereas soft and translucent materials are realized for the lowest PEO content. This discrepancy can be likely explicated by the degree of crystallinity of the blends. For Li$_{0,2}$BL serie, self-standing films are obtained up to 30wt.% of PEO; above, gel type materials were observed. On the opposite, better mechanical integrity is reached for Li$_{0,5}$BL serie, even with 25wt.% of PEO.

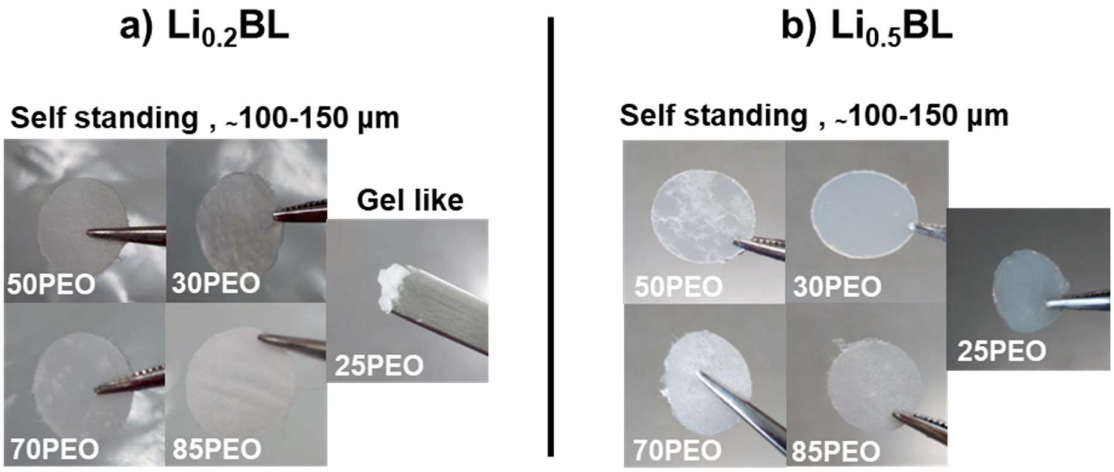

Figure 6: Film aspects of Li$_{0,2}$BL and Li$_{0,5}$BL series depending on PEO content (wt.%)

Thermal properties of Li$_{0,2}$BL and Li$_{0,5}$BL series were evaluated by DSC (Experimental method in Appendix A3). Evolution of DSC traces depending on PEO content can be seen in Figure 7.a. and Figure 7.b. For each Li$_x$BL, PEO's crystallinity continues to decrease while copolymer content rises in the blend formulation. This is confirmed by the reduced area of the endothermic melting transition peaks. Compared to previously reported PEO-poly(LiMTFSI) blends, these transitions look to be composed of two overlapped peaks, suggesting two kinds of PEO crystals within the blends. This difference can be interpretated as different environments for PEO chains in presence of LiMTFSI and PEGM moieties.

Characteristic thermal transition temperatures (T_g and T_m) were determined and compiled in Table 2 and Table 3. From 66ºC (pure PEO films), T_m drops to 48,8ºC and 50,83ºC for $Li_{0,2}$BL and $Li_{0,5}$BL respectively, at the lowest PEO content. This evolution further confirms the amorphization of PEO phases. The degree of crystallinity X_c was calculated for each blend composition and reported in Table 2 and Table 3. X_c is determined to be 56% and 4% for $Li_{0,2}$BL and $Li_{0,5}$BL respectively, at 25wt.% of PEO. In comparison, pure PEO films were evaluated to have X_c=60%. The high X_c observed for $Li_{0,2}$BL is quite surprising. This discrepancy must be explained by the low LiMTFSI content compared to $Li_{0,5}$BL, as Olmedo-Martinez & al previously described that PEO complexation with LiMTFSI was responsible of its crystallinity decrease[8].

For both Li_xBL series, one T_g is detected by DSC, implying that the copolymer and PEO are miscible. For $Li_{0,2}$BL compositions, T_g drops from -55.12ºC to -58ºC, which suggests higher chain mobility (T_g of PEO=-49.8ºC). PEGM moiety of the copolymer must plasticize PEO crystalline phases. On the other hand, the T_g of $Li_{0,5}$BL films are bigger but tend to go down with the addition of copolymer, from -10,5ºC to -40ºC for the lowest PEO content.

Table 2. Summary of thermal and electrochemical properties of $Li_{0,2}$BL material serie

$Li_{0.2}$BL with y= PEO content (wt.%)	T_m (°C)	T_g (°C)	X_c (%)	$\sigma_{25°C}$ (S/cm)	$\sigma_{60°C}$ (S/cm)
y=0	-	-51,53	-	6.10^{-6}	3.10^{-5}
y=25	48,88	-58	55,88	2.10^{-6}	4.10^{-5}
y=30	53,46	-52,66	56,39	$1,6.10^{-6}$	$3,7.10^{-5}$
y=50	56,43	-53,2	57	$6,4.10^{-7}$	$2,9.10^{-5}$
y=70	61,75	-54,42	57,88	5.10^{-7}	$1,5.10^{-5}$
y=85	61,54	-55,12	60,64	4.10^{-7}	6.10^{-6}
y=100 (pure PEO film)	65,63	-49,77	60,79	-	-

Table 3. Summary of thermal and electrochemical properties of $Li_{0,5}$BL material serie

$Li_{0.5}$BL with y= PEO content (wt.%)	T_m (°C)	T_g (°C)	X_c (%)	$\sigma_{25°C}$ (S/cm)	$\sigma_{60°C}$ (S/cm)
y=0	-	-20	-	$2,4.10^{-8}$	1.10^{-6}
y=25	50,83	-40,06	3,68	$2,3.10^{-9}$	9.10^{-6}
y=30	50,65	-42,38	48,96	$4,4.10^{-9}$	$6,5.10^{-6}$
y=50	58,33	-27,35	51,72	$8,8.10^{-10}$	7.10^{-6}
y=70	61,42	-22,1	58,6	$4,8.10^{-10}$	1.10^{-6}
y=85	61,44	-10,5	59	$3,7.10^{-10}$	6.10^{-7}

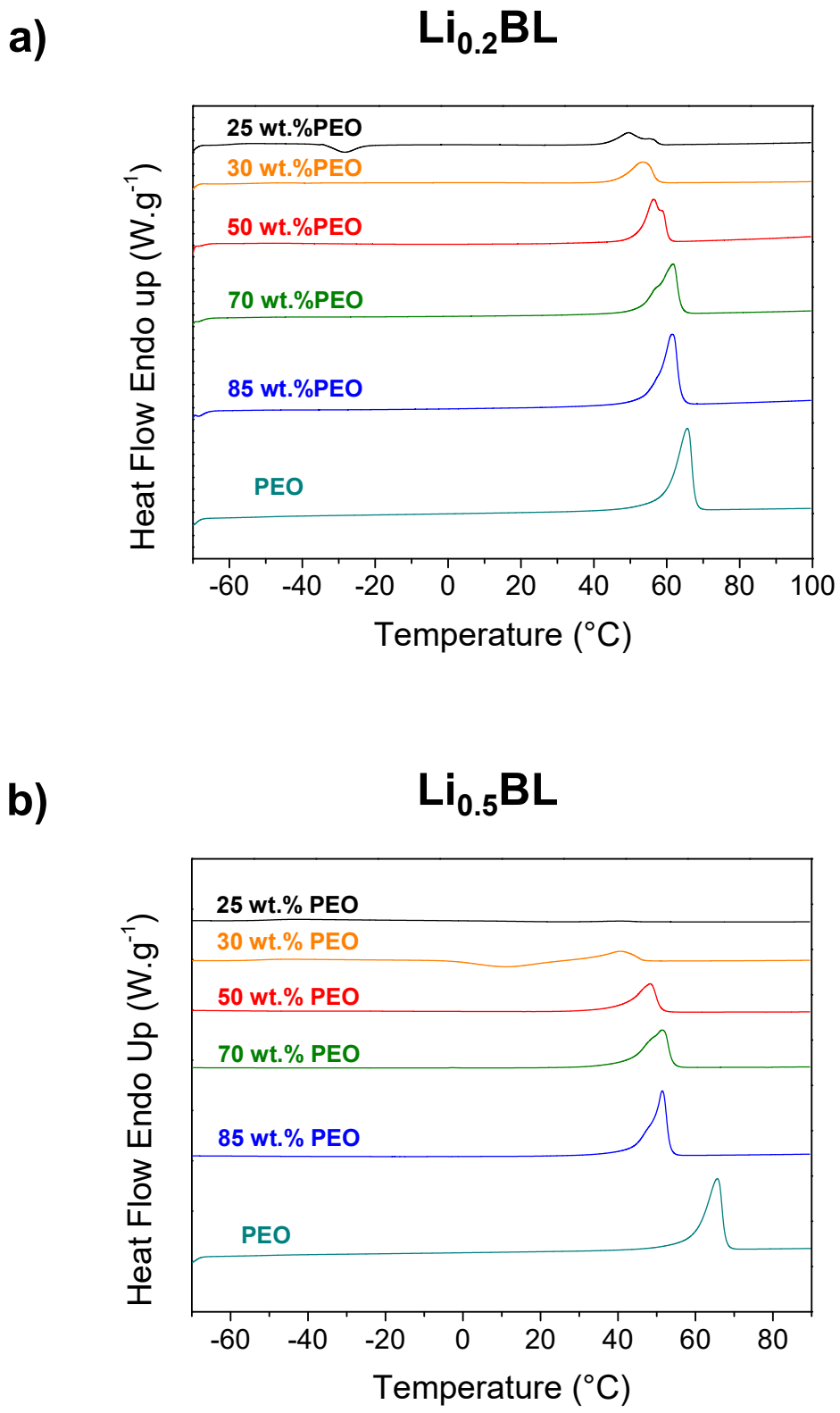

Figure 7: Thermal characterization (DSC traces) of a) $Li_{0,2}BL$, b) $Li_{0,5}BL$ series

Ionic conductivities of $Li_{0,2}$BL and $Li_{0,5}$BL series were assessed by EIS (Experimental method in Appendix B1). Figure 8 displays their evolution as function of the temperature and PEO content and are compared to poly(LiMTFSI$_x$-co-PEGM$_{1-x}$) copolymers. As Li_xBL are semi-crystalline, the ionic conduction follows a Vogel-Tamman-Fulcher (VTF) tendency, with an inflexion point situated around 60°C. This temperature corresponds to the melting transition of PEO phases. The ionic conductivity is badly affected for high PEO compositions, whichever poly(LiMTFSI$_x$-co-PEGM$_{1-x}$) copolymer used. Nevertheless, the ionic conductivity continues to increase while the copolymer composition rises in the blend formulation. The biggest improvement is observed for $Li_{0,5}$BL, which outreaches the copolymer's ionic conductivity up to 50ºC, starting at 30 wt.% of PEO (Figure 8.a). On the other hand, at the lowest PEO content (25 wt.%), $Li_{0,2}$BL displays faster ionic conduction than $Li_{0,5}$BL despite its superior crystallinity (Figure 8.a). At room temperature, $1,3.10^{-6}$ and $4,4.10^{-9}$ S/cm are estimated for $Li_{0,2}$BL and $Li_{0,5}$BL respectively.

In comparison to $Li_{0,2}$BL, similar value was reported by Olmedo-Martinez and co-workers for low molecular weight p(LiMTFSI) (5,000 g.mol^{-1}). In their study, the ionic conductivity starts to go down when high molecular weight p(LiMTFSI) is blended with PEO (superior to 50,000 g.mol^{-1}), despite of complete inhibition of PEO's crystallinity. The low conductivity obtained for $Li_{0,5}$BL likely comes from the presence of strong ionic clusters which impedes fast Li ion mobility at room temperature, in spite of its nearly amorphic nature[13]. However, acceptable ionic conductivities of 4.10^{-5} and $9,3.10^{-6}$ S/cm at 60ºC were measured for $Li_{0,2}$BL and $Li_{0,5}$BL respectively.

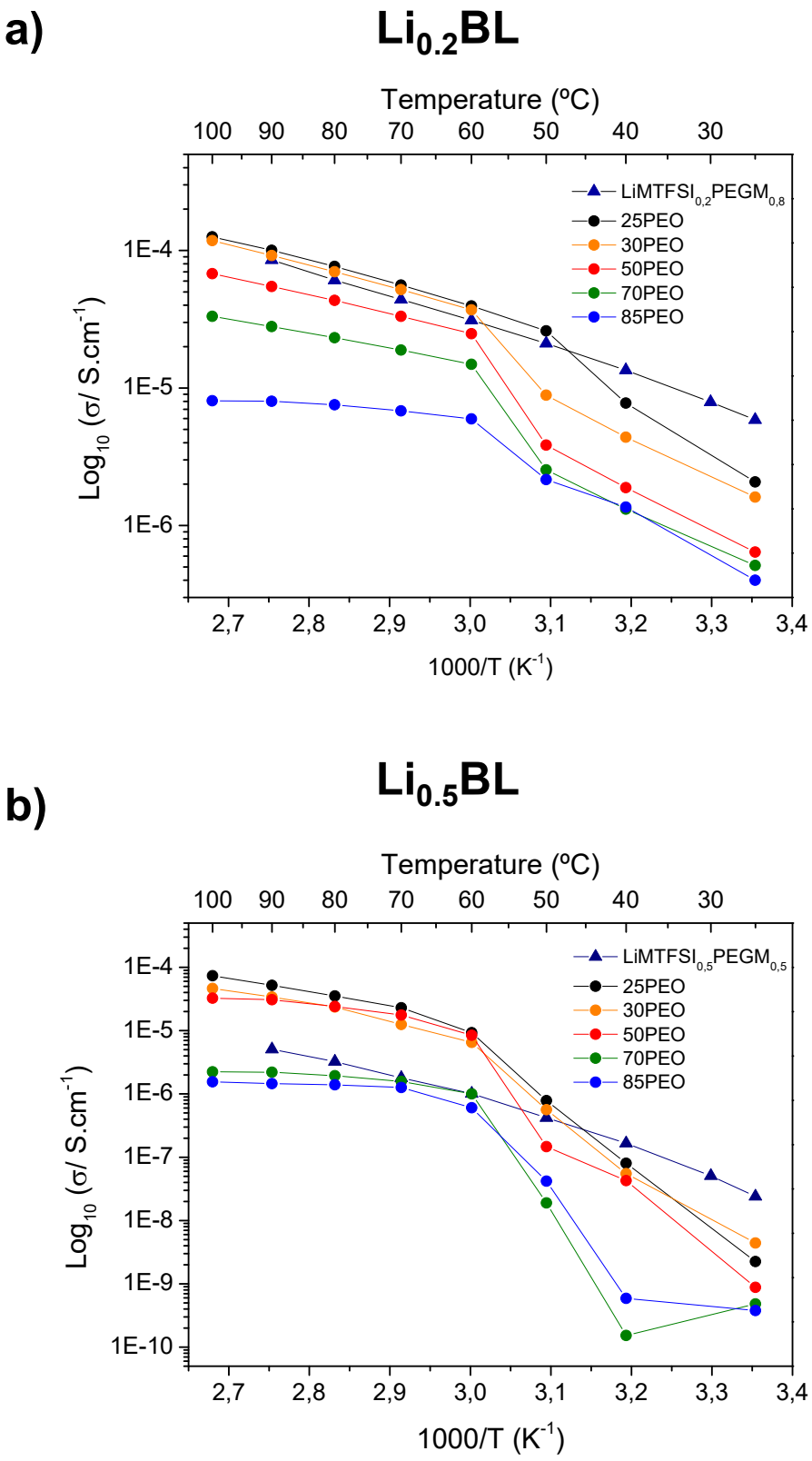

Figure 8: VTF plots for a) $Li_{0,2}BL$, b) $Li_{0,5}BL$ series

In a view of getting the best compromise between mechanical stability and ionic conductivity, Li_xBL formulation was fixed for the rest of this study to **30 wt.% PEO- 70wt.% poly(LiMTFSI$_x$-co-PEGM$_{1-x}$)**. To ascertain the relationship between Li_xBL crystallinity and LiMTFSI content, random free p(LiMTFSI) has been mixed with 30 wt.% of PEO to compare the evolution of the ionic conductivity (Figure 9). Unlike previous Li_xBL series, Li_1BL has an Arrhenius trend, implying that the blend is almost totally amorphous at room temperature. However, its ionic conductivity is extremely low compared to others blends, even at high temperatures. This tendency proves that blend's crystallinity is directly linked to LiMTFSI composition and explains why $Li_{0,2}BL$ has the highest X_c. On the other hand, high salt concentration in the blend leads to low ionic conductivity. This highlights the complementarity effect of PEGM and LiMTFSI moieties on the ionic conduction of the blend, by plasticizing effect or by ionic complexation with PEO. That is the reason why $Li_{0,2}BL$ achieves higher ionic conductivity than its counterparts $Li_{0,5}BL$ and Li_1BL.

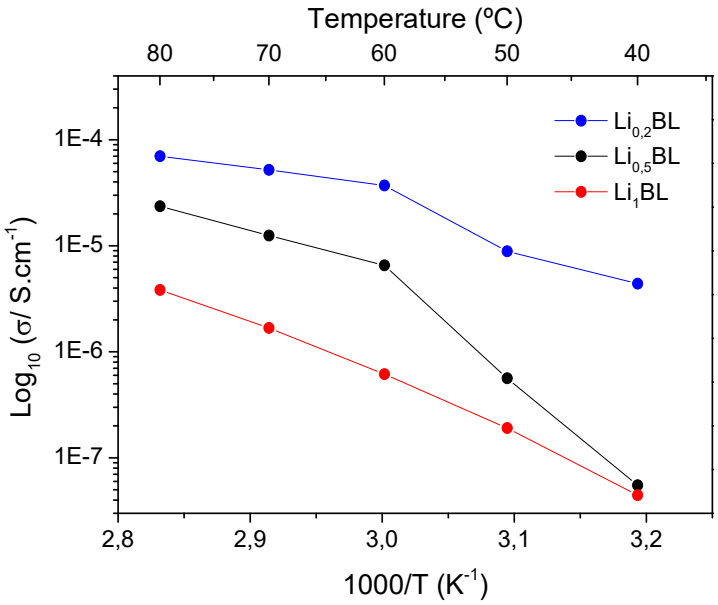

Figure 9: VTF plots of Li_xBL (x=0,2;0,5;1) at fixed PEO content (30wt.%)

To further confirm this hypothesis, ATR-FTIR was conducted on these blends to observe the complexation of PEO phase with LiMTFSI moiety (Experimental method in Appendix A1). As a matter of fact, the presence of interactions tends to broaden and decrease the bands intensity of involved vibration modes. Figure 10 shows the spectrum of pure PEO, along with its characteristic bands. Noteworthy vibrations to pay attention to are the band 3 and 5, as they are greatly sensible to PEO's crystallinity[14]. CH_2 bending mode tends to form a single band at 1350 cm^{-1} once PEO becomes amorphous. In addition, C-O-C stretching mode band at 1149 cm^{-1} totally disappears for amorphous PEO. Table 4 summarizes the bands to observe in order to conclude about PEO's crystallinity in the blends.

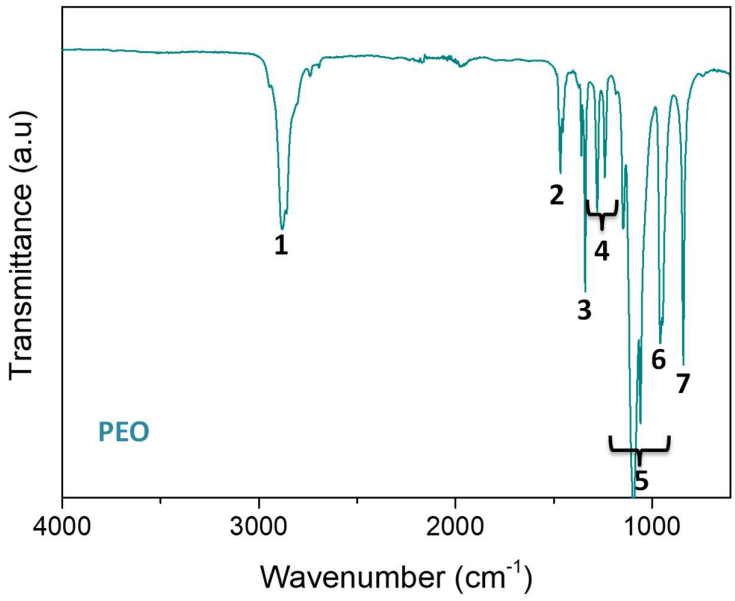

Figure 10: Representative ATR-FTIR spectrum of a pure PEO film

Table 4. Indexation of bands in Figure 10

Bands	ATR-FTIR vibrations	Wavenumber
1	CH_2 symmetric stretching	2880 cm^{-1}
2	CH_2 scissoring	1474 cm^{-1}
3	CH_2 bending	1360 & 1343 cm^{-1}
4	s+as CH_2 twisting	1279 & 1240 cm^{-1}
5	C-O-C stretching	1149, 1110 & 1061 cm^{-1}
6	CH_2 twisting	963 cm^{-1}
7	CH_2 wagging	842 cm^{-1}

Figure 11 compares ATR-FTIR spectra of pure PEO and Li_xBL (x=0,2;0,5 and 1). Black lines highlight the modifications of the characteristic bands of PEO once it is blended with the poly($LiMTFSI_x$-co-$PEGM_{1-x}$) copolymer. Complexation between ether oxygen of PEO and LiMTFSI happens in the blends as Li_1BL presents the bigger modifications in all CH_2 and C-O-C modes of PEO. Higher concentration of LiMTFSI leads to a decrease of intensity and broadening of the bands. Especially, modes related to PEO's crystallinity (1360, 1343 and 1149 cm^{-1}) completely disappear once poly(LiMTFSI) is mixed with PEO. $Li_{0,2}BL$ and $Li_{0,5}BL$ show slight changes, due to the lower LiMTFSI concentration. In addition, PEGM moieties have similar structure to PEO and their bands tend to overlap the concerned modes. Nevertheless, most of the bands related to PEO tend to broaden and are smaller. This proves that PEO amorphization is linked to its interaction with LiMTFSI and this explains the different properties obtained for the Li_xBL electrolytes.

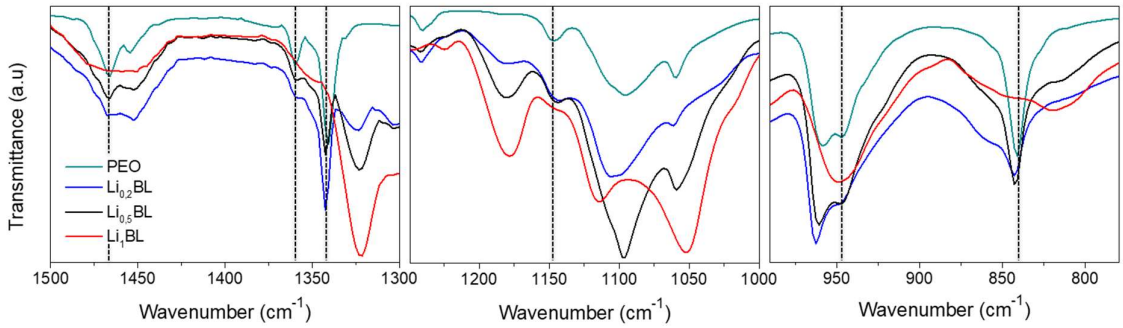

Figure 11: Comparison of ATR-FTIR spectra of pure PEO and Li_xBL (x=0,2;0,5;1)

To conclude, LiMTFSI interaction with PEO is a key parameter to reduce the blend crystallinity. Nevertheless, blends-based poly(LiMTFSI) homopolymer show low ionic conductivity due to their high salt concentration. The use of the copolymer is strongly beneficial as it acts as Li ion source and plasticizer at the same time. However, remaining crystalline PEO phases at low temperatures impedes to use these materials for practical applications. Above 60ºC, acceptable ionic conductivity can be reached but blends do not have any mechanical integrity.

4.3.3. UV crosslinking of the Li_xBL blends

UV crosslinking of PEO can be a promising compromise in order to obtain optimal electrochemical and mechanical properties[15,16]. Under irradiation, benzophenone UV initiator reacts with ethylene chains, generating unstable macro-radicals. These radicals can recombine once they meet, forming a 3D network. Crosslinked PEO matrices are reported to be totally amorphous, achieving superior ionic conductivity at room temperature. Thanks to PEO crosslinking, plasticizers such as glymes or ionic liquids can be added without compromising the mechanical stability of the electrolyte. For this reason, PEO crosslinking was carried out into our blends by addition of benzophenone and UV irradiation of cast Li_xBL films. Transparent and highly stretchable materials, later on named as **CLi_xBL**, then were obtained (Figure 12.b).

Ionic conductivities of crosslinked CLi_xBL and unreticulated Li_xBL electrolytes are compared in Figure 12.a (Experimental method in Appendix B1). For both CLi_xBL series, the ionic conductivity is enhanced below 60ºC. Nonetheless, the two curves still exhibit a VTF type behaviour, which signifies that unreticulated PEO remains. In the case of $CLi_{0,2}BL$, the ionic conductivity is slightly improved at low temperatures (σ=2,6.10^{-6} instead of 1,3.10^{-6} S/cm at 25°C). PEGM comonomer units, which are also composed of ethylene oxide units, may also participate in the PEO crosslinking. This can explain why no improvement is observed at high temperatures, as PEGM mobility is reduced. On the opposite, the most considerable change is noted for $CLi_{0,5}$ BL, in the whole range of temperatures. The ionic conductivity at room temperature is still limited (6.10^{-7} S/cm) but this electrolyte achieves high conductivity at mild temperatures (up to 2.10^{-4} S/cm at 60ºC).

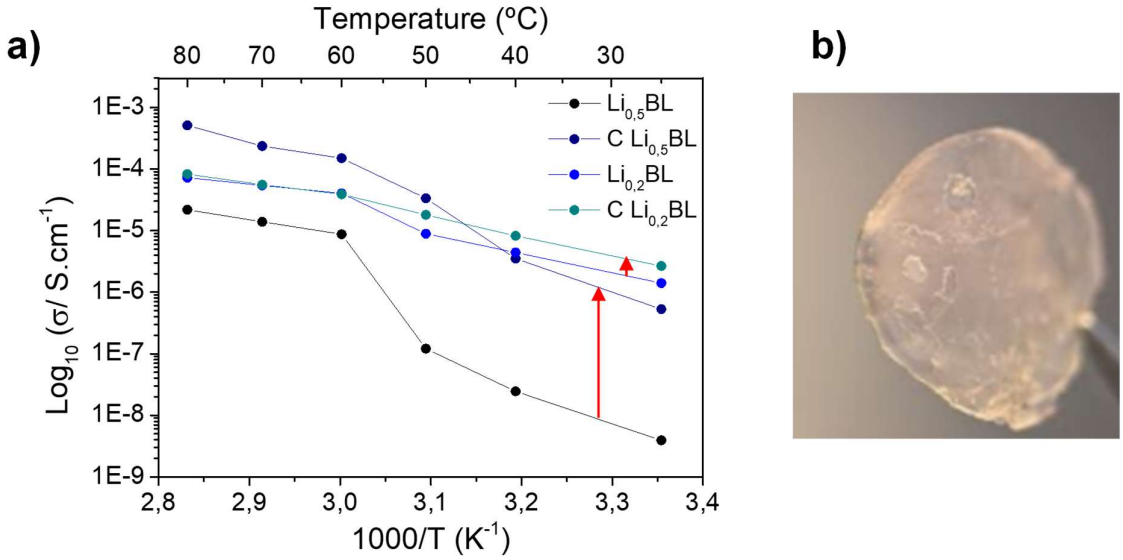

Figure 12: a) Arrhenius plot of crosslinked CLi_xBL and no crosslinked Li_xBL electrolytes, b) Picture of a $CLi_{0.5}BL$ membrane after irradiation.

XRD measurements were undertaken to verify the crosslinking efficiency of PEO component in the blends. The resulted diffractograms are shown in Figure 13. Crystalline peaks of PEO are located at 19° and 23° [17]. Firstly, blank PEO is strongly amorphized thanks to the addition of the copolymer, whichever its LiMTFSI composition. However, crosslinked CLi_xBL present distinct diffractograms. PEO's crystallinity is highly inhibited for $CLi_{0,5}BL$, crystalline peaks can be hardly distinguished (Figure 13.a). On the other hand, $CLi_{0,2}BL$ displays almost no change compared to the unreticulated blend, minor intensity decrease and broadness of the peaks can be only observed in Figure 13.b. This explains the poor improvement of ionic conductivity observed for $CLi_{0,2}BL$ compared to $CLi_{0,5}BL$.

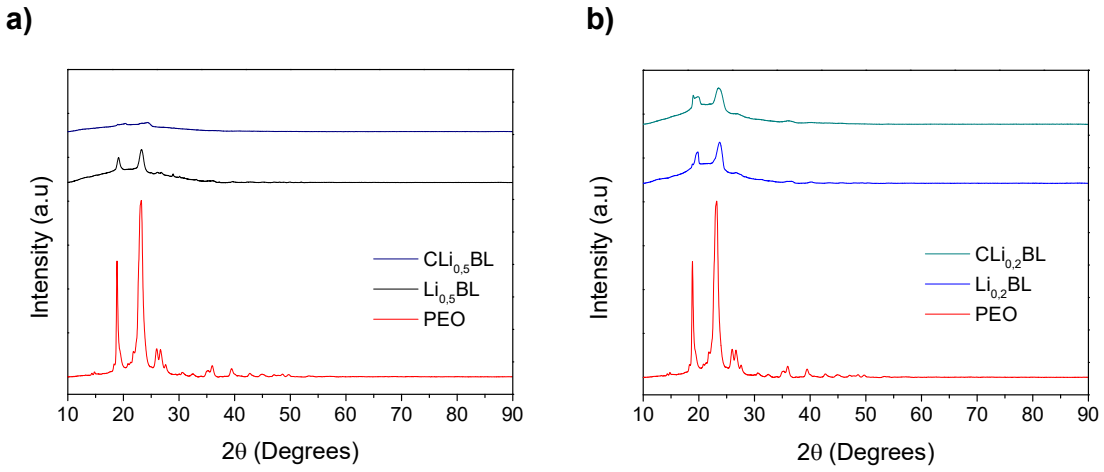

Figure 13: Comparison of XRD diffractograms of PEO, Li_xBL and CLi_xBL: a) x=0,5; b) x=0,2

To conclude this section, UV curing of PEO seems an efficient method to amorphize the blends, at the condition to use high LiMTFSI content in the copolymer formulation. Additional improvement is the use of active inorganic particles such as LLZO which can both affect left crystalline PEO and improve ionic dissociation in the blends. Hybrid electrolytes based on $Li_{0,5}BL$ and $CLi_{0,5}BL$ were then studied.

4.3.4. Physicochemical characterization of HSE and ionic conductivity study of crosslinked polymer and hybrid PEO-($LiMTFSI_x$-co-$PEGM_{1-x}$) blends

The HSEs were prepared by wet mixing of the three components (copolymer, PEO and LLZO). A focus on the particles stability towards the solvent used for the HSE film process is mandatory. Acetonitrile was chosen as solvent for the preparation of the polymer blends as it has an excellent chemical stability towards LLZO. In spite of being anhydrous, acetonitrile may have some traces of water which can contaminate the particles[18]. If they are exposed to H_2O impurities, Li^+/H^+ exchange occurs at the particle surface as it follows[19]:

$$Li_7La_3Zr_2O_{12} + xH_2O \rightarrow Li_{7-x}H_xLa_3Zr_2O_{12} + xLiOH$$

In presence of CO_2 traces, it can further react as:

$$LiOH + ½\ CO_2 \rightarrow ½\ Li_2CO_3 + ½\ H_2O$$

Formation of Li_2CO_3 needs to be limited, as it affects badly LLZO's ionic conductivity. In addition, it has been confirmed that Li_2CO_3 contamination can be at the origin of dendrites formation in sintered LLZO pellets[19]. Its prevention within LLZO solid electrolyte improves its critical current density, from 0,1 to 0,5 $mA.cm^{-2}$.

To verify the formation of Li_2CO_3 phase, pH determination and ATR-FTIR measurements were carried out. The first method consists of confirming the presence of LiOH induced by Li^+/H^+ exchange with water. For this purpose, LLZO particles were dispersed with the polymers in two acetonitrile solvents, one used as received and one dried beforehand in molecular sieves for several weeks (called SD). Only from the non-treated acetonitrile dispersions, basic pH was detected by pH paper (10). ATR-FTIR allows to detect Li_2CO_3 phase and reacted protons in the garnet structure[20]. Table 5 summarizes their related bands. Hybrid films made from the untreated and home dried solvents were used for comparison. The spectra are shown in Figure 14. Reacted water can be noticed at 3545 cm^{-1} (exchanged protons) and 1615 cm^{-1}, which can be clearly distinguished for the sample processed with no treated acetonitrile. Li_2CO_3 characteristic modes are located at 1508, 1443 and 865 cm^{1}. Appearance of big bands in the 1500-1400 wavenumber region removes any doubt about LLZO contamination by water traces when acetonitrile is not further dried in molecular sieves. Li_2CO_3 formation is highly limited once the hybrid film is processed with the SD solvent. Only a small shoulder at 865 cm^{-1} can suggest potential water contamination. Despite its easiness and process efficiency, solvent casting is not recommended for hybrid LLZO polymers electrolytes[21]. Solid state film processes, such as hot pressing or blending with the help of torque rheometer, are more appropriate to limit the presence of water. Nonetheless, thanks to

the adequate drying of acetonitrile, extremely dried hybrid films were obtained with preserved LLZO particles.

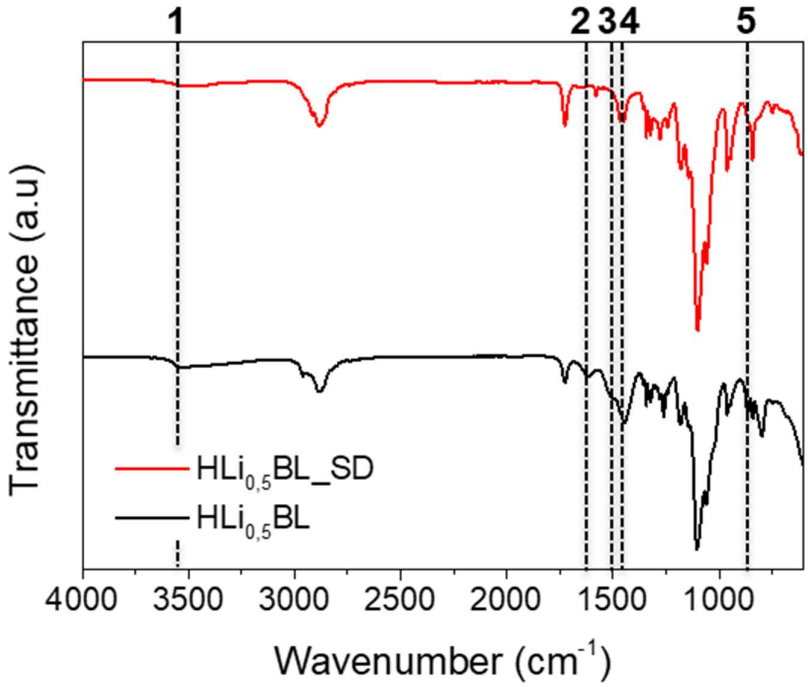

Figure 14: Comparison of ATR-FTIR spectra of hybrid $Li_{0.5}BL$ (25 wt.% LLZO) processed with no treated and home dried (SD) solvents.

Table 5. Indexation of bands in Figure 14

Bands	ATR-FTIR vibrations	Wavenumber
1	Li^+/H^+ exchange	3545 cm^{-1}
2	H-O from H_2O impurities	1615 cm^{-1}
3	Li_2CO_3	1508 cm^{-1}
4		1443 cm^{-1}
5		865 cm^{-1}

The preparation of the HSE based on $Li_{0,5}BL$ was conducted by two methods, doctor blade and spray coating, so as to elect the best technique to process the hybrid films. LLZO tends to agglomerate easily in acetonitrile, stable dispersions are then challenging to be obtained. Besides, low viscosity of polymer solutions (10 wt.% in acetonitrile) does not prevent particles' sedimentation during the film drying. It was then necessary to examine the LLZO dispersion within the hybrid electrolytes. Figure 15 exhibits the SEM pictures of cast and spray coated hybrid films containing 25 wt.% LLZO, taken at their top and bottom faces (Experimental method in Appendix A5).

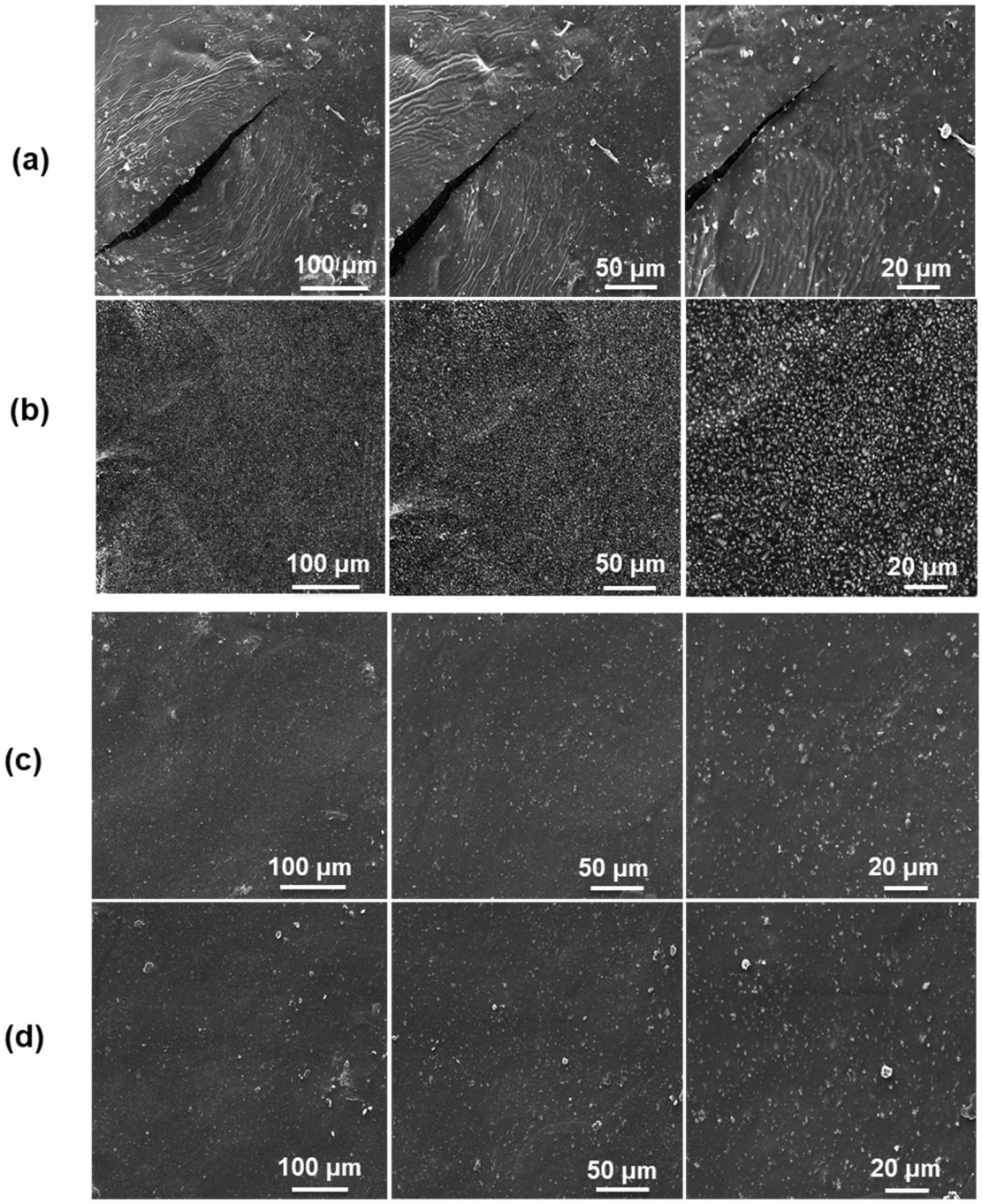

Figure 15: SEM pictures of the hybrid electrolyte with 25 wt.% LLZO processed by doctor blade a) top part and b) bottom part; by spray coating c) top part and d) bottom part.

The film processed by doctor blade shows high agglomeration of particles. Mostly polymer phase is noticed on the top face (Figure 15.a) whereas mainly LLZO are seen on the down face Figure 15.b). The film is extremely brittle when cut with liquid N_2 (fracture appearing on the top) because of the poor LLZO dispersion. On the opposite, spray coating is highly effective to disperse LLZO particles within the blend. Almost no differences between the top and bottom faces can be distinguished (Figure 15.c and Figure 15.d). LLZO particles are completely embedded by the polymer phase and no aggregates can be noticed. Spray coating was then chosen to process the hybrid films. x is defined as LLZO content in wt.% and hybrids are named **$HLi_{0,5}BL$-x**.

Films with low, intermediate and high LLZO compositions (x=10,25 and 50) were synthesized as shown in Figure 16. These materials are extremely thin thanks to spray coating (below 200 µm). No change of colour was noticed for the stored hybrid electrolytes, which implies that no or minimal contamination of LLZO happens. $HLi_{0,5}BL$-10 is fragile (Figure 16. a) while $HLi_{0,5}BL$-50 is rigid and self-standing (Figure 16.c). $HLi_{0,5}BL$-25 looks to have intermediate mechanical properties but can withstand deformation without being torn.

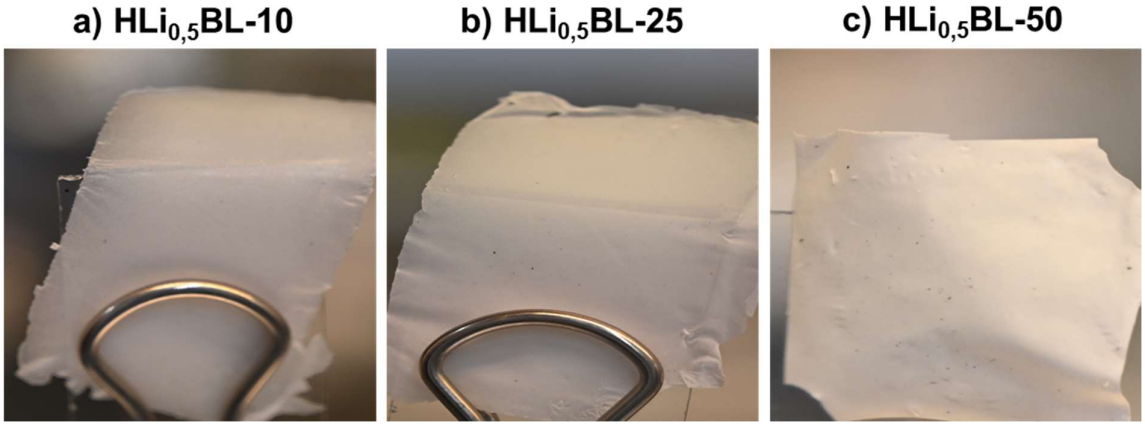

Figure 16: Images of $HLi_{0,5}BL$-x hybrid polymer electrolytes depending on x= LLZO in wt.%

The first step was to investigate the effect of LLZO on the ionic conductivity of unreticulated $Li_{0,5}BL$ blend matrix. It was also coupled to XRD to evaluate how PEO's crystallinity is affected by the addition of particles. Figure 17 summarizes these results. $HLi_{0,5}BL$-x electrolytes follow the VTF trend. After adding the inorganic particles, the ionic conductivity can be enhanced slightly below 60ºC up to 25 wt.% LLZO (Figure 17.a). From 4.10^{-9} S/cm, it reaches 8.10^{-9} S/cm at room temperature. At higher composition (50wt.%), the conductivity starts to go down. This tendency has been already reported for PEO-LiTFSI-LLZO systems with high particles content[22,23]. If no percolation threshold is achieved, the Li ion motion occurs in the polymer phase. Nevertheless, the polymer is highly confined due to large presence of the inorganic particles, which hinders fast ionic conduction. LLZO looks to inhibit PEO's crystallinity since its crystalline peaks at 19° and 23° almost completely disappear for $HLi_{0,5}BL$-25 electrolyte (Figure 17.b). Above 60°C, once left crystalline PEO melt, the pristine $Li_{0,5}BL$ polymer electrolyte displays superior ionic conductivity than its hybrid counterparts. For x superior to 10 wt.%, the ionic conduction is dropping in the high temperature range. LLZO appears to be an obstacle

to Li motion in the polymer phase. To summarize, the particles look to be beneficial below 60°C as they can amorphize the blend.

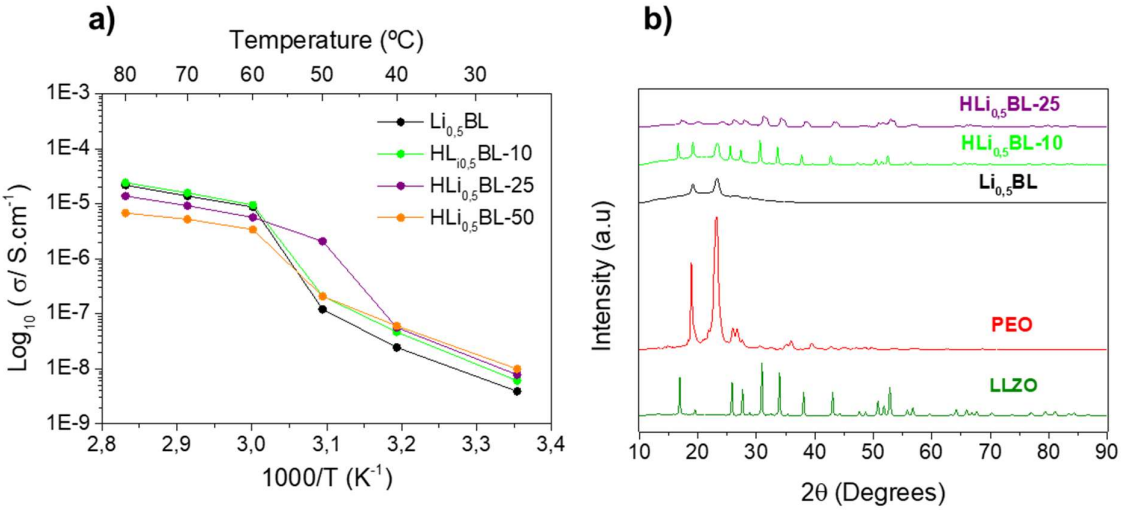

Figure 17: Characterization hybrid $HLi_{0.5}BL$-x polymer electrolytes by a) EIS; b) XRD

$HLi_{0,5}BL$-25 composition was kept for UV crosslinking and is going to be called as **$HCLi_{0,5}BL$-25**. The aim was to observe if the ionic conductivity of the hybrid can be further improved at low and mild temperatures. After UV curing, the electrolyte gains in flexibility and is a truly self-standing film as it is shown in Figure 18.a. EIS coupled with XRD were carried out (Figure 18.b and Figure 18.c). The ionic conductivity of $HCLi_{0,5}BL$-25 is one-fold bigger than unreticulated hybrid. Surprisingly, the electrolyte follows a VFT law. Its XRD diffractogram is very similar to $HLi_{0,5}BL$-25, suggesting no big improvement in term of PEO's amorphization. Nevertheless, the hybrid present lower performance in the whole temperature range when compared to the crosslinked polymer matrix $CLi_{0,5}BL$. The hybrid outreaches 10^{-5} S/cm at 60ºC whereas the pristine blend achieves 10^{-4} S/cm.

The discrepancies between the not crosslinked and crosslinked hybrids can be interpreted by two manners. Firstly, LLZO particles can inhibit PEO's crystallinity, which enhances the ionic motion in the polymer phase. Finally, LLZO can help to dissociate the ionic aggregates: in other words, the undissociated salt due to high LiMTFSI content. Experimental evidences of strong interactions between LLZO particles and immobilized anionic moieties from single ion polymers were reported in the literature and attested in our project (Chapter 3). By interacting with tethered anions, LLZO can free the Li ions, which can complex with the PEO phase. The drop of crystallinity in $HLi_{0,5}BL$-x blends is then not fully related to the increase of disorder in the polymer phase. That may be the reason why the ionic conductivity increases for $HLi_{0,5}BL$-10 composition, where the crystalline PEO phase is poorly affected by the low LLZO content. To verify this last hypothesis, ATR-FTIR was conducted on $HLi_{0,5}BL$-x compositions.

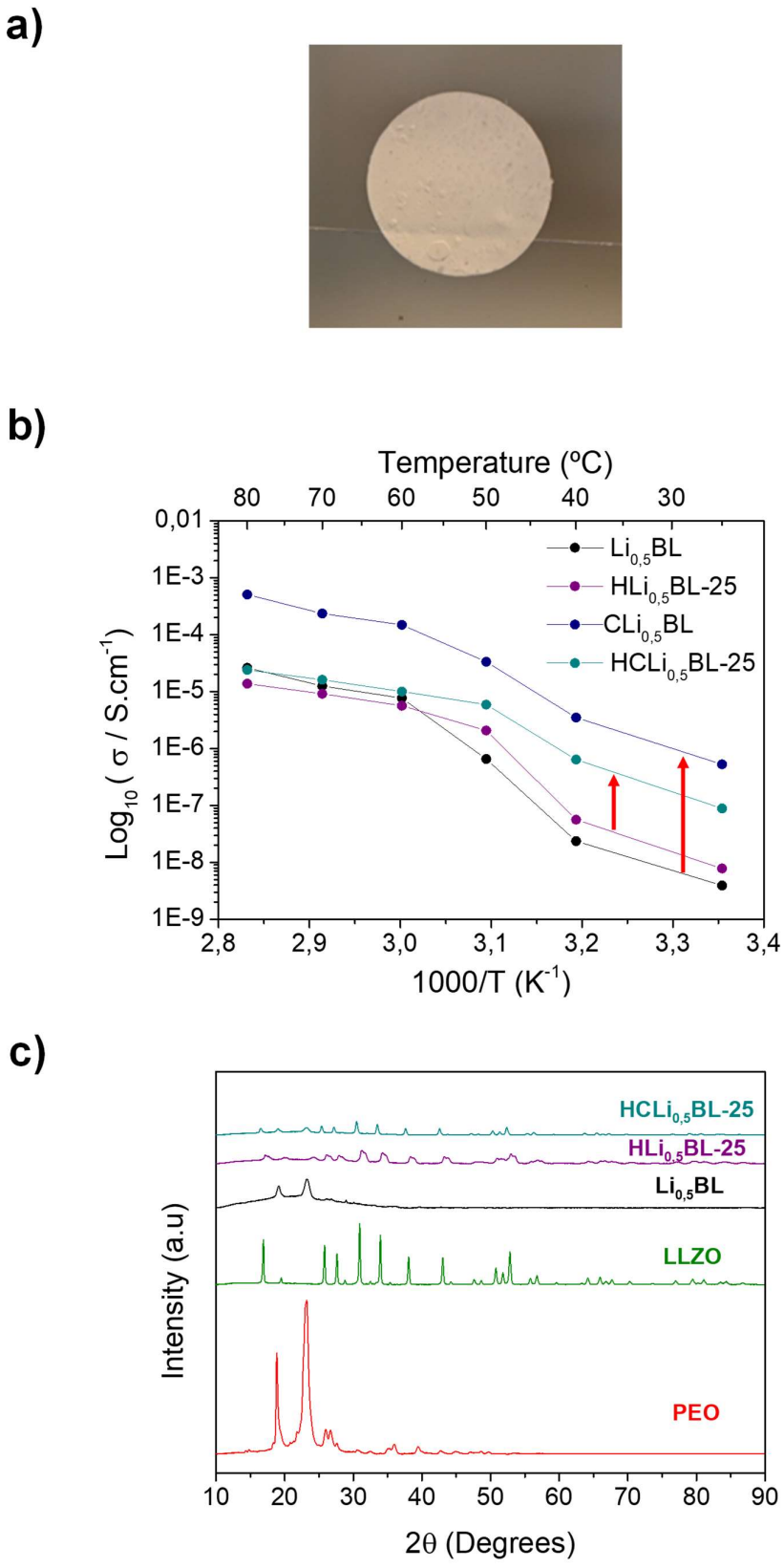

Figure 18: Photograph of hybrid HCL$i_{0.5}$BL film and characterization of hybrids based on L$i_{0.5}$BL and CL$i_{0.5}$BL polymers by b) EIS; c) XRD.

New bands associated to ion pairs can be observed in polymer matrices once salt concentration becomes too high. Polymers-salt or polymer-ionic liquids systems composed of TFSI anions present a supplementary band related $Li^{+}\cdots TFSI^{-}$ interactions which appears around 1220-1215 cm^{-1} [24,25]. Figure 19 displays the ATR-FTIR spectra of the polymer $Li_{0,5}BL$ and hybrid $HLi_{0,5}BL$-x. Red lines assign for band modification of LiMTFSI moieties while black line refers to PEO's crystalline phase alteration after LLZO addition.

Interestingly, major changes take place for LiMTFSI bands once LLZO is added. Firstly, a band at 1224 cm^{-1} confirms the presence of ionic aggregates in $Li_{0,5}BL$ electrolyte. Dramatic decrease of intensity of this mode appears once 25 wt.% LLZO is added to the blend. This implies that LLZO can interact with LiMTFSI moieties and dissociate the ionic clusters. In addition, characteristic bands of LiMTFSI tend to broaden and to become smaller, suggesting complexation of immobilized $TFSI^{-}$ with the particles[26]. Especially, ν(S-N) stretching and δ(SO_2) bending located at 712 and 618 cm^{-1}, completely disappear for each $HLi_{0,5}BL$-x compositions. ν_{as} (SO_2) and ν_{as} (CF) stretching also become wider for $HLi_{0,5}BL$-25. Concerning PEO crystalline phase, major band of ν(C-O-C) stretching shifts blue (from 1090 to 1101 cm^{-1}), which implies complexation of [EO] chains. By interacting with tethered anions, it can be hypothesized that LLZO particles are freeing Li ions, which can be able to complex with the PEO phase and decrease its crystallinity. Once the polymer is crosslinked, the PEO phase is totally amorphous, which fastens the ionic conduction in the material. Nevertheless, the combination of inorganic fillers and the chemical network may strengthen the electrolyte, which reduces the chain mobility in the polymer phase. Subsequently, $CLi_{0,5}BL$ has superior ionic conductivity than $HCLi_{0,5}BL$-25.

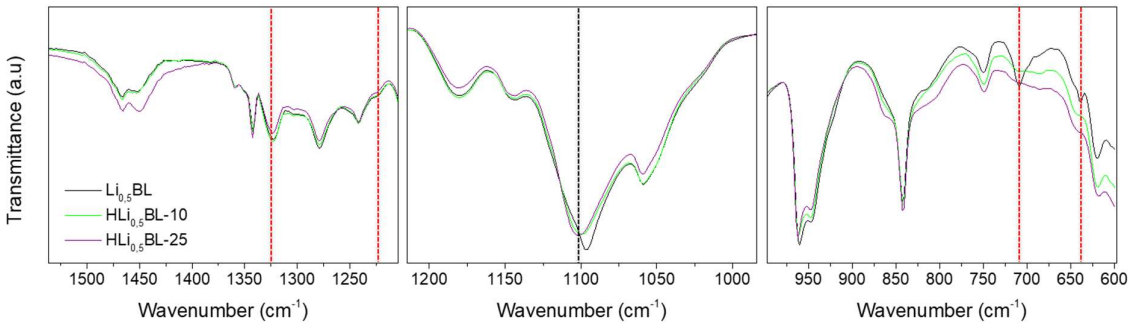

Figure 19: ATR-FTIR spectra comparison of polymer $Li_{0.5}BL$ and hybrid $HLi_{0.5}BL$-x

4.3.5. Electrochemical application in Li/Li symmetrical cells

Both polymer $CLi_{0,5}BL$ and hybrid $HCLi_{0,5}BL$-25 were implemented in Li symmetrical cells to evaluate their performance as solid electrolytes. The tests were conducted at 60°C to achieve sufficient ionic conductivity ($1{,}4.10^{-4}$ and 1.10^{-5} S/cm for the pristine and the hybrid). Before testing the selected materials, SEI additives need to be added to stabilize the electrolyte towards the Li. The SEI in PEO based Li metal cells is usually formed by the decomposition of the polymer chains and the salt, as well as impurities such as water traces[27]. As $TFSI^-$ is anchored to the polymer backbone, it cannot be degraded on Li metal to form the SEI. Unlikely to Chapter 3, it was not possible to use fluorinated solvents as the UV curing of the blends was performed at 80°C. Then, it was decided to add to the blend formulation small amount of LiFSI salt, which is known to form stable SEI on the lithium anode[28]. This salt has been previously used as additive in PEO electrolyte coupled with Li metal[29,30].

The evolution of the resistance in lithium symmetrical cells over time was carried out firstly for pristine and modified polymer $CLi_{0.5}BL$ with 5wt.% of LiFSI salt (Figure 20, experimental method in Appendix B2). The thicknesses of the electrolytes were between 50 and 180 µm for the pristine and modified polymers respectively. The cell pressure was set up to 3,2 N.m. Each spectrum is composed of two semi circles, which are related to the electrolyte bulk resistance R_{bulk} and SEI resistance R_{SEI}. The Equivalent Circuit Model (ECM) used for determining the resistances was composed of three CPEs: the two first ones were assigned to the amorphous and crystalline phases of the electrolyte; the last one to the SEI formation. The model is shown in Figure 21. Surprisingly, $CLi_{0.5}BL$ polymer electrolyte has a low R_{SEI} (504 Ω), but this latter tends unstably to increase over time (up 1000 Ω). On the opposite, the modified polymer $CLi_{0.5}BL$+LiFSI has a large R_{SEI} (825 Ω) but remains constant once the SEI is formed (R_{SEI} stabilizes up to 1100 Ω). This high resistance maybe comes from inadequate interfacial contact between the Li and the electrolyte, as the electrolyte was made ex situ. $HCLi_{0,5}BL$-25 composition was also modified with 5 wt.% salt in order to be further tested in Li symmetrical cells.

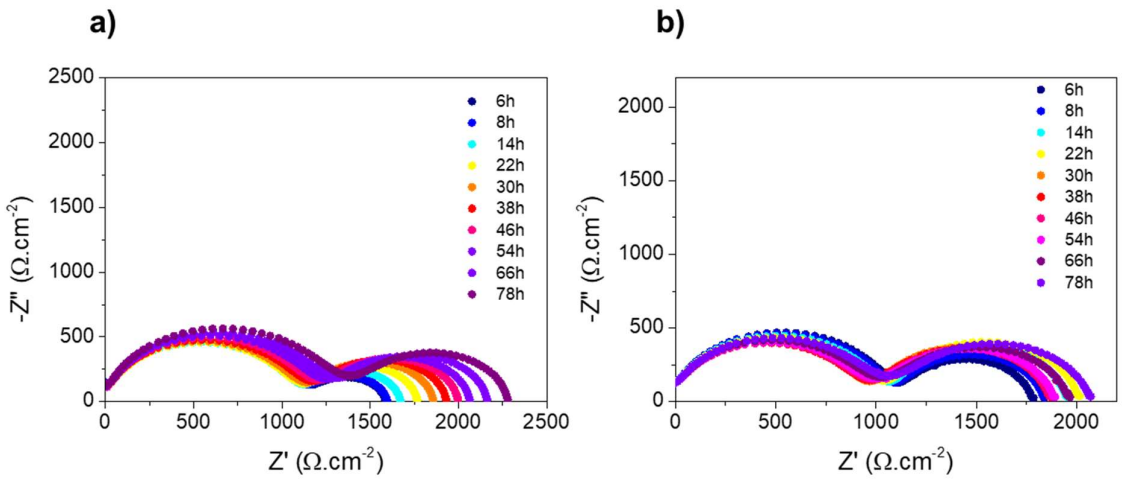

Figure 20: Evolution of the resistance over time of Li|$CLi_{0,5}BL$|Li and Li|$CLi_{0,5}BL$+LiFSI|Li cells

Transference numbers (TN) were calculated following Bruce's method (Experimental method in Appendix B4). Representative EIS spectra and intensity decays are shown in Figure 21. Equivalent circuit model was used to determine the resistances R_{bulk} and R_{SEI}. Red dot lines represent the fitting of the model.

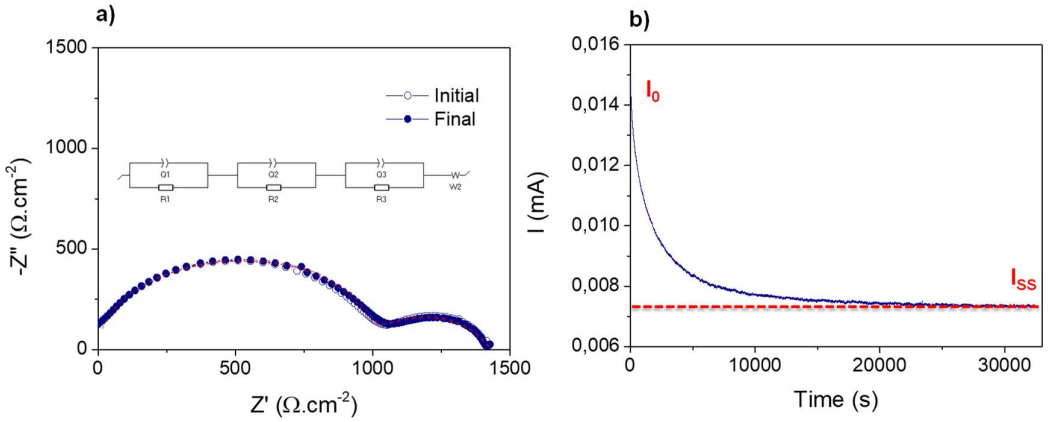

Figure 21: Transference number determination for $CLi_{0.5}BL$+LiFSI electrolyte: a) EIS spectra before and after chronoamperometry; b) Intensity decay after polarization

TN values are summarized in Table 6 and are coupled to the ionic conductivities of the electrolytes:

Table 6. Transference numbers and ionic conductivity determined at 60°C.

Electrolyte	TN	Ionic conductivity σ (S.cm ^{1})
$CLi_{0.5}BL$	0,84	$1,4.10^{-4}$
$CLi_{0.5}BL$+LiFSI	0,45	$2,4.10^{-5}$
$HCLi_{0.5}BL$-25+LiFSI	0,51	$2,2.10^{-5}$

First of all, it is confirmed by TN that single ion conduction happens in the polymer electrolyte $CLi_{0,5}BL$. In addition to its single ion motion, this electrolyte achieves high ionic conductivity without the help of plasticizer. Once small LiFSI additive is added, TN drops down to 0,45. Nevertheless, it is still high value for PEO electrolytes with lithium salt, which is generally comprised between 0,1 and 0,2. This highlights the beneficial effect of the single ion copolymer phase, which can restrain ion concentration gradients in the cell. Unfortunately, the ionic conductivity starts to decrease in presence of LiFSI. The addition of salt, even at low content, may favour the formation of ionic clusters. Especially, FSI^- anions are less bulky and delocalized than $TFSI^-$ moieties, which complicates the complete dissolution of the lithium in the polymer. After addition of LLZO particles, the transference number rises to 0,51. The ionic conductivity is also slightly enhanced. The inorganic particles are known to help the ionic dissociation in HSE by interacting with anions and TN values were reported to increase in the presence of active fillers (Table Chapter 1).

To corroborate the existence of interactions between LLZO and FSI^- anions, ATR-FTIR was performed to compare the polymer $CLi_{0,5}BL$ and the hybrid $HCLi_{0,5}BL$-25 in presence of

LiFSI. Their spectra are compiled in Figure 22. Characteristic bands of LiFSI salt can be recognized in the spectra of $CLi_{0,5}BL$ polymer such as ν_{as} (SO_2) and ν_{as} (S-N-S) stretching at 1380 and 825 cm^{-1} (Green lines) [31]. Band related to ionic pairs at 1224 cm^{-1} appears to be more intense and narrower than the polymer $CLi_{0.5}BL$ without LiFSI salt (Orange line). In addition, tethered $TFSI^-$ moieties vibrations occur to increase in intensity in presence of the salt additive (Red lines). In conclusion to these observations, it is more challenging for the single ion monomer to dissociate efficiently once LiFSI is added. However, the situation is inverted once LLZO particles are dispersed in the polymer. Both bands related to FSI^- and $TFSI^-$ anions strongly widen and decrease in presence of LLZO. This implies strong complexation of anionic species with the inorganic particles. LLZO is then highly beneficial for the Li ionic mobility in the polymer.

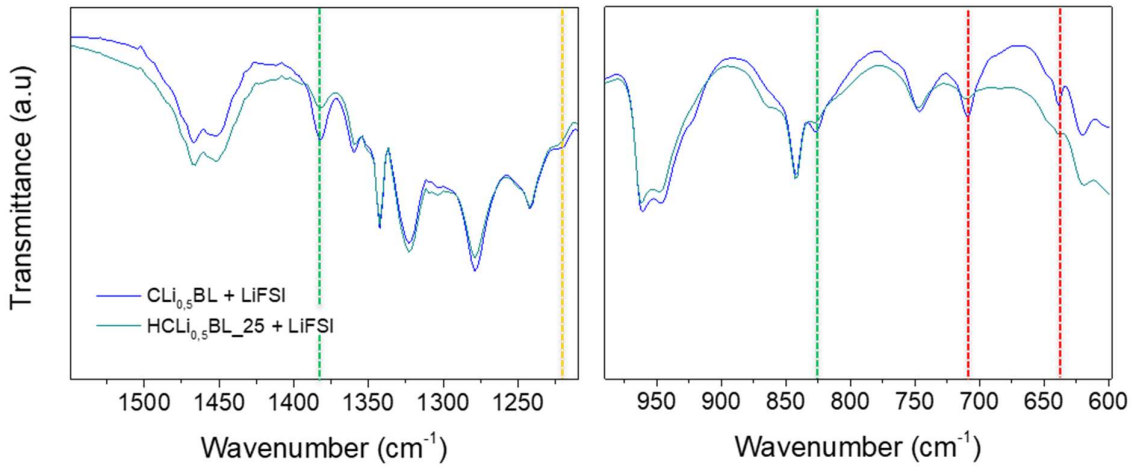

Figure 22: Comparison of ATR-FTIR spectra of $CLi_{0.5}BL$ and $HCLi_{0.5}BL$-25 in presence of LiFSI

Galvanostatic cycling was conducted on the polymer electrolyte $CLi_{0.5}BL$ with and without SEI additive in a view of analysing their cyclability. Both polymers were extremely thin, below 200 µm. Figure 23 compares their performance in Li symmetrical cells. The polymer $CLi_{0,5}BL$ without LiFSI has a poor cycling performance towards Li metal (Figure 23.a.i). Voltage spikes can be detected even at low current densities. The electrolyte achieves with difficulty a CCD of 0,25 $mA.cm^{-2}$. Above, the voltage suddenly drops down; likely the cell short-circuited. Cell failure was further confirmed by Electrochemical Impedance Spectroscopy (EIS) in Figure 23.b.i. After cycling, the resistance was measured to be null. On the other hand, the modified polymer $CLi_{0.5}BL$ displays a superior cycling performance thanks to the salt additive (Figure 23.b.i). Despite intermediate TN value (0,45), mossy like stripping/plating happens, as neck shaped voltage profiles can be noted starting from 0,25 $mA.cm^{-2}$. The electrolyte reaches a CCD of 0,5 $mA.cm^{-2}$ but can withstand higher current densities up to 4 $mA.cm^{-2}$. Nonetheless, this strongly damages the electrolyte as erratic voltages can be observed above 0,5 $mA.cm^{-2}$. This indicates that the uneven Li dissolution/deposition likely led to dendrites formation. Starting from 2 $mA.cm^{-2}$, the voltage is dropping continuously. Dramatic reduction of resistances after the test further supports the apparition of dendrites in the electrolyte. R_{SEI}

drops from 1019 Ω to a few ohms. For comparison, the CCD of PEO membrane intercrosslinked with a polymethacrylate is 0,2 mA.cm^{-2} at 25ºC [32]. At 60°C, the CCD tends to double thanks to the enhanced ionic conductivity and better Li deformation at high temperature. Then, it can be considered that its CCD should reach around 0,4 mA.cm^{-2} at 60°C, which is lower than our electrolyte presented in this chapter.

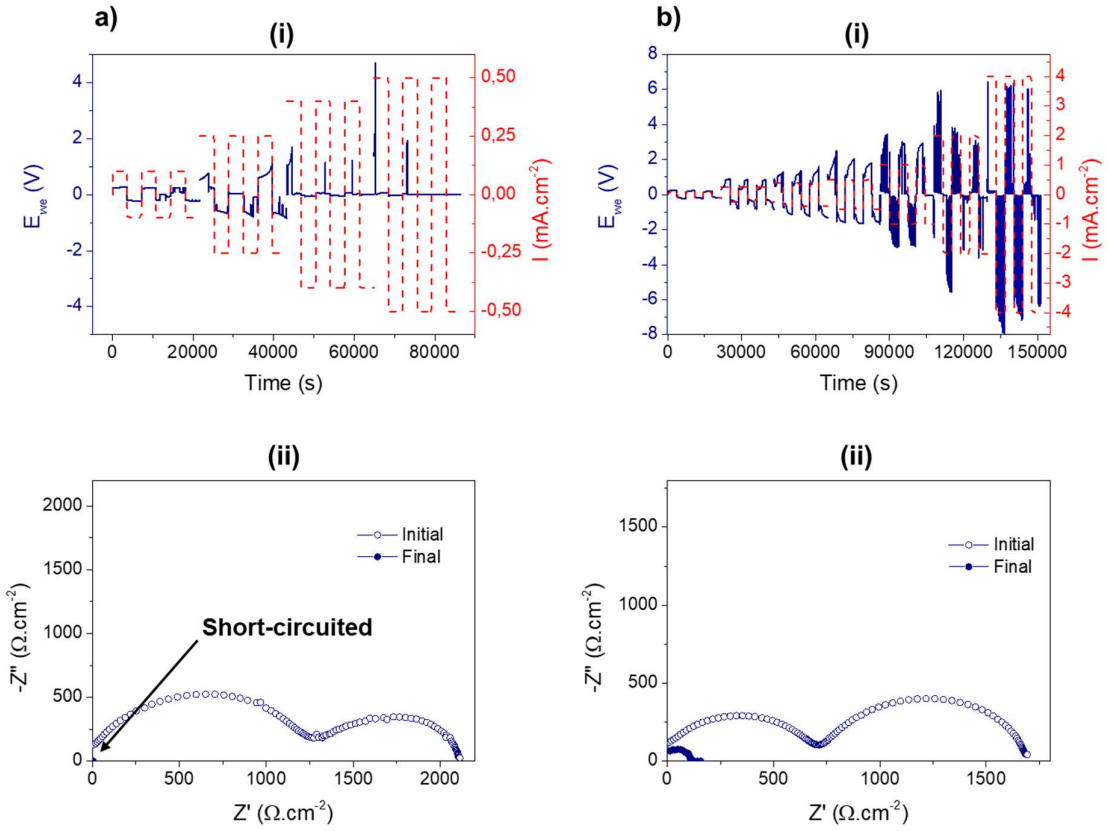

Figure 23: Galvanostatic cycling performance of CLi$_{0.5}$BL and CLi$_{0.5}$BL+LiFSI in Li symmetrical cells at 60°C; a) Voltage profiles with increasing current densities; b) EIS spectra before and after cycling.

Hybrid HCLi$_{0,5}$BL-25 was also tested by galvanostatic cycling to investigate the potential effect of LLZO on the cycling performance of the polymer matrix. The hybrid electrolyte can cycle up to 0,5 mA.cm^{-2} (Figure 24.a). Therefore, LLZO particles do not improve the cycling performance of the polymer matrix. However, erratic voltages happen to occur sooner, starting from 0,4 mA.cm^{-2}. Consequently, the electrolyte achieves lower current densities, up to 1 mA.cm^{-2}, at which the voltage decreases dramatically. After cycling, the resistance of the cell fiercely goes down, confirming the presence of dendrites within the electrolyte (Figure 24.b). In comparison with Chapter 3, the polymer can achieve higher current densities than the hybrid. It can be hypothesized that this difference is linked to the distinct interactions between LiMTFSI and LLZO. HCLi$_{0,5}$BL-25 electrolyte does not experience any change of colour previously described in hybrid gels. Nevertheless, the CCD of HCLi$_{0,5}$BL-25 is superior to the reported limits of the garnet, estimated to be 0,3 mA.cm^{-2}. Existence of ionic interactions between LiMTFSI and LLZO particles (confirmed by ATR-FTIR) can maybe help the hybrid to achieve an acceptable cycling.

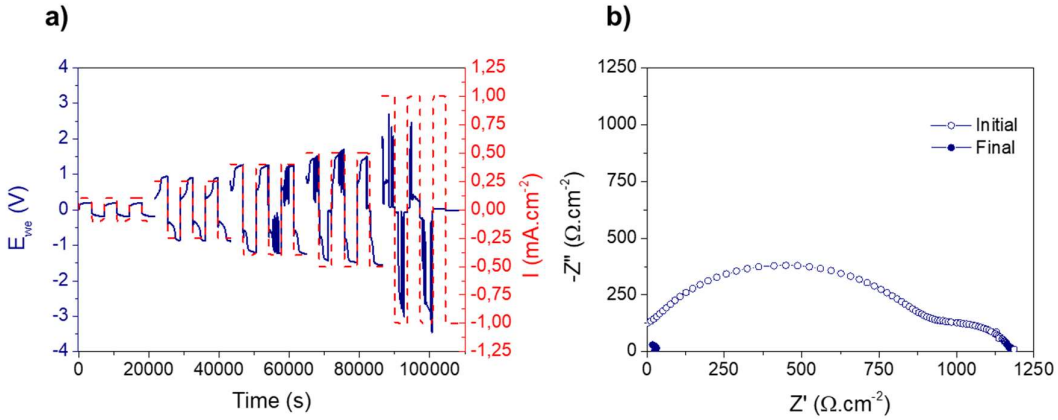

Figure 24: Galvanostatic cycling performance of $HCLi_{0.5}BL$-25+LiFSI in Li symmetrical cells at 60°C; a) Voltage profiles with increasing current densities; b) EIS spectra before and after cycling.

The addition of LLZO deteriorates the cycling of the polymer at high current densities. This is unexpected as the hybrid shows enhanced ionic dissociation and similar ionic conductivity than the polymer matrix. Besides, improved SEI was noted for the hybrid. As a matter of fact, the polymer $CLi_{0,5}BL$ has a bigger SEI resistance than the hybrid $HCLi_{0,5}BL$-25. With similar thicknesses (190 and 180 µm for the polymer and the hybrid), R_{SEI} is divided by half for $HCLi_{0,5}BL$-25. Chemical compatibility in Li cells was previously reported to be enhanced with the use of LLZO hybrid electrolytes (Chapter 1). Nevertheless, the promising features of $HCLi_{0,5}BL$-25 are not enough to provide a stable Li stripping and plating.

The polymer and the hybrid presented here present lower ionic conductivity and transference number than the previous materials presented in Chapter 3. These latter may explain the lower CCD achieved for both these electrolytes, but not the facilitated dendrites formation. Their high resistances seem to be related to the poor interfacial contact between the electrolyte and the lithium. Many researchers examined the cause of the poor cycling performance of PEO based electrolytes. In addition to the formation of unstable SEI, the "mechanical" interfacial contact was evoked as potential origin of dendrites growth in lithium metal cell[33]. Generally, high molecular weight PEO is used thanks to its optimal ionic conductivity. However, unoptimized Li wetting is obtained with this electrolyte, because of void spaces and limited contact points with the anode, mainly due to the chain entanglement of the polymer. This unfortunately leads to non-uniform interphase, with favorized spots for Li nucleation. Despite being composed of small oligomers (high PDI determined by SEC-GPC), the copolymer used in the blend does not provide sufficient wetting. Potential remedy is to add a small content of plasticizer, such as glymes, in order to have a softer contact with the Li anode[34].

Electrochemical stability window (ESW) of the polymer $CLi_{0,5}BL$ and hybrid $HCLi_{0,5}BL$-25 were further determined as depicted in Figure 25 (Experimental method in Appendix C5). $CLi_{0,5}BL$ has an improved ESW than PEO based polymer electrolytes, up to 5.37 V. Small peak around 4V is observed, which may come from the oxidation of uncrosslinked PEO (OH groups oxidation happens at 4.05V). This impressive improvement mainly comes from -OCH_3 terminal groups from PEGM moieties[35]. Addition of particles in the polymer can further enhance the

ESW up to 5.6V, which confirms the beneficial effect of LLZO particles on the stabilization of the interface with the lithium.

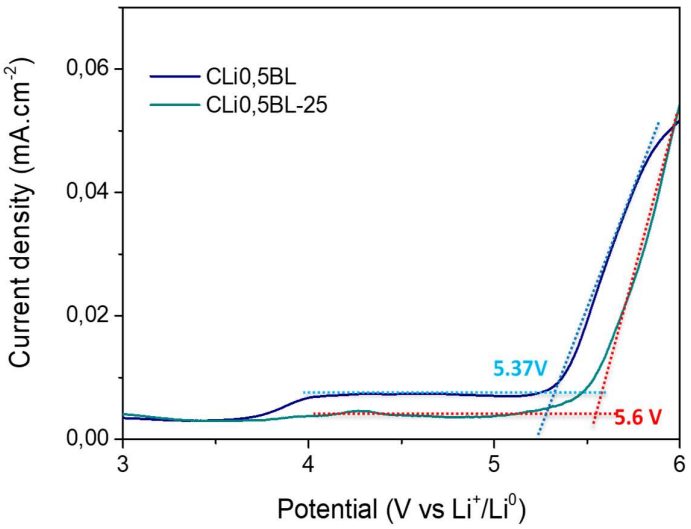

Figure 25: Oxidation stability towards Li metal for $CLi_{0,5}BL$ and $HCLi_{0,5}BL$-25 electrolytes at 60°C

To summarize, acceptable cycling performance was obtained for the polymer $CLi_{0,5}BL$. LiFSI additive was necessary to form a stable SEI. Nevertheless, the presence of dual salt tends to decrease the ionic conductivity of the electrolyte. The CCD is then lower as expected (0,5 $mA.cm^{-2}$). Sluggish ionic conduction is unfortunately not the sole drawback of this electrolyte. Insufficient wetting of the anode leads to preferred spots for Li stripping/plating, leading to uneven Li dissolution/deposition. That is probably why the addition of LLZO does not improve the cycling efficiency of the polymer, despite numerous qualities in term of ionic dissociation and interfacial chemical stability. Small content of glyme (plasticizer) in the blend formulation can be a solution to improve cyclability of these electrolytes.

4.4. Conclusions

In this chapter, crosslinked hybrid and polymer blend electrolytes based on lithium single ion copolymers, PEO and LLZO particles were investigated. For this purpose, we carried out first the synthesis of new poly($LiMTFSI_x$-co-$PEGM_{1-x}$) random copolymers by free radical copolymerization and studied the optimum composition for obtaining the highest ionic conductivity. Blends containing low PEO amount ($\leq$ 30 wt.%) show the best ionic conductivity (up to 10^{-6} S/cm at room temperature) but suffer from poor mechanical stability. It was observed that the crystallinity of the blends between PEO and poly($LiMTFSI_x$-co-$PEGM_{1-x}$) electrolytes is strongly affected by the concentration of LiMTFSI in the copolymer. The copolymer acts as a single ion Li source and plasticizer, by complexing its LiMTFSI moieties with the PEO phase and improving the flexibility thanks to its PEGM component. An additional treatment by UV curing was carried out to provoke the crosslinking of PEO and enables to get self-standing membranes, allowing their use at high temperatures in an ASSB set up.

The HSE were successfully prepared by spray-coating of a solution of the three components (copolymer, PEO and LLZO). Spray coating gives a uniform dispersion of inorganic particles within the polymer matrix and thin hybrid films (< 200 µm). pH detection and FTIR-ATR analysis was carried during HSE process to verify the possible contamination of LLZO particles by water traces. Extremely dried HSE films were successfully obtained by simple wet method. LLZO does not look to be actively participating to the ionic processes but can interact with LiMTFSI moieties. This affinity was proved by FTIR-ATR analysis. Formation of an “interphase” between LLZO and LiMTFSI seems to not occur in these materials, as no change of colour was observed as in the first chapter when LiMTFSI monomer was used.

These solid electrolytes were tested in lithium symmetrical cells to conclude about their potential use as anolyte in Li metal batteries. Use of additive - LiFSI salt- was primordial to stabilize the polymer towards the lithium. The polymer blend loses its single-ion conduction after the addition of the SEI stabilizer: from 0,84, the transference number decreases to the intermediate value of 0,45. Nevertheless, fixed anionic moieties in the polymer architecture helps to mitigate concentration gradients, as the developed electrolyte withstands higher current densities that similar polymers reported in the literature. The CCD was determined to be 0,5 $mA.cm^{-2}$, which is however still too low for practical applications in industrial batteries. Possible remedies to enhance the cycling performance might be to have a softer interfacial contact, higher ionic conductivity and maybe a better design of the SEI. The use of glymes as plasticizer can be the easiest solution for the first and second requirements. Regarding the last one, addition of several dual salt additives (LiFSI+$LiNO_3$ for example) was proved to form highly stable interphases on the lithium. Concerning the hybrid, it presents improved mechanical and electrochemical properties, such as Li ion transport and oxidative stability. However, the addition of particles does not help the electrolyte to have a better interfacial contact with the electrodes. Unfortunately, no enhancement in term of cyclability was observed for the hybrid blend HSE.

4.5. References

1. Xue, Z., He, D. & Xie, X. Poly(ethylene oxide)-based electrolytes for lithium-ion batteries. *J. Mater. Chem. A* **3**, 19218–19253 (2015).

2. Jiang, Y. *et al.* Development of the PEO based solid polymer electrolytes for all-solid state lithium ion batteries. *Polymers (Basel).* **10**, 1–13 (2018).

3. Zhao, S., Wu, Q., Ma, W. & Yang, L. Polyethylene Oxide-Based Composites as Solid-State Polymer Electrolytes for Lithium Metal Batteries: A Mini Review. *Front. Chem.* **8**, 1–7 (2020).

4. Porcarelli, L. *et al.* Single-ion triblock copolymer electrolytes based on poly(ethylene oxide) and methacrylic sulfonamide blocks for lithium metal batteries. *J. Power Sources* **364**, 191–199 (2017).

5. Chang, C. ., Sun, Y. . & Kim, D. . Blended polymer electrolytes based on poly(lithium 4-styrene sulfonate) for the rechargeable lithium polymer batteries. *Electrochim. Acta* **50**, 375–378 (2004).

6. Cao, C. *et al.* A solid-state single-ion polymer electrolyte with ultrahigh ionic conductivity for dendrite-free lithium metal batteries. *Energy Storage Mater.* **19**, 401–407 (2019).

7. Meziane, R., Bonnet, J.-P., Courty, M., Djellab, K. & Armand, M. Single-ion polymer electrolytes based on a delocalized polyanion for lithium batteries. *Electrochim. Acta* **57**, 14–19 (2011).

8. Olmedo-Martínez, J. L. *et al.* High Lithium Conductivity of Miscible Poly(ethylene oxide)/Methacrylic Sulfonamide Anionic Polyelectrolyte Polymer Blends. *Macromolecules* **53**, 4442–4453 (2020).

9. Merrill, L. C. *et al.* Polymer-Ceramic Composite Electrolytes for Lithium Batteries: A Comparison between the Single-Ion-Conducting Polymer Matrix and Its Counterpart. *ACS Appl. Energy Mater.* **3**, 8871–8881 (2020).

10. Porcarelli, L. *et al.* Single-Ion Block Copoly(ionic liquid)s as Electrolytes for All-Solid State Lithium Batteries. *ACS Appl. Mater. Interfaces* **8**, 10350–10359 (2016).

11. Porcarelli, L. *et al.* Design of ionic liquid like monomers towards easy-accessible single-ion conducting polymer electrolytes. *Eur. Polym. J.* **107**, 218–228 (2018).

12. Kim, G. T. *et al.* UV cross-linked, lithium-conducting ternary polymer electrolytes containing ionic liquids. *J. Power Sources* **195**, 6130–6137 (2010).

13. Molinari, N., Mailoa, J. P. & Kozinsky, B. Effect of Salt Concentration on Ion Clustering and Transport in Polymer Solid Electrolytes: A Molecular Dynamics Study of PEO-LiTFSI. *Chem. Mater.* **30**, 6298–6306 (2018).

14. Polu, A. R. & Rhee, H. W. Ionic liquid doped PEO-based solid polymer electrolytes for lithium-ion polymer batteries. *Int. J. Hydrogen Energy* **42**, 7212–7219 (2017).

15. Rupp, B., Schmuck, M., Balducci, A., Winter, M. & Kern, W. Polymer electrolyte for lithium batteries based on photochemically crosslinked poly(ethylene oxide) and ionic liquid. *Eur. Polym. J.* **44**, 2986–2990 (2008).

16. Porcarelli, L., Gerbaldi, C., Bella, F. & Nair, J. R. Super Soft All-Ethylene Oxide Polymer Electrolyte for Safe All- Solid Lithium Batteries. *Nat. Publ. Gr.* 1–14 (2016)

doi:10.1038/srep19892.

17. Marzantowicz, M., Dygas, J. ., Krok, F., Nowiński, J. . & Tomaszewska, A. Crystalline phases, morphology and conductivity of PEO:LiTFSI electrolytes in the eutectic region. *J. Power Source* **159**, 420–430 (2006).

18. Kun, R. *et al.* Structural and Computational Assessment of the Influence of Wet-Chemical Post-Processing of the Al-Substituted Cubic Li7La3Zr2O12. *ACS Appl. Mater. Interfaces* **10**, 37188–37197 (2018).

19. Huo, H. *et al.* Li2CO3: A Critical Issue for Developing Solid Garnet Batteries. *ACS Energy Lett.* **5**, 252–262 (2020).

20. Liu, C. *et al.* Reversible ion exchange and structural stability of garnet-type Nb-doped Li7La3Zr2O12 in water for applications in lithium batteries. *J. Power Sources* **282**, 286–293 (2015).

21. Huang, Z., Tong, R. ao, Zhang, J., Chen, L. & Wang, C. A. Blending Poly(ethylene oxide) and Li6.4La3Zr1.4Ta0.6O12 by Haake Rheomixer without any solvent: A low-cost manufacture method for mass production of composite polymer electrolyte. *J. Power Sources* **451**, 227797 (2020).

22. Keller, M. *et al.* Electrochemical performance of a solvent-free hybrid ceramic-polymer electrolyte based on Li7La3Zr2O12 in P(EO)15LiTFSI. *J. Power Sources* **353**, 287–297 (2017).

23. Langer, F., Bardenhagen, I., Glenneberg, J. & Kun, R. Microstructure and temperature dependent lithium ion transport of ceramic–polymer composite electrolyte for solid-state lithium ion batteries based on garnet-type {Li}7La3Zr2O12. *Solid State Ionics* **291**, 8–13 (2016).

24. Zhu, C., Cheng, H. & Yang, Y. Electrochemical Characterization of Two Types of PEO-Based Polymer Electrolytes with Room-Temperature Ionic Liquids. *J. Electrochem. Soc.* **155**, A569 (2008).

25. Abitelli, E. *et al.* Electrochimica Acta Polyethylene oxide electrolyte membranes with pyrrolidinium-based ionic liquids. *Electrochim. Acta* **55**, 5478–5484 (2010).

26. Wen, S. J. *et al.* FTIR characterization of PEO + LiN(CF3SO2)2 electrolytes. *J. Electroanal. Chem.* **408**, 113–118 (1996).

27. Xu, C., Sun, B., Brandell, D. & Hahlin, M. Interface layer formation in solid polymer electrolyte lithium batteries : an XPS study. *J. Chem.* **A**, 7256–7264 (2014).

28. Wang, M. *et al.* Effect of LiFSI Concentrations to Form Thickness- and Modulus-Controlled SEI Layers on Lithium Metal Anodes. *J. Phys. Chem. C* **122**, 9825–9834 (2018).

29. Judez, X. *et al.* Lithium Bis(fluorosulfonyl)imide/Poly(ethylene oxide) Polymer Electrolyte for All Solid-State Li-S Cell. *J. Phys. Chem. Lett.* **8**, 1956–1960 (2017).

30. Santiago, A. *et al.* Improvement of Lithium Metal Polymer Batteries through a Small Dose of Fluorinated Salt. *J. Phys. Chem. Lett.* **11**, 6133–6138 (2020).

31. Kerner, M., Plylahan, N., Scheers, J. & Johansson, P. Thermal stability and decomposition of lithium bis(fluorosulfonyl)imide (LiFSI) salts. *RSC Adv.* **6**, 23327–23334 (2016).

32. Zhang, Y. *et al.* Cross-linking network based on Poly(ethylene oxide): Solid polymer electrolyte for room temperature lithium battery. *J. Power Sources* **420**, 63–72 (2019).

33. Brown, N. R., Makkapati, T. & Teeters, D. Stabilization of the polymer electrolyte/lithium metal electrode interface with increased ion conduction using PEO polymer/low molecular weight PE-b-PEO diblock copolymer composite bi-layer films. *Solid State Ionics* **288**, 207–212 (2016).

34. Falco, M. *et al.* UV-Cross-Linked Composite Polymer Electrolyte for High-Rate, Ambient Temperature Lithium Batteries. *ACS Appl. Energy Mater.* **2**, 1600–1607 (2019).

35. Yang, X. *et al.* Determining the limiting factor of the electrochemical stability window for PEO-based solid polymer electrolytes: Main chain or terminal -OH group? *Energy Environ. Sci.* **13**, 1318–1325 (2020).

CHAPTER 5.

Hybrid and polymer electrolytes based on pseudo-zwitterionic semi-interpenetrated networks.

5.1. Introduction.

Zwitterions are organic salts which bear both anionic and cationic components in their structure[1]. As the positive and the negative charges are covalently bonded and equal in number, the overall charge of the zwitterion is neutral. Zwitterions can be then considered as stable dipoles. This property led to considerate them as promising additive in liquid and polymer-based electrolytes, such as ionic dissociators and SEI stabilizers [2,3,4]. Thanks to their positive and negative charges, zwitterions can interact with both the mobile cations and anions. It was reported that small content of this additive in polymer formulations enhances the ionic dissociation of the salt from the polymer and controls the anion decomposition at the surface of the electrodes. Then, higher ionic conductivity, larger transport number and stabler SEI were observed in SPE coupled with zwitterions.

Polyzwitterions are ionic polymers comprising immobilized zwitterionic moieties in their polymer backbone. They were deeply investigated as anti-fouling materials for medical and environmental applications such as drug delivery or filtration[5]. Recently, polyzwitterions were studied to develop new electrolytes for Li batteries. Firstly, they spark off a growing interest for enhancing the ionic conductivity of polymer electrolytes, thanks to their ability to weaken the complexation between ethylene oxide units and Li cations [6,7]. Finally, these materials show, as their mobile counterparts, higher stability with Li metal and homogeneous Li cycling at moderate and high current densities[8]. Zwitterionic moieties are thought to regulate the ion flux within the electrolyte by immobilizing mobile anions. This property mitigates the formation of high concentration gradients over cycling, resulting in a better protection towards dendrites growth.

In addition, polyzwitterions show interestingly tunable properties such as mechanical strength or swelling in presence of salt, ionic liquids (IL) or another polyzwitterions. Despite the complexity of these ionic interactions, it is generally accorded that the zwitterionic moieties can strongly associate with other ionic species[9]. Gel type electrolytes were obtained by physical crosslinking of tethered zwitterionic moieties with other polyzwitterions or ILs[10,11]. Some studies show that polyzwitterions can pair up with high concentration of salt[12,13]. This last property could be promising to develop new and highly conductive polymer-in-salt systems.

However, the formation of polyzwitterions or their related zwitterionic monomers is still challenging due to complex multistep synthesis and purification processes[14]. Polymerization of zwitterionic monomers is extremely complicated as they can strongly interact or even react with the present chemical species such as the solvent, the salt etc. That is why we decide to investigate on a new type of ionic polymer, namely pseudo-polyzwitterion. This polymer differs

from the original poly(zwitterion) by its simple synthetic method and distinct chemical structure. This technique was inspired by the pioneer work of Ohno & co-workers, who synthesized a variety of ionic liquid monomers by ionic exchange[15]. The addition of an anionic monomer in an aqueous solution, where a cationic monomer was previously dissolved, leads to the precipitation of a stable pseudo-zwitterionic monomer. This latter is therefore formed by the strong complexation between independent monomeric anionic and cationic moieties. These distinct polymer architectures are represented in Figure 1. Pseudo-polyzwitterions can then be more easily synthesized than typical polyzwitterions by conventional radical polymerization and offer a larger variety of chemical structures and composition possibilities.

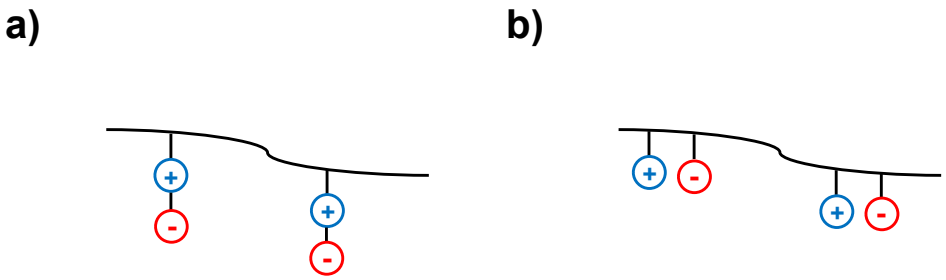

Figure 1: Schematic representation of a) Polyzwitterion; b) Pseudo-polyzwitterion

In this chapter, new polymer electrolytes were prepared by mixing cationic and pseudo-zwitterionic copolymers based on an anionic sulfonylimide monomer (LiMTFSI), a cationic trimethyl ammonium monomer (NTFSI) and an ethylene glycol monomer (PEGM). These polymer electrolytes were further reinforced by the formation of a semi-interpenetrated network (s-IPN), leading to self-standing, flexible and highly deformable films. Hybrid solid electrolytes (HSE) were also synthesized to analyse the effect of LLZO particles on the electrochemical properties of the polymer matrix. Investigation on polyzwitterions with active inorganic particles has not been carried out to our knowledge. However, several studies reported beneficial effects of combined IL and ionic polymers with inorganic ionic conductors, in term of filler dispersion, ionic dissociation and electrochemical stability [16,17].

Ionic interactions between immobilized charged moieties, free salt and inorganic particles were explored to understand the final performance of these hybrid and polymer electrolytes. Finally, the practical application of these materials was evaluated in Li symmetrical cells.

5.2. Experimental part

This experimental section is organized as follows:

- Firstly, the synthesis of cationic and new pseudo-zwitterionic monomers is detailed. Then, their copolymerization with poly(ethylene glycol) methyl ether methacrylate (PEGM) is addressed.

- Secondly, the preparation of pseudo-zwitterionic polymer blends is discussed. Quasi-solid gel materials were formed by simply mixing the pseudo-zwitterionic copolymer with anionic or cationic copolymers.

- Finally, the formation of a semi-interpenetrated networks (s-IPN) was carried out. This process allows to get self-standing pseudo-zwitterionic films with acceptable ionic conductivity at mild temperatures. Hybrid Solid Electrolytes (HSEs) were finally prepared in order to conclude about LLZO effect on the solid electrolyte properties and its performance in lithium symmetrical cells.

All the experimental methods (electrolyte characterization, battery set up) are fully described in the Appendix section.

5.2.1. Materials

Poly(ethylene glycol) methyl ether methacrylate (500 g/mol), Poly(ethylene glycol) dimethacrylate (550 g/mol), [2-(Acryloyloxy)ethyl]trimethylammonium chloride solution (75 wt.% in water), Azobis(2-methylpropionitrile) (AIBN thermal initiator, 98% purity), tetraethylene glycol dimethyl ether (TEGDME) and anhydrous acetonitrile (98%) were purchased from Sigma Aldrich. PEGM and PEGDM were further dried with 10 wt.% molecular sieves before use (4 Å, activated under vacuum for 24h at 300°C). Anhydrous acetonitrile and TEGDME were also dried with the same method to minimize the risk of LLZO contamination in presence of H_2O traces.

Diethyl ether (Et_2O), methanol (MeOH) and dichloromethane (DCM) were supplied from Acros.

Lithium Bis(fluorosulfonyl)imide LiFSI salt was provided by TCI (98% purity). Before use, LiFSI was dried under vacuum at 130°C for 24h and stored in Argon glovebox. LiMTFSI single ion monomer was synthesized according to the reaction reported in Chapter 3.

Cubic Al doped $Li_{7-3x}Al_xLa_3\ Zr_2O_{12}$ (LLZO) particles were received from MSE under argon atmosphere and were used as received (99.9% purity, 400-600 nm particles size).

Li foils (120 µm thickness) were purchased from Rockwood Lithium (USA).

5.2.2. Synthesis of cationic poly(NTFSI$_{0,2}$-co-PEGM$_{0,8}$) copolymer

NTFSI monomer was obtained by a simple ionic exchange of chloride anions by bis(trifluoromethanesulfonyl)imide anions (TFSI) as illustrated in Figure 2. A concentrated solution of ([2-(Acryloyloxy)ethyl]trimethylammonium chloride) (1 g; 5,2 mmol) was further diluted in 20 mL of distilled water. LiTFSI salt (1,5 g; 5,2 mmol) was dissolved in 4 mL of distilled water. This equimolar salt solution was added dropwise the diluted [2-(Acryloyloxy)ethyl]trimethylammonium chloride) under agitation. Immediately, a precipitate appeared. This latter was diluted in DCM and washed several times with Brine. The solvent was then gently evaporated under reduced pressure (Yield: 53%).

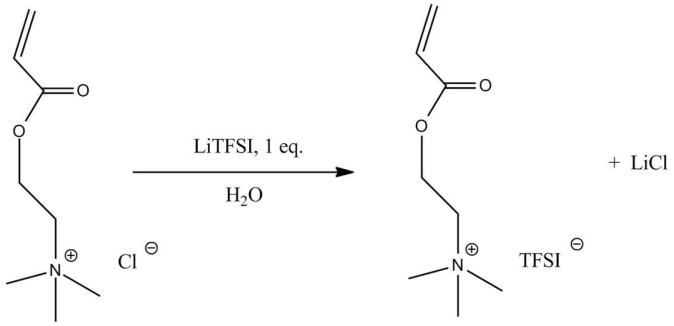

Figure 2: NTFSI monomer obtained by ionic exchange.

NTFSI monomer was then copolymerized with PEGM according to the same method described in Chapter 4. The reaction scheme is shown in Figure 3. Poly(NTFSI$_x$-co-PEGM$_{1-x}$) composition was fixed to x=20% mol in order to compare with the previously developed anionic copolymer poly(LiMTFSI$_{0,2}$-co-PEGM$_{0,8}$). NTFSI (2,4 g, 5,5 mmol) and PEGM (11 g, 22 mmol) was dissolved in methanol (MeOH, 35 mL) in a Schlenk tube. AIBN (2wt.%) was added to the reaction mixture as thermal initiator. Freeze Vacuum Thaw degassing was processed at least 4 times to remove the oxygen. The reaction was launched by immersing the reaction flask in oil bath (70°C) for at least 6h. The yield was calculated to be 97%.

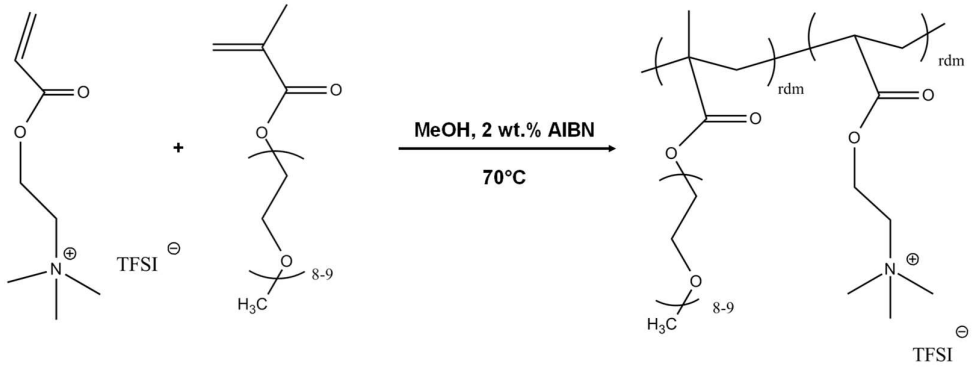

Figure 3: Synthesis of Poly(NTFSI$_{0,2}$-co-PEGM$_{0,8}$) copolymer

5.2.3. Synthesis of pseudo-zwitterionic poly($ZI_{0,2}$-co-$PEGM_{0,8}$) copolymer

Pseudo-zwitterionic monomer (ZI) was obtained by the complexation of cationic NTFSI and anionic LiMTFSI monomers in water as displayed in Figure 4. NTFSI monomer (1 g, 5,2 mmol) was diluted in distilled water (10mL). An equimolar aqueous solution of LiMTFSI monomer (1,8 g, 5,2 mmol) was added dropwise under agitation. Straightaway, the pseudo zwitterionic monomer precipitated. This latter was then diluted in DCM and washed several times with Brine. The solution was finally evaporated under reduced pressure (Yield: 38%)

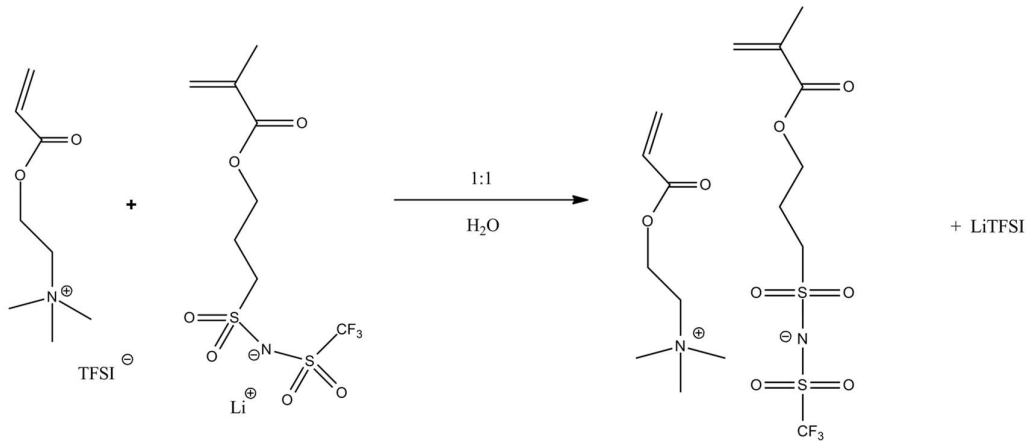

Figure 4: Synthesis of pseudo-zwitterionic monomer ZI

ZI monomer was afterward copolymerized with PEGM as shown in Figure 5 to obtain the poly($ZI_{0,2}$-co-$PEGM_{0,8}$) copolymer, with x=20% mol. Previous method was applied for this synthesis: ZI monomer (1,9 g, 3,9 mmol), PEGM monomer (7,8 g, 15,6 mmol) and AIBN thermal initiator (2 wt.%) were dissolved in MeOH (30 mL) in a Schenk tube. The reaction mixture was purged several times by using Freeze Vacuum Thaw technique. Finally, the reactional flask was immersed in hot oil bath (70°C) for at least 6h. The yield was calculated to be 73%.

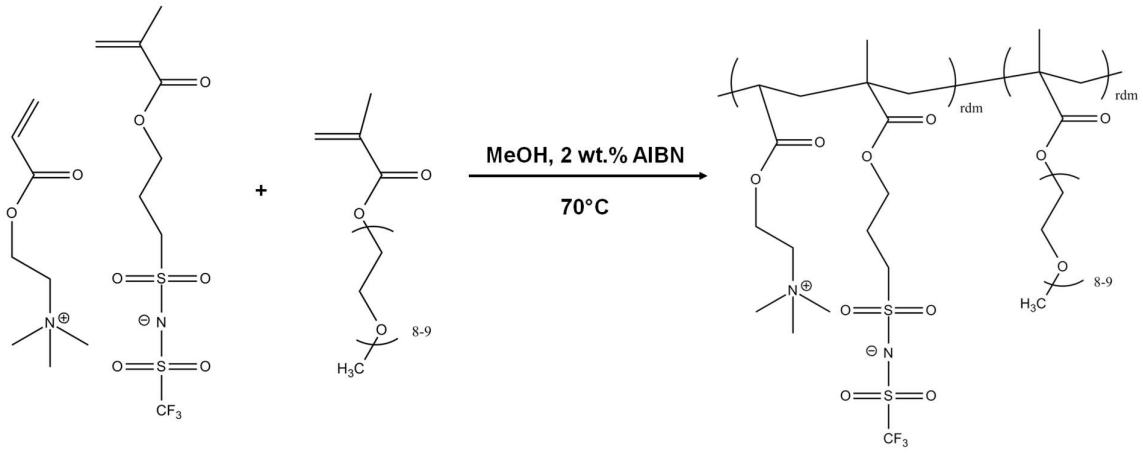

Figure 5: Synthesis of Poly($ZI_{0,2}$-co-$PEGM_{0,8}$) copolymer

5.2.4. Preparation of pseudo-zwitterionic blends based on poly($ZI_{0,2}$-co-$PEGM_{0,8}$) copolymer.

Blends were prepared by mixing the pseudo-zwitterionic poly($ZI_{0,2}$-co-$PEGM_{0,8}$) copolymer with its cationic and anionic counterparts, namely poly($NTFSI_{0,2}$-co-$PEGM_{0,8}$) and poly($LiMTFSI_{0,2}$-co-$PEGM_{0,8}$) copolymers. Their composition was fixed to 50/50 (wt.%) in order to form quasi solid electrolytes thanks to the physical interactions between the immobilized cationic and anionic moieties. Blend process was carried out under inert atmosphere in an Argon glovebox. Firstly, the copolymers (and the salt if needed) were diluted at 12 wt.% in anhydrous acetonitrile, which was previously dried over molecular sieves. The copolymers were mixed for one day to get a homogeneous mixture. Next, the solution was cast on a silicon mould to form a film. This latter was dried at room temperature in the glovebox, then under vacuum at 60°C to remove residual traces of solvent.

5.2.5. Formation of a semi-interpenetrated networks based on poly($ZI_{0,2}$-co-$PEGM_{0,8}$) copolymer, LiFSI and LLZO particles.

To form a semi-interpenetrated network (s-IPN), Poly(ethylene glycol) dimethacrylate (PEGDM) monomer and AIBN were added in the batch solution. The film was processed and dried in the glovebox as described previously. Then, the obtained films were cured under vacuum at 70°C for 24h to crosslink PEGDM monomer within the pseudo-zwitterionic blend. In the case of the hybrid s-IPN, LLZO was added in the batch and mixed a couple of hours before processing the film. Spray coating was chosen to disperse efficiently the particles, as it was previously demonstrated in Chapter 4. Finally, same method was applied than the polymer s-IPN: the HSE film was dried at room temperature in the glovebox and cured at 70°C under vacuum for 24h.

5.3. Results and discussion

5.3.1. Poly(NTFSI$_{0,2}$-co-PEGM$_{0,8}$) and poly(ZI$_{0,2}$-co-PEGM$_{0,8}$) synthesis and their characterization

Firstly, we characterized the cationic poly(NTFSI$_{0,2}$-co-PEGM$_{0,8}$) copolymer. Figure 6 displays its spectra before and after reaction obtained by ^{1}H NMR (Experimental method in Appendix A1). Vinyl groups, located between 6,1 and 5,8 ppm, completely disappeared after 6h reaction. Both signals from PEGM and NTFSI chemical structures can be observed in the final product (NTFSI ^{1}H spectrum is displayed in the Annex). FTIR-ATR was used to further verify the copolymer architecture and confirm the ionic exchange of chloride anions by bis(trifluoromethanesulfonyl)imide anions (TFSI^{-}). Figure 7 display its infrared spectrum (Experimental method in Appendix A1). Table 1 summarizes the main bands noticed for poly(NTFSI$_{0,2}$-co-PEGM$_{0,8}$). Bands related to PEGM monomer such as C-H stretching, carbonyl C=O stretching, CH_2 scissoring and C-O-C stretching are distinguished at 2870, 1750, 1450 and 1099 cm ^{1}. The trimethylammonium moiety vibrations modes are CH_2-N and the quaternary ammonium N^+ stretching, located at 1031 and 950 cm^{-1}. Characteristic bands of TFSI^{-} are noticed such as SO_2 asymmetric, C-S and S-N-S stretching respectively at 1350, 787 and 759 cm^{-1} [18]. Other TFSI^{-} bands are fully annotated in Figure 6. It can be concluded that the ionic exchange was successful and that poly(NTFSI$_{0,2}$-co-PEGM$_{0,8}$) is cationic copolymer.

Differential Scanning Calorimetry (DSC) was carried out to determine the glass transition (T_g) of poly(NTFSI$_{0,2}$-co-PEGM$_{0,8}$) (Experimental method in Appendix A3). The cationic copolymer is an oily material and is totally amorphous. The T_g was observed at -57,2°C. This value is similar to its anionic counterpart described in the previous chapter, poly(LiMTFSI$_{0,2}$-co-PEGM$_{0,8}$) (T_g=-58,6°C).

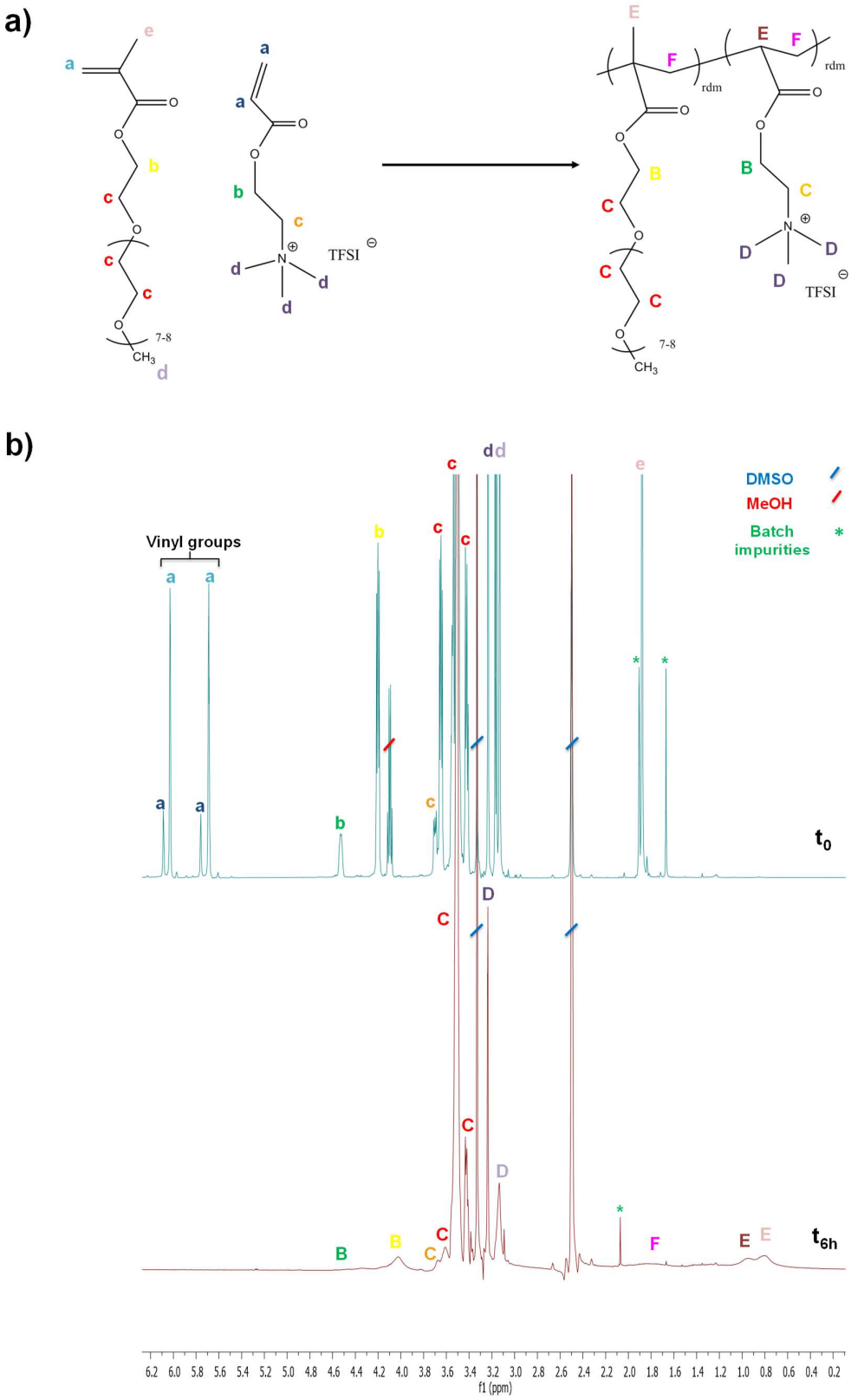

Figure 6: a) Reactional scheme of poly($NTFSI_{0,2}$-co-$PEGM_{0,8}$) synthesis; b)^{1}H NMR spectra of unreacted NTFSI and PEGM monomers (upper spectrum) and poly($NTFSI_{0,2}$-co-$PEGM_{0,8}$) (lower spectrum)

Table 1: Indexation of bands in Figure 7

Bands	ATR-FTIR vibrations	Wavenumber
1	C-H stretching	2870 cm^{-1}
2	C=O stretching	1750 cm^{-1}
3	CH_2 scissoring	1450 cm^{-1}
4	CH_2 bending and SO_2 stretching	1350 cm^{-1}
5	s+as CH_2 twisting	1270 & 1245 cm^{-1}
6	as CF stretching	1189 cm^{-1}
7	s SO_2, C-O-C and s C-F stretching	1132,1099 & 1058 cm^{-1}
8	CH_2-N stretching	1031 cm^{-1}
9	Quaternary ammonium and methacrylate backbone	950 & 848 cm^{-1}
10	TFSI characteristic bands: C-S, S-N-S and C-F stretching and C-F, S-N-S and SO_2 bending	787, 759, 748, 738, 653 & 617 cm^{-1}

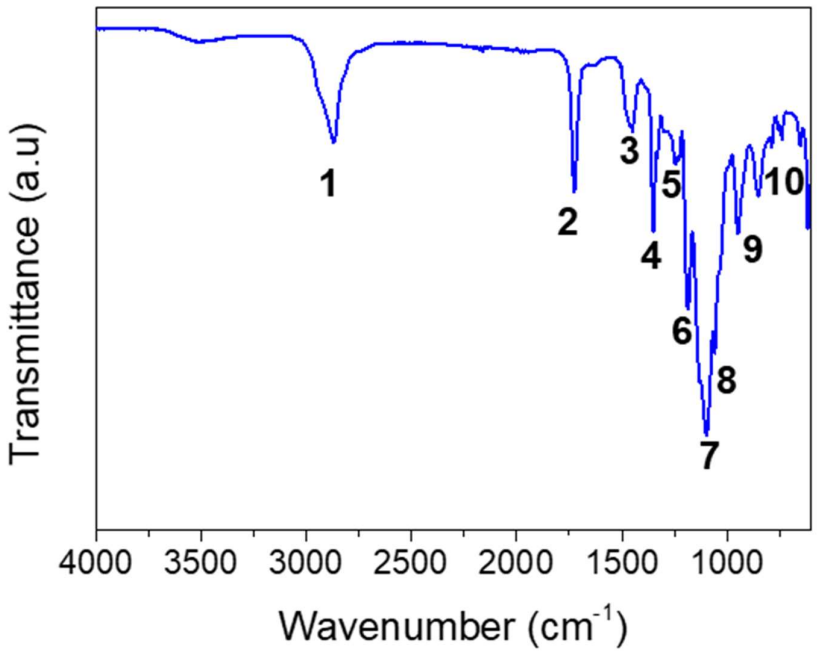

Figure 7: Verification of poly($NTFSI_{0,2}$-co-$PEGM_{0,8}$) chemical structure by ATR-FTIR

Same techniques were used to characterize poly($ZI_{0,2}$-co-$PEGM_{0,8}$) copolymer. ^{1}H NMR spectrum of the ZI monomer (presented in the Appendix) verifies the complexation of the anionic LiMTFSI and cationic NTFSI monomers. Both signals from PEGM, LiMTFSI and NTFSI chemical architectures can also be detected in the ^{1}H NMR spectrum of the final copolymer (Figure 8). Vinyl groups almost disappear after polymerization. Only small traces of monomers are discernible. The yield was estimated to 73%. The high viscosity of the reactive medium can explain this relatively low value in contrast with high yield of the previous free radical polymerization reactions.

Figure 9 displays the ATR-FTIR spectrum of the poly($ZI_{0,2}$-co-$PEGM_{0,8}$) copolymer. Table 2 summarizes the main bands related to poly($ZI_{0,2}$-co-$PEGM_{0,8}$) chemical structure. LiMTFSI moiety and $TFSI^-$ anion are chemically similar and share common vibrations bands. Nevertheless, after complexation of LiMTFSI and NTFSI monomers, many bands disappear such as 1350, 787 or 760 cm^{-1}. These vibration modes were attributed previously to the mobile $TFSI^-$ anion. This suggests that the ionic exchange was successful. Besides, the appearance of a new band at 1323 cm^{-1} further confirms the replacement of $TFSI^-$ by LiMTFSI moieties.

Then, the poly($ZI_{0,2}$-co-$PEGM_{0,8}$) copolymer can be considered as a “pseudo-zwitterionic” material. The term “pseudo-zwitterionic” was preferred, as the negative and the positive charges are not borne by a unique monomer moiety. On the contrary, the “pseudo-zwitterionic” charge in the poly($ZI_{0,2}$-co-$PEGM_{0,8}$) copolymer is shared by the two complexed adjacent monomer units of LiMTFSI and NTFSI.

Compared to the anionic poly($LiMTFSI_{0,2}$-co-$PEGM_{0,8}$) and cationic poly($NTFSI_{0,2}$-co-$PEGM_{0,8}$) copolymers, the pseudo-zwitterionic electrolyte has a very different aspect. It is extremely sticky and gummy. This structural change hints about the potential ionic interactions taking place in this polymer.

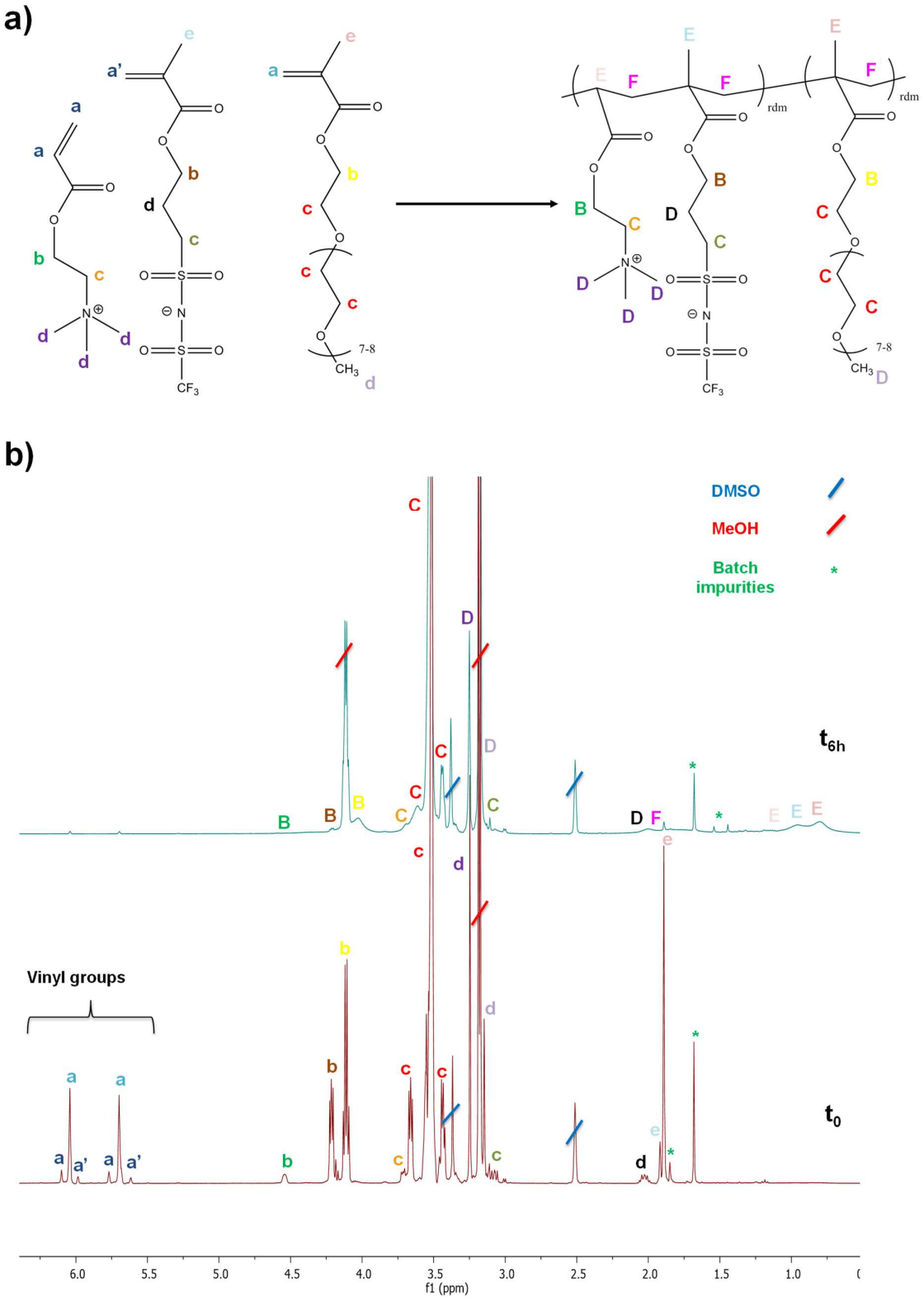

Figure 8: a) Reactional scheme of poly($ZI_{0,2}$-co-$PEGM_{0,8}$) synthesis; b)^{1}H NMR spectra of unreacted NTFSI and PEGM monomers (lower spectrum) and poly($ZI_{0,2}$-co-$PEGM_{0,8}$) (upper spectrum)

Table 2: Indexation of bands in Figure 9

Bands	ATR-FTIR vibrations	Wavenumber
1	C-H stretching	2870 cm^{-1}
2	C=O stretching	1750 cm^{-1}
3	CH_2 scissoring	1450 cm^{-1}
4	CH_2 bending and SO_2 stretching	1350 and 1323cm^{-1}
5	s+as CH_2 twisting	1271 & 1247 cm^{-1}
6	as CF stretching	1178 cm^{-1}
7	s SO_2, C-O-C and s C-F stretching	1136 & 1099 cm^{-1}
8	CH_2-N stretching	1031 cm^{-1}
9	Quaternary ammonium and methacrylate backbone	949 & 848 cm^{-1}
10	LiMTFSI characteristic bands: C-F, S-N-S and SO_2 bending	748, 650 & 621 cm^{-1}

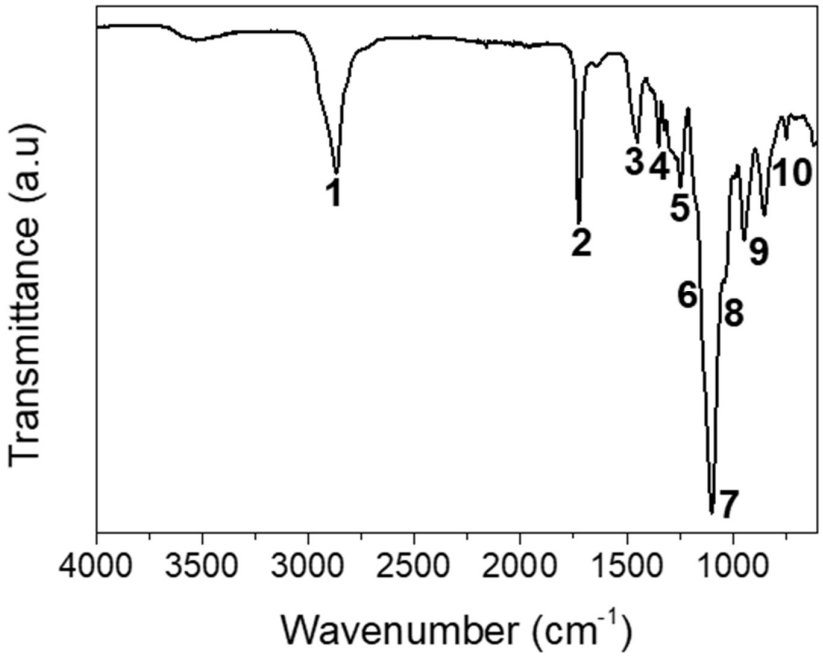

Figure 9: Verification of poly($ZI_{0,2}$-co-$PEGM_{0,8}$) chemical structure by ATR-FTIR

Electrochemical Impedance Spectroscopy (EIS) was used to determine the ionic conductivity of these electrolytes (Experimental method in Appendix B1). To be more concise, the cationic, anionic and pseudo-zwitterionic copolymers are going to be named respectively **C**, **A** and **ZI**. To ascertain the pseudo-zwitterionic nature of ZI copolymer, a mixture of A+C was also tested to see if their ionic behaviours are distinct or not. Figure 10 exhibits the corresponding Arrhenius plot. In addition, Table 3 reports the ionic conductivities at room and mild temperatures (25 and 60°C), with the activation energies. C shows higher ionic conductivity than A thanks to the well-known mobile nature of $TFSI^-$ anions as compared to Li ions. This is further emphasized by the difference of activation energies for these two copolymers. ZI shows the lowest ionic conductivity, implying that the ionic species are attached to the polymer backbone. Both cationic and anionic mobile species must remain, as its activation energy is an intermediate between C and A. The blend A+C is strongly different from ZI in term of ionic conductivity. This discrepancy originates by the presence of the additional counterions of Li^+ and $TFSI^-$.

Table 3. Summary of thermal and electrochemical properties of anionic, cationic and pseudo-zwitterionic copolymers

Copolymers	T_g (°C)	$\sigma_{25°C}$ (S/cm)	$\sigma_{60°C}$ (S/cm)	E_a (kJ/mol)
A=$LiMTFSI_{0,2}$-$PEGM_{0,8}$	-58,6	6.10^{-6}	3.10^{-5}	16,3
C=$NTFSI_{0,2}$-$PEGM_{0,8}$	-57,2	$1,9.10^{-5}$	$8,6.10^{-5}$	11
ZI=$ZI_{0,2}$-$PEGM_{0,8}$	-	4.10^{-7}	$2,4.10^{-6}$	15,8
A+C	-	$1,4.10^{-6}$	$7,6.10^{-6}$	16

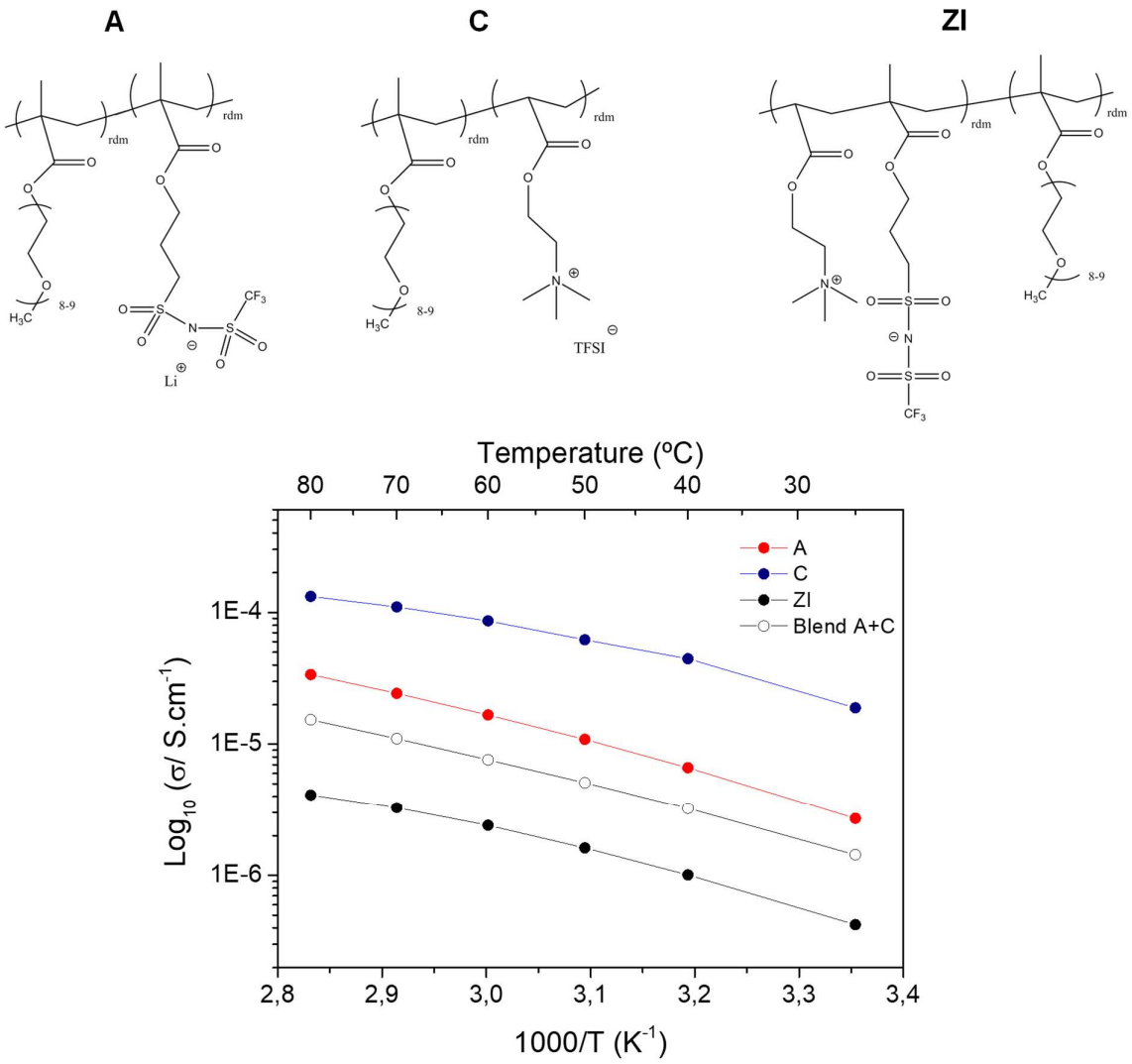

Figure 10: Chemical structure and Arrhenius plot of anionic, cationic and pseudo-zwitterionic copolymers

5.3.2. Physicochemical characterization and ionic conductivity study of pseudo-zwitterionic blend based on poly($ZI_{0,2}$-co-$PEGM_{0,8}$) copolymer.

Pseudo-zwitterionic poly($ZI_{0,2}$-co-$PEGM_{0,8}$) copolymer was further blended with the anionic poly($LiMTFSI_{0,2}$-co-$PEGM_{0,8}$) and cationic poly($NTFSI_{0,2}$-co-$PEGM_{0,8}$) copolymers. Sticky and jelly like materials were synthesized by simple mixing.(Figure 11.a). These electrolytes are going to be called later on as **ZI-A** and **ZI-C** electrolytes. This big discrepancy in term of mechanical properties implies the formation of a physical network thanks to the interactions of ZI moieties with the anionic or the cationic copolymer (Figure 11.a). In addition, the solid like properties are only maintained at low temperatures. Above 40°C, the blends, whether the copolymer used, start to be liquid. This feature further confirms the formation of reversible physical network. The ionic conductivity of these ionogels was evaluated and compared with the pristine copolymers (Figure 11.b)

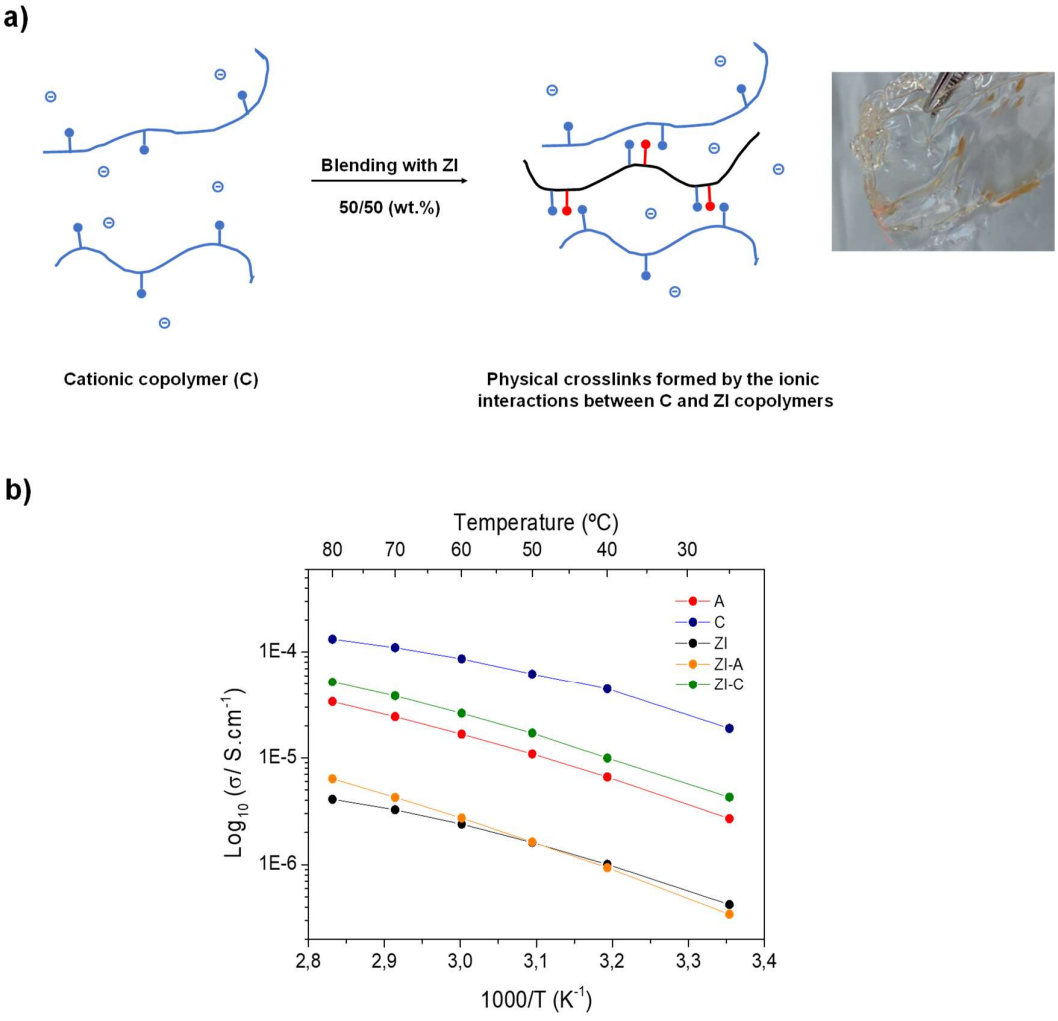

Figure 11: a) Schema representing the possible interactions between cationic (blue) and pseudo-zwitterionic (black) copolymers (ZI-C) and the photograph of the resulting blend; b) Comparison of the ionic conductivity of the ionic polymer blends and their anionic, cationic and pseudo-zwitterionic copolymers.

ZI-A and ZI-C ionic polymer electrolytes present lower ionic conductivity than the individual anionic and cationic copolymers. Mobile ions may be trapped into ionic crosslinks, explaining the lower ionic conductivity and increased activation energies (Table 4). ZI-C may form weaker ionic complexes than ZI-A, as its E_a is lower. Sulfonate based PILs were reported to form strong interactions with salts[19]. Wohde and co-workers highlight that Li ions are greatly immobilized by their interactions with sulfonated zwitterionic salts. This characteristic can explain the low conductivity and the high activation energy of ZI-A blend. Then, ZI-C was preferred as potential pseudo-zwitterionic polymer matrix to have a comprise between mechanical stability and ionic conduction.

Table 4. Summary of the ionic conductivities (25°C and 60°C) and the activation energies of the ionic polymer blends ZI-A and ZI-C

Ionic polymer blends	$\sigma_{25°C}$ (S/cm)	$\sigma_{60°C}$ (S/cm)	E_a (kJ/mol)
ZI-A	$3{,}4.10^{-7}$	$2{,}7.10^{-6}$	20,2
ZI-C	$4{,}3.10^{-6}$	$2{,}6.10^{-5}$	17,4

ATR-FTIR was carried out to better understand the ionic interactions taking place in this complex ionic polymer electrolyte. The resulted spectra of C, ZI and ZI-C are shown and compared in Figure 12. FTIR-ATR verifies the existence of interactions between ZI and C moieties. Blue lines in Figure 12 indicate the major changes of $TFSI^-$ bands once C is mixed with ZI. A red shift and an intensity decrease for mobile $TFSI^-$ bands are noted. For example, υ_{as}(CF) stretching and δ_s (S-N-S) bending located at 1187 cm^{-1} and 653 cm^{-1} move to 1183 and 650 cm^{-1}. This indicates that the interaction between the trimethylammonium moiety and $TFSI^-$ is weakened[20]. Left vibrations bands decrease in intensity and become wider, such as υ_s (SO_2) and +υ_s (CF) stretching at 1134 and 1058 cm^{1}. This suggests that $TFSI^-$ is dissociated thanks to the presence of ZI moieties. The disappearance of the band related to ion pairs at 1224 cm^{-1} further confirms the dissociation of $TFSI^-$ anions (denoted by the red line in Figure 12). Besides, the vibration mode corresponding to the quaternary ammonium ($\upsilon_s(CH_2\text{-}N)$ stretching) from C and ZI copolymers become broader in the blend, implying potential interactions. The lower ionic conductivity measured for ZI-C is then not linked to the $TFSI^-$ agglomerates but come from the decreased flexibility of the polymer matrix due the physical crosslinks formed in the electrolyte.

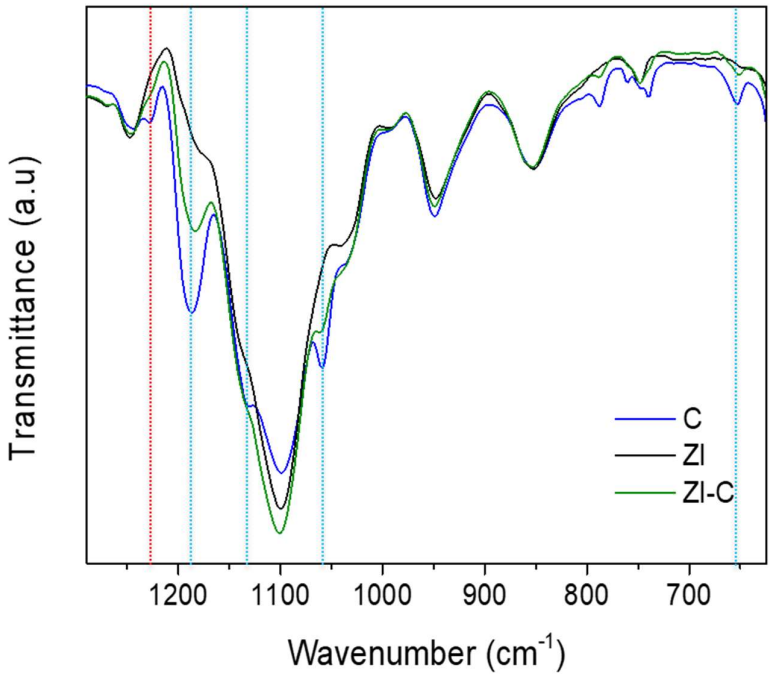

Figure 12: Comparison of FTIR-ATR spectra of the anionic and pseudo-zwitterionic copolymers (C and ZI) and their respective ionic polymer blend ZI-C

5.3.3. Physicochemical characterization and ionic conductivity study of pseudo-zwitterionic blend based on poly($ZI_{0,2}$-co-$PEGM_{0,8}$) copolymer and LiFSI salt.

LiFSI salt was added in the ionic polymer blend ZI-C to increase the concentration of mobile Li^+ ions and for its ability to form stable SEI layer. ZI-C is an interesting polymer matrix to be mixed with high salt content, as the pseudo-zwitterionic moieties can play the role of ionic dissociator. As shown previously, poly($ZI_{0,2}$-co-$PEGM_{0,8}$) enables to lessen the interaction between $TFSI^-$ anions and the cationic copolymer. It can be also considered that the presence of pseudo-zwitterionic moieties in the blend can help to dissociate to some extent high concentration of salt. This property is extremely promising as polymer-in-salt systems present stable SEI toward Li metal. Firstly, no depletion of salt occurs near the electrodes, which favourizes a stable Li stripping/plating. Secondly, if the SEI is fractured by Li dendritic growth, this latter can be reformed easily thanks to the large salt content.

Besides, the cationic poly($NTFSI_{0,2}$-co-$PEGM_{0,8}$) copolymer can also help to break ionic clusters by interacting with the anions. Recently, PMMA and polycation poly(diallyldimethylammonium) bis (trifluoromethanesulfonyl)imide (PDADMATFSI) were compared as polymer host to form gels. PDADMATFSI electrolyte was reported to have higher ionic conductivity than the usual PMMA gel, thanks to its interactions with anionic species[21]. Then, the use of a cationic copolymer can be strongly beneficial for the ionic dissociation. To apply this hypothesis, 30 and 45 wt.% LiFSI was added to the blend formulation. The ionic polymer blend tends to strengthen upon the addition of salt. The resulted electrolytes are named **ZI-C_30** and **ZI-C_45**. Figure 13 exhibits the Arrhenius plot of these materials and Table 5 summarizes the ionic conductivities along with their activation energies.

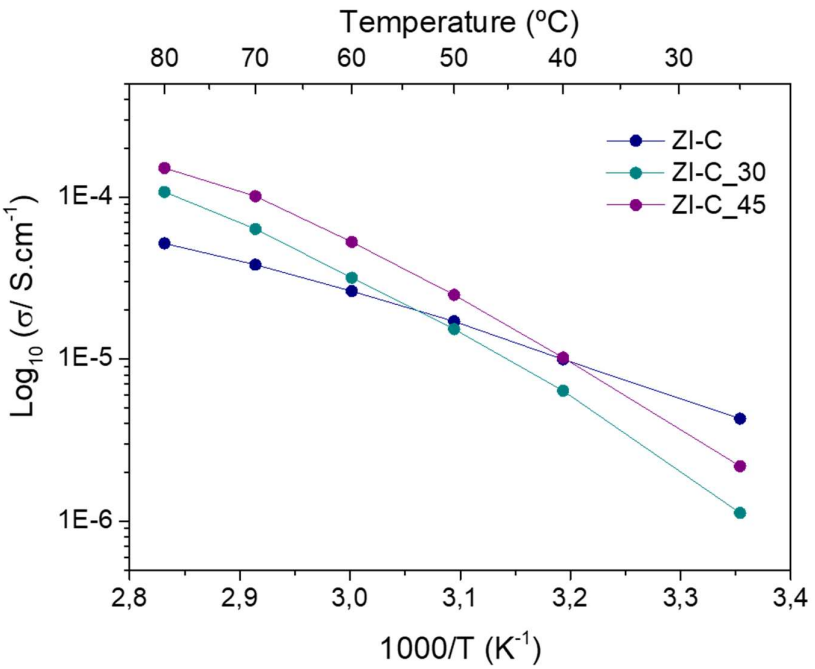

Figure 13: Arrhenius plot of the ionic polymer blends ZI-C with increased LiFSI content (wt.%)

Table 5: Summary of the ionic conductivities (25°C and 60°C) and the activation energies of the ionic polymer blends ZI-C doped with LiFSI salt.

Ionic polymer blends with salt	$\sigma_{25°C}$ (S/cm)	$\sigma_{60°C}$ (S/cm)	E_a (kJ/mol)
ZI-C	$4{,}3.10^{-6}$	$2{,}6.10^{-5}$	17,4
ZI-C_30	1.10^{-6}	$3{,}2.10^{-5}$	31,4
ZI-C_45	$2{,}2.10^{-6}$	$5{,}3.10^{-5}$	28

First of all, the change of slope of the ionic polymer blends doped with LiFSI salt indicates a distinct ionic conduction mechanism than the blend ZI-C. At room temperature, the ionic conductivity is slightly impacted by the large addition of LiFSI, whether the composition studied. The ionic polymer blend ZI-C achieves $4{,}3.10^{-6}$ S/cm, instead of 1.10^{-6} and $2{,}2.10^{-6}$ S/cm for ZI-C_30 and ZI-C_45 respectively. This decrease can be explained by the higher activation energies calculated for these electrolytes: from 17,4 kJ/mol, it almost doubles in presence of LiFSI. Ion pairs between poly($NTFSI_{0,2}$-co-$PEGM_{0,8}$), poly($ZI_{0,2}$-co-$PEGM_{0,8}$) and LiFSI salt must happen, rigidifying the blend at low temperatures. However, ZI-C_30 and ZI-C_45 both have better ionic conductivities at mild and high temperatures. With the heat, the doped ionic polymer blends soften, as physical interactions fade off with the temperature. The composition ZI-C_45 reaches 5.10^{-5} S/cm at 60ºC, which is the double than the ionic polymer blend ZI-C. Surprisingly, this highest composition of salt presents the best ionic conductivity in the whole range of temperature. In addition, its large LiFSI concentration is expected to help to passivate the SEI. This feature may lead to propitious environment for stable Li stripping/plating. Unfortunately, it was not possible to increase further LiFSI content in the ionic polymer blend ZI-C. Difficult homogenisation of the polymer batch and poor film formation limited our study to 45 wt.% of salt.

FTIR-ATR was used to shed light on the additional physical interactions in presence of LiFSI (Figure 14). Characteristic bands of FSI can be noticed such as $\upsilon_{as,\,oop}(SO_2)$, $\upsilon_{s,\,oop}(SO_2)$, υ_{as} (S-N-S) and υ_s (S-N-S) stretching situated at 1380, 1178 and 1217, 825 and 739 cm^{-1} (Blue lines) [22]. The two last vibration modes are closely related to ionic clusters $Li^{+}\cdots FSI^{-}$ [23]. They tend to shift blue with increased LiFSI content. This greatly implies the formation of large ionic aggregates. However, the ionic conductivity of the doped ionic polymer blends is slightly affected by these clusters, even at 45 wt.% LiFSI. Beneficial ionic environment must be accounted to explain this high ionic conductivity, especially above 40°C. Cationic poly($NTFSI_{0,2}$-co-$PEGM_{0,8}$) and pseudo-zwitterionic poly($ZI_{0,2}$-co-$PEGM_{0,8}$) copolymers enable to dissolve high content of LiFSI in the polymer matrix. Decreased intensity and wider bands can be observed for $\upsilon_s(CH_2\text{-}N)$ stretching and δ_s (SO_2) bending, located at 1031 and 618 cm^{-1} (Red lines). These modes are associated to tethered $TFSI^-$ and trimethylammonium $N^+(CH_3)_3$ from poly($NTFSI_{0,2}$-co-$PEGM_{0,8}$) and poly($ZI_{0,2}$-co-$PEGM_{0,8}$). This suggests potential interactions between LiFSI and the ionic copolymers at the expense of $TFSI^-$ anions. Its band at 1350 cm^{-1} shifts blue and its intensity becomes higher with the increase of LiFSI. PEGM also helps the ionic dissociation of LiFSI salt to some extent. Vibration modes of the carbonyl and ethylene oxide units tends to decrease in intensity and become broader, such as υ_s(C=O) and δ_s (CH_2) scissoring observed at 1750 and 1450 cm^{1}.

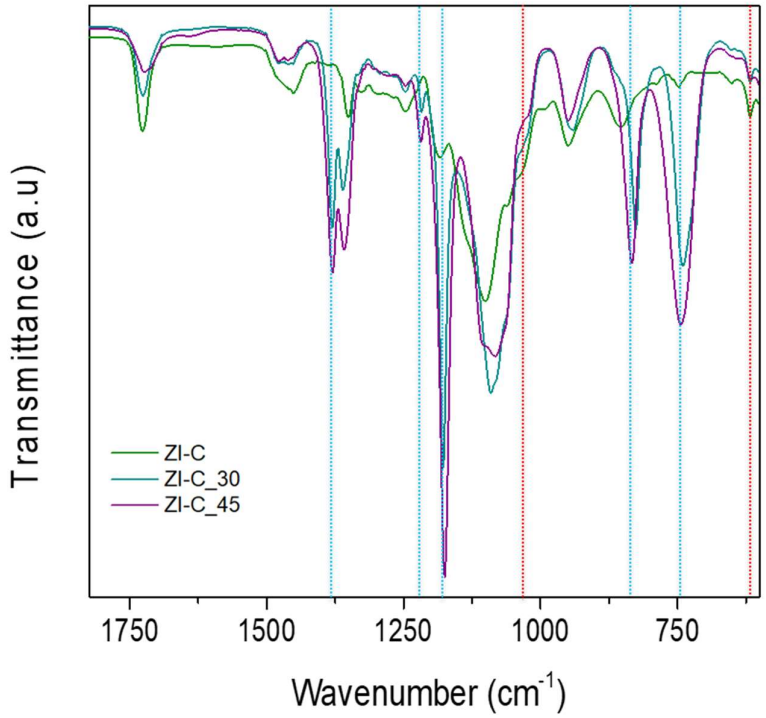

Figure 14: Comparison of FTIR-ATR spectra of the ionic polymer blends ZI-C doped with LiFSI salt.

Figure 15 depicts the possible interactions in the ionic polymer blend ZI-C in presence of high concentration of LiFSI salt.

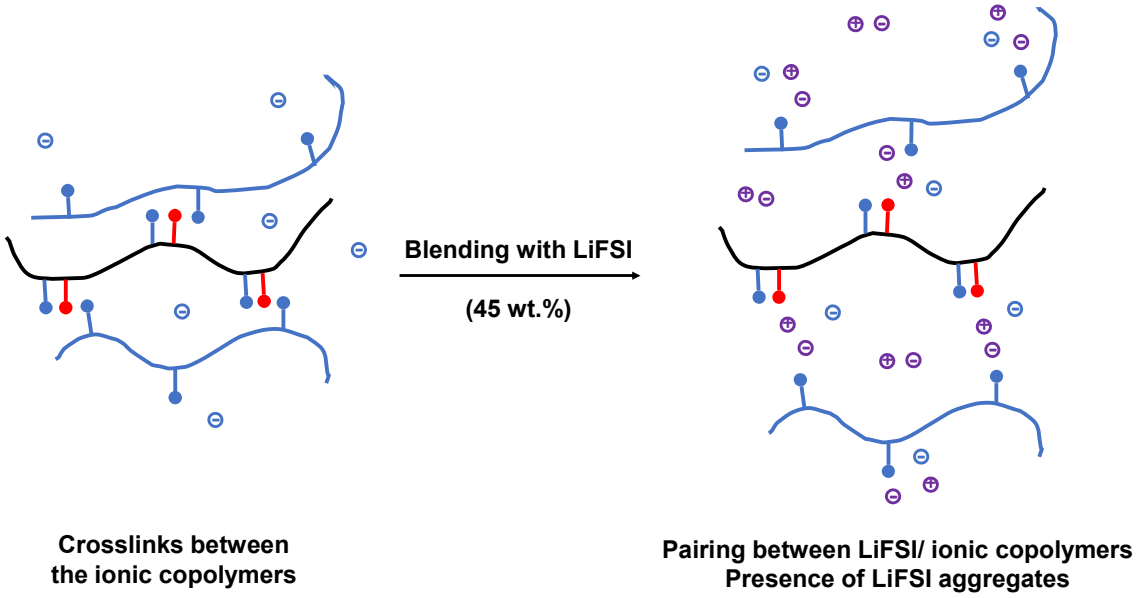

Figure 15: Schema representing the possible interactions between the cationic poly($NTFSI_{0,2}$-co-$PEGM_{0,8}$) copolymer (blue) , the pseudo-zwitterionic poly($ZI_{0,2}$-co-$PEGM_{0,8}$) copolymer (back) and the LiFSI salt (purple).

This representation considers the observations from our FTIR-ATR analysis and examples from the literature[12]. Several studies reported the “swelling” behaviour of polyzwitterions complexing with salts. As a matter of fact, strong intra and interchain associations happen in such ionic polymers because of the presence of dipole-dipole interactions[9]. In presence of salt, polyzwitterions are often observed to “expand” (in other worlds their polymer chains disentangle), as extra ionic species weaken the coulombic interactions between the zwitterionic pendants. Then, we can hypothesize that LiFSI salt screen the complexation between the cationic poly($NTFSI_{0,2}$-co-$PEGM_{0,8}$) and the pseudo-zwitterionic poly($ZI_{0,2}$-co-$PEGM_{0,8}$) copolymers. The formation of strong ion pairs at room temperature limits fast Li^+ conduction. However, these interactions soften at higher temperatures, which explains the bigger ionic conductivity observed for the ionic polymer blends ZI-C after salt doping.

To conclude, even if the high LiFSI content generates large ionic aggregates, the presence of the cationic poly($NTFSI_{0,2}$-co-$PEGM_{0,8}$) and the pseudo-zwitterionic poly($ZI_{0,2}$-co-$PEGM_{0,8}$) copolymers promote beneficial ionic environment for Li ion conduction, especially at high temperature. Unfortunately, these electrolytes are not properly self-standing as the physical crosslinks fade once the temperature is risen to 40°C. The formation of a semi-interpenetrated network (s-IPN) within the ionic polymer blends may enable a compromise of flexibility and mechanical stability at mild temperature. Such solid electrolytes were simply synthesized by the addition of the poly(ethylene glycol) dimethacrylate (PEGDM) monomer and a thermal initiator in the ZI-C composition. Then, thermal treatment of the films leads to the crosslinking of PEGDM in the ionic polymer blend. In addition to the superior mechanical properties, the increased concentration of ethylene oxide units should further dissociate LiFSI salt. ZI-C_45 composition was then selected to form pseudo-zwitterionic polymer and hybrid s-IPNs.

5.3.4. Physicochemical characterization and ionic conductivity study of hybrid and polymer semi-interpenetrated networks (s-IPN) based on pseudo-zwitterionic poly($ZI_{0,2}$-$PEGM_{0,8}$) copolymer, LiFSI salt and LLZO particles.

Semi-IPN formation was easy to be implemented to get free-standing polymer films from the previously described materials. A photograph and a schematic representation of this complex ionic polymer s-IPN are depicted in Figure 16. The PEGDM crosslinking leads to improve the mechanical stability of the ionic polymer blend, but without compromising the flexibility and the stickiness. For hybrids, 10 wt.% LLZO was chosen. Polymer and hybrid semi-IPNs electrolytes are going to be labelled **I-ZI-C_45** and **HI-ZI-C_45** respectively. Their thicknesses were comprised between 200 and 300 µm.

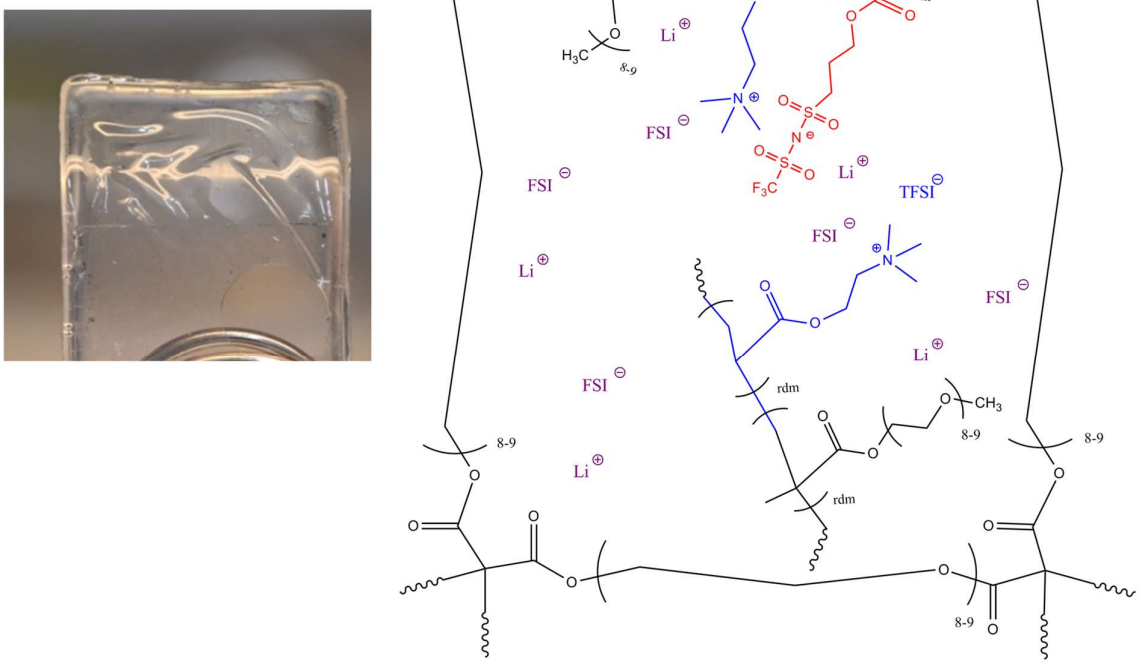

Figure 16: Photograph and schematic representation of the polymer s-IPN electrolyte

Figure 17 presents the Arrhenius plot comparing the s-IPN to the original ionic polymer blend ZI-C_45. The ionic conductivity is lightly decreased at room temperature because of the solid architecture induced by the s-IPN. From $2{,}2.10^{-6}$ S/cm, it drops to 9.10^{-7} S/cm for the polymer s-IPN I-ZI-C_45. Table 6 reports the ionic conductivity and the activation energy of the s-IPNs. After thermal curing, the activation energy rises to the large value of 38 kJ/mol. Up

to 60°C, the IPN electrolyte achieves identic ionic conductivity than the previous ionic blend polymer ZI-C_45 (5,3.10^{-5} S/cm). This is extremely engaging as this electrolyte can perform in solid state cells. The addition of LLZO particles in the polymer s-IPN matrix slightly improves the ionic conductivity in the whole range of temperature. This latter increases to 1,3.10^{-6} and 5,5.10^{-5} S/cm at 25°C and 60°C respectively. Small content of LLZO can also reduce the activation energy, from 38,4 to 37,3 kJ/mol. As elucidated in the previous chapters, LLZO particles can interact with mobile and tethered anions. It can be supposed that the particles are able to break LiFSI ionic clusters, increasing the Li mobility.

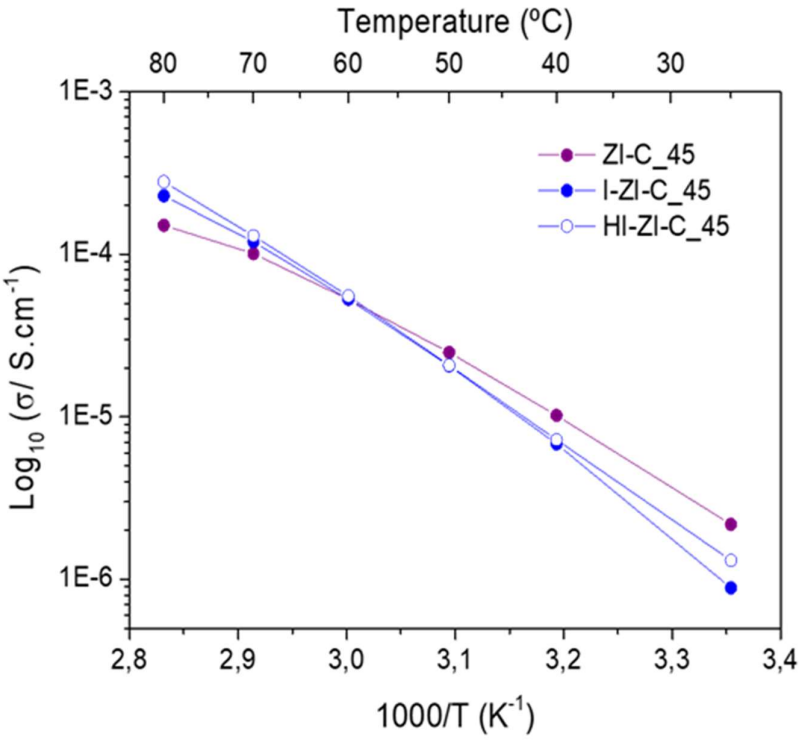

Figure 17: Arrhenius plot of polymer and hybrid s-IPNs

Thermal properties of the polymer and hybrid s-IPN were also examined. Figure 18 exhibits the DSC traces of these electrolytes. The incorporation of PEGDM reticulated network in the ionic polymer blend ZI-C induces a decrease of the chain mobility. The glass transition temperature can be clearly distinguished at T_g =-11,7°C in the DSC trace of the polymer s-IPN I-ZI-C_45. Unfortunately, the T_g is not discernible for the hybrid composition HI-ZI-C_45. Surprisingly, an additional thermal transition can be noticed for the polymer s-IPN: an exothermic peak, likely a cold crystallisation, appears at T_c=75°C. This is startling, as the polymer s-IPN is supposed to be fully amorphous. Such transition does not occur in the hybrid s-IPN.

It was reported that zwitterionic ionic liquids can form crystals by self-assembly[24].Qiao and co-workers observed for these materials similar thermal transitions and attributed them to the crystallization of dissociated zwitterionic species[25]. In other words, this type of transition is

related to the rearrangement of zwitterions during the cooling and heating steps. This interesting similarity goes along with the assumption developed in section 5.3.3, which explains the formation of strong ion pairs between the LiFSI salt, the cationic poly($NTFSI_{0,2}$-co-$PEGM_{0,8}$) and the pseudo-zwitterionic poly($ZI_{0,2}$-co-$PEGM_{0,8}$) copolymers. We can imagine that the ionic polymer blend phase within the s-IPN can be structurally modified by the succeeding heating and cooling steps. This results to the appearance of a cold crystallization transition on the DSC trace. The absence of such transition for the hybrid s-IPN maybe comes from the possible "immobilization" of ionic species (anchored and mobile) in presence of LLZO particles, limiting their rearrangement during the cooling and the heating steps.

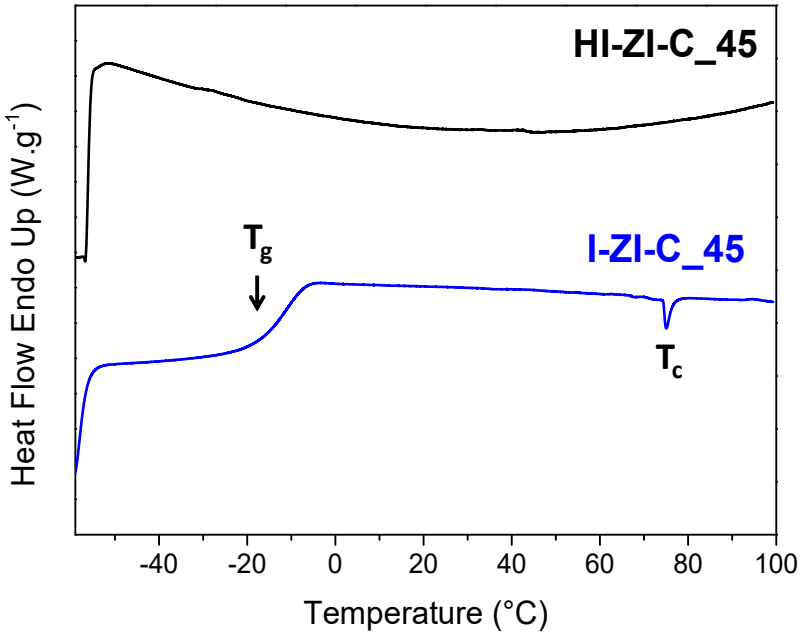

Figure 18: DSC traces of polymer and hybrid s-IPNS I-ZI-C_45 and HI-ZI-C_45

Table 6: Summary of thermal and electrochemical properties of polymer and hybrid s-IPNs

s-IPN	T_g (°C)	Tc (°C)	$\sigma_{25°C}$ (S/cm)	$\sigma_{60°C}$ (S/cm)	E_a (kJ/mol)
I-ZI-C_45	-11,7	75	9.10^{-7}	$5,3.10^{-5}$	38,4
HI-ZI-C_45		-	$1,3.10^{-6}$	$5,5.10^{-5}$	37,3

FTIR-ATR was performed on polymer and hybrid s-IPNs to analyse the modifications of the ionic interactions after PEGDM crosslinking and the addition of LLZO particles. Figure 19 compiles the spectra of the ionic polymer blend ZI-C_45, the polymer s-IPN I-ZI-C_45 and the hybrid s-IPN HI-ZI-C_45.

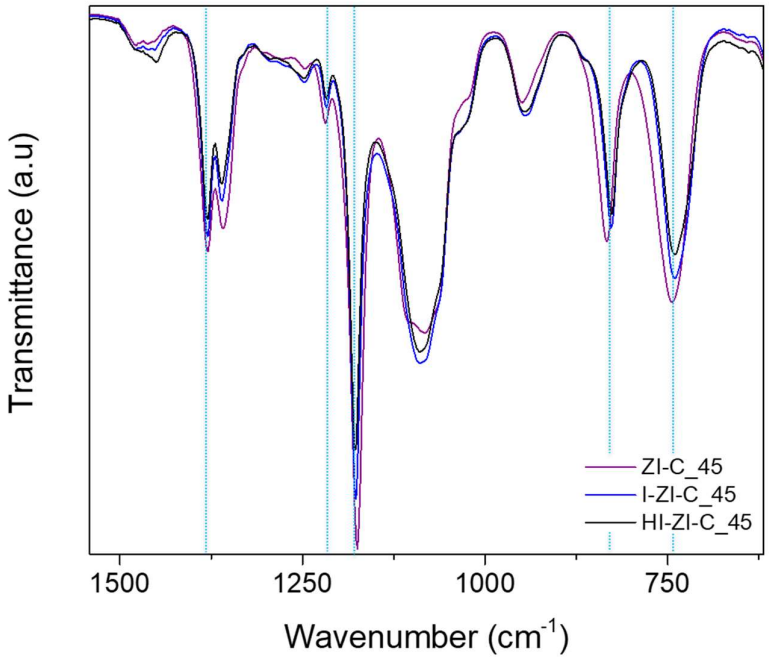

Figure 19: Comparison of FTIR-ATR spectra of the ionic polymer blend (ZI-C_45), the polymer s-IPN (I-ZI-C_45) and the hybrid s-IPN (HI-ZI-C_45)

The intensity decrease of LiFSI vibration modes are noticed in the polymer s-IPN when compared to the previous ionic polymer blend. These bands are shown in Figure 19 by the blue lines in the spectra. The addition of LLZO particles further emphasizes the intensity decrease of the concerned modes. Especially, bands related to ion pairs (830 and 740 cm^{1}) shift red for polymer and hybrid s-IPNs. This suggests the break-up of LiFSI ion pairs by the help of additional ethylene oxide units and their interactions with the inorganic particles. LLZO particles , even at low content, are beneficial to the ionic conductivity. However, shoulders are observed at 1451 and 865 cm^{1}, which are characteristic of Li_2CO_3 formation. Small contamination of LLZO particles by water impurities cannot be moved aside, despite extra care about solvent dryness. The polymer and hybrid s-IPN I-ZI-C_45 and HI-ZI-C_45 were then selected for electrochemical tests.

5.3.4. Electrochemical application in Li/Li symmetrical cells

Compared to the previous solid electrolytes investigated in this project, no SEI stabilizer are needed in I-ZI-C_45 and HI-ZI-C_45 formulations. Large LiFSI content must be enough to form a stable SEI. However, the ionic conductivity is still critical (below 10^{-4} S/cm). To reach high current densities, small of content of dried TEGDME (10 wt.%) was added to boost the ionic conduction at 60°C while maintaining the mechanical stability of the electrolyte. The resulted ionic conductivity was measured to be 9.10^{-5} S/cm for both the pristine and hybrid electrolytes. Then, plasticized I-ZI-C_45 and HI-ZI-C_45 IPNs were assembled in Li symmetrical cells to evaluate their stability towards the lithium (Experimental method in Appendix B2). The cell pressure was set up to 3,2 N.m. The ECM used for resistance determination was composed of two CPEs, assigned to R_{bulk} and R_{SEI} (the model is shown in Figure 21). The stability of I-ZI-C_45 and HI-ZI-C_45 towards the Lithium is displayed in Figure 20.

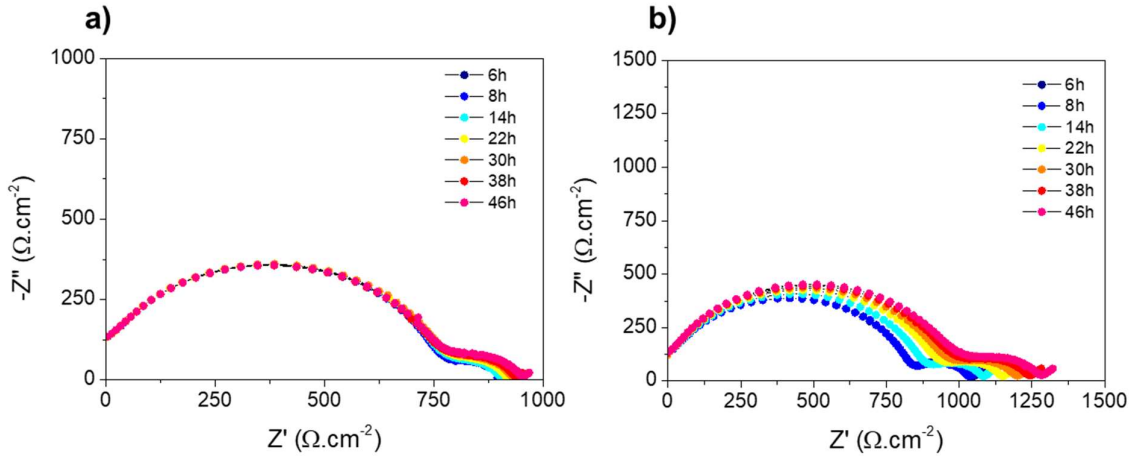

Figure 20: Evaluation of the electrolyte stability towards the lithium by monitoring the resistances in Li symmetrical cells over time: a) EIS spectra of Li| I-ZI-C_45 |Li; b) EIS spectra of Li| HI-ZI-C_45 |Li.

Extremely stable interface with low resistance is formed when the Li metal is coupled with the plasticized polymer s-IPN I-ZI-C_45 (Figure 20.a). The high concentration of FSI anions, regulated by the pseudo-zwitterionic and cationic moieties, allows to form a LiF rich and thin SEI. R_{SEI} grows from 180 to only 230 Ω in 46h. Compared to plasticized polymer s-IPN, the hybrid has a bigger SEI resistance and looks to take more time to stabilize (Figure 20.b). Both R_{bulk} and R_{SEI} increase from 810 Ω and 230 Ω to 900 Ω and 290 Ω up to 38h of stabilization. Then, the resistances start to remain steady. This difference can be explained by Li reaction with LLZO or the reduced decomposition of FSI anions due to their interaction with the particles. Potential LLZO contamination by water traces can be also considered to explain this behaviour. Nevertheless, both hybrid and polymer s-IPN electrolytes have excellent chemical stability towards Li metal thanks to high LiFSI content.

Transference numbers were also calculated for the polymer and hybrid s-IPNs, without the presence of plasticizer (Experimental method in Appendix B4). Figure 21 exhibits the representative EIS spectra before and after polarization, along with the intensity decay, of the polymer s-IPN I-ZI-C_45. Red lines on EIS spectra represent the fitting of the equivalent circuit model used for the determination of R_{bulk} and R_{SEI} (Figure 21.b). Compared to the plasticized I-ZI-C_45, the dry electrolyte shows a dramatic increase of bulk and interfacial resistance. R_{bulk} increases from 735 to 2450 Ω without the addition of the glyme plasticizer. R_{SEI} is also affected, rising from 180 to 860 Ω. TEGDME improves the ionic conductivity (so R_{bulk}) by breaking LiFSI ion pairs, but its most beneficial effect is the enhancement of the interfacial contact between the electrolyte and the lithium. The liquid plasticizer allows to "wet" the Li surface, leading to an optimized interface.

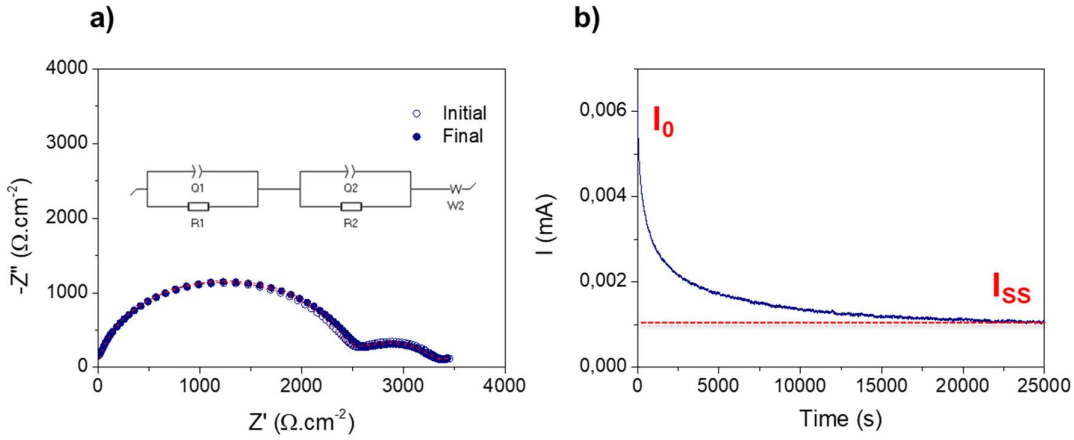

Figure 21: Determination of the transference number of I-ZI-C_45 by Bruce's method: a) Intensity decay after polarization of Li| I-ZI-C_45 |Li cell; b) Resulted EIS spectra before and after cell polarization.

Lithium transference numbers (TN) are reported in Table 7. Despite acceptable ionic conductivity at 60ºC, a value of 0,14 is determined for the polymer s-IPN I-ZI-C_45. This value is highly similar to the ones calculated for diluted PEO-LiFSI and PEO-LiTFSI systems[26], in spite of the high salt content of I-ZI-C_45. Pozycska and co-workers investigated the evolution of the transference number of PEO-LiTFSI electrolyte at elevated temperatures, according to the weight fraction of LiTFSI[27]. They demonstrated that the Li^+ transport number drops slightly with the addition of salt and then starts to rise for the highest compositions. The increase of viscosity and the formation of ionic aggregates tend to slow down the ionic motion of the polymer phase for low salt content. Intermediate compositions (between 40 and 60 wt.%) present the lowest TN values. Above 60 wt.%, the electrolyte shifts to the polymer-in-salt regime, where only the Li ions can move through the percolation of ionic aggregates. Thanks to this study, it can be estimated that PEO electrolyte with 45 wt.% LiTFSI salt has a low TN equal to 0,09. This value is quite distinct from I-ZI-C_45. This discrepancy can be explicated by the presence of tethered cationic and pseudo-zwitterionic moieties which can enhance the ionic dissociation of LiFSI. Then, the ionic conductivity mainly relies of the mobility of anions or negatively charged ionic aggregates. On the other hand, the transport number is almost doubled for the hybrid. This result emphasizes the potential of LLZO as ionic dissociator in

dual salt polymer electrolytes. Anions are efficiently immobilized by small content of garnet particles. The incorporation of plasticizer (TEGDME) in polymer and hybrid s-IPN may further enhance the salt dissociation and increase the transference number.

Li^+ diffusion coefficients were determined by the method developed by Ma and co-workers[28] and are reported in Table 7 (Experimental method in Appendix B3). These results are in good agreement with values previously reported on ionic liquids-based gel polymer electrolytes. Porthault et al. evidence the relationship between transport number and Li^+ diffusion coefficient in presence of high concentration of LiTFSI and N-propyl-N-methylpyrrolidinium bis(trifluoromethanesulfonyl)imide (PYR13TFSI) ionic liquid in a crosslinked methacrylate polymer host[29]. These low values confirm the high concentration of ionic aggregates. The distinct D_{Li+} values between the polymer and hybrid s-IPN can be further clarified by the nature of ionic aggregates, due to the immobilization of FSI anions by the LLZO particles.

Table 7. Summary of the Li^+ transport properties of pristine and hybrid IPNs at 60°C

IPN	Transference number	Li^+ diffusion coefficient D_{Li+}(cm^2/s)
I-ZI-C_45	0,14	$4{,}27.10^{-13}$
HI-ZI-C_45	0,26	$1{,}67.10^{-13}$

Li symmetrical cells based on dry and plasticized polymer s-IPNs I-ZI-C_45 were assembled to assess their cycling performance. Dry I-ZI-C_45 can cycle up to 0,25 $mA.cm^{-2}$ (Figure 22.i.a). Above this value, voltage drop occurs, along with intense voltage spikes. Nevertheless, the dry electrolyte can cycle up to 2 $mA.cm^{-2}$. Surprisingly, the cell resistance does not go down after the test, implying that no dendrites formed over cycling (Figure 22.i.b). R_{SEI} increases only from 490 Ω to 750 Ω. This limited CCD may come from insufficient ionic conductivity or poor interfacial contact between the lithium and the electrolyte. R_{bulk} is impressively big (3230 Ω). Nevertheless, the electrolyte can withstand higher current densities without dendrites penetration. Presence of high salt content can reform instantaneously the SEI despite the uneven Li deposition/dissolution. Upon addition of the glyme plasticizer, the performance of the polymer s-IPN I-ZI-C_45 is greatly enhanced (Figure 22.ii.a). R_{bulk} decreases drastically in presence of the plasticizer (844 Ω before cycling). Homogeneous stripping/plating processes are taking place up to 0,25 $mA.cm^{-2}$. Above, high polarization occurs, generated by the formation of salt concentration gradients. Mossy like deposition/dissolution happen clearly at the high current density of 1 $mA.cm^{-2}$, thanks to the observation of neck shaped voltage profiles. The electrolyte cannot be cycled efficiently above, its CCD was then established to 1 $mA.cm^{-2}$. Figure 22.ii.b displays the EIS spectrum after cycling. Cell resistance did not drop, which indicates that no dendrites were formed. R_{SEI} only increases from 240 Ω to 360 Ω. This electrolyte is then extremely promising as potential anolyte for Li metal-based batteries.

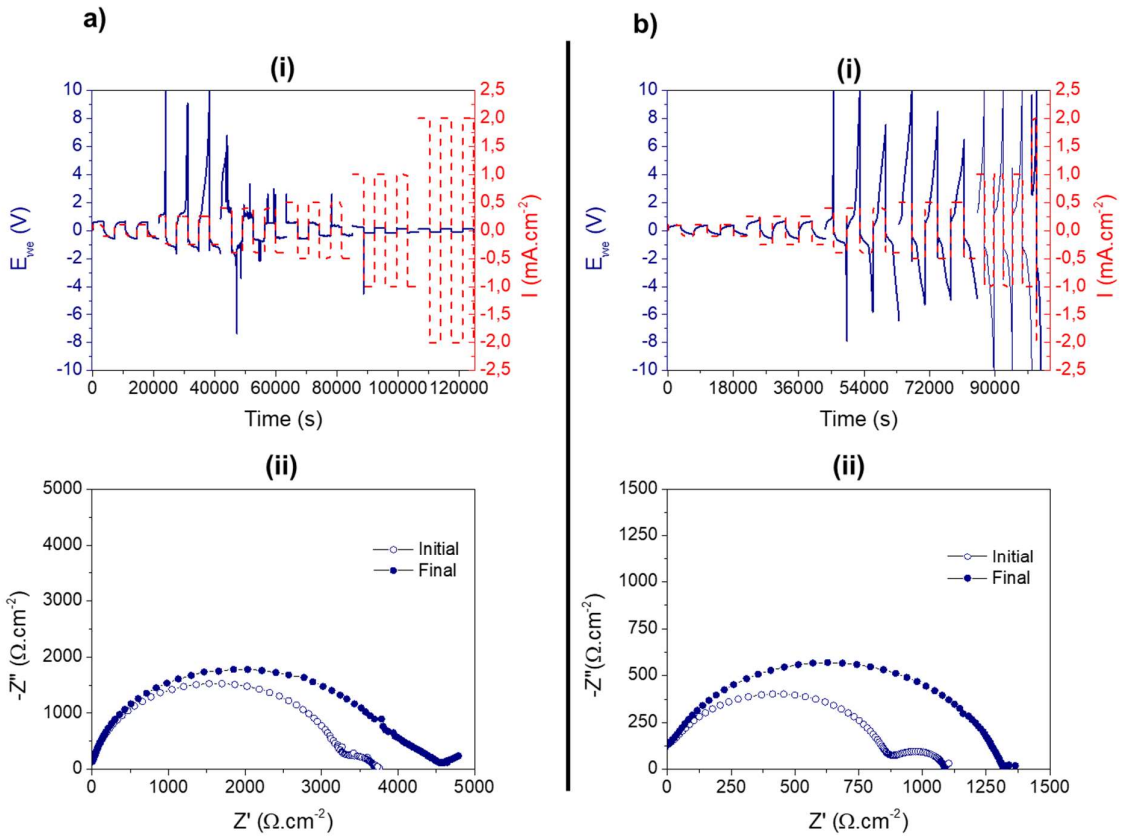

Figure 22: Galvanostatic cycling performance of i) Li| I-ZI-C_45 |Li and ii) Li| I-ZI-C_45 + TEGDME|Li cells composed of a) Voltage profiles regarding increased current densities; b) EIS spectra before and after cycling.

Galvanostatic test was then applied to the hybrid s-IPN HI-ZI-C_45 in Li symmetrical cell. The result is shown in Figure 23.a. Unfortunately, LLZO worsens the cycling performance of the polymer s-IPN. The electrolyte can cycle up to 0,25 mA.cm^{-2}, despite high polarization. The voltage starts to drop down at 0,5 mA.cm^{-2}. The current density of 0,4 mA.cm^{-2} was then designated as CCD. Typical voltage spikes can be noticed above this current density, sign of heterogenous Li stripping/plating. Nevertheless, the electrolyte can withstand up to 2 mA.cm^{-2}. Dendrites do not form during cycling as R_{bulk} and R_{SEI} both increase after cycling, despite the observation of erratic voltage above the CCD (Figure 23.b). This poor performance is quite surprising considering the superior cyclability of the polymer s-IPN. It was expected that the addition of LLZO can further improve the cycling efficiency, thanks to the improvement of the Li transference number and a better interface with Li metal. Compared to the hybrid developed in Chapter 4, HI-ZI-C_45 achieves higher ionic conductivity, better interfacial contact and enhanced SEI than HCLi$_{0.5}$BL-25. However, this latter manages to reach a CCD of 0,4 mA.cm^{-2}. The biggest distinction between these two hybrid electrolytes is the transference number. In this study, the transport number is extremely low, which causes a significant mismatch between the polymer and the garnet phases. It was reported that high polarization losses at the interface between Li inorganic conductor and polymer electrolyte was the main cause of the poor cyclability of sandwich type HSE at high current densities[30]. Then, the addition of LLZO in the polymer s-IPN matrix must create high polarizations between the polymer and the

ceramic phases, which unfortunately impacts badly the Li stripping/plating processes. Maybe a beneficial effect of LLZO could be observed in a polymer-in-salt system, namely where the salt content exceeds 50 wt.%. In these electrolytes, the transference number rises thanks to the immobilization of anions in large clusters, where only the Li ions are able to move[31]. A good illustration of this assumption is the PEO-in-salt hybrid electrolyte with 10wt.% LLZO nanofibers[32]. This material accomplishes high transference number (0,57) and superior cycling performance (up to 2 $mA.cm^{-2}$). One way to improve HI-ZI-C_45 cyclability might be to increase LiFSI content in order to reach the polymer-in-salt regime.

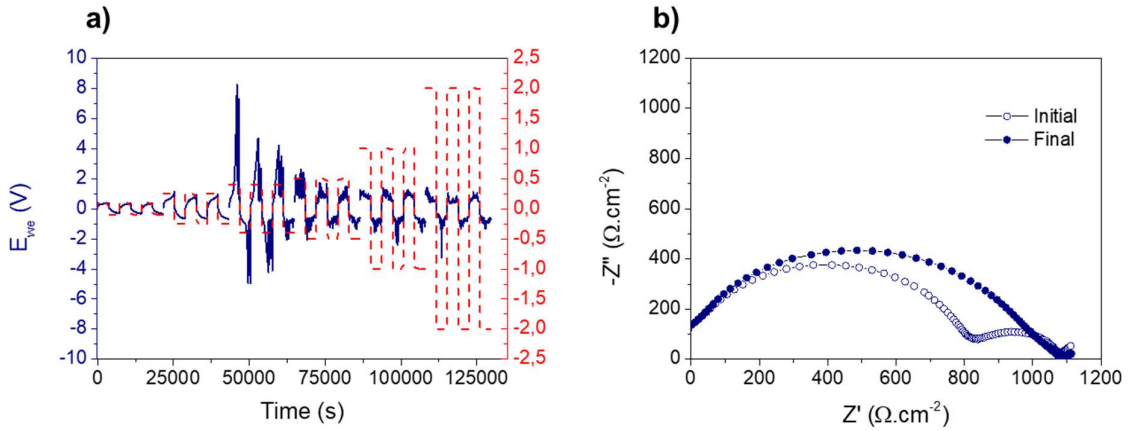

Figure 23: Galvanostatic cycling performance of Li| HI-ZI-C_45 + TEGDME|Li a) Voltage profiles regarding increased current densities; b) EIS spectra before and after cycling.

The Electrochemical Stability Window (ESW) of the polymer and the hybrid s-IPNs were also studied (Experimental method in Appendix B5). Figure 24 reports their oxidation stability towards Li metal. Slight enhancement of ESW is noticed for the hybrid, thanks to the LLZO particles. The inorganic conductor does help the polymer to improve its electrochemical stability. Anodic stability for the polymer s-IPN is similar to the one measured in Chap.4, as the copolymers used have similar structure. The terminal groups of $–(OCH_3)$ for PEGM moieties improve the stability of the polyether towards Li metal.

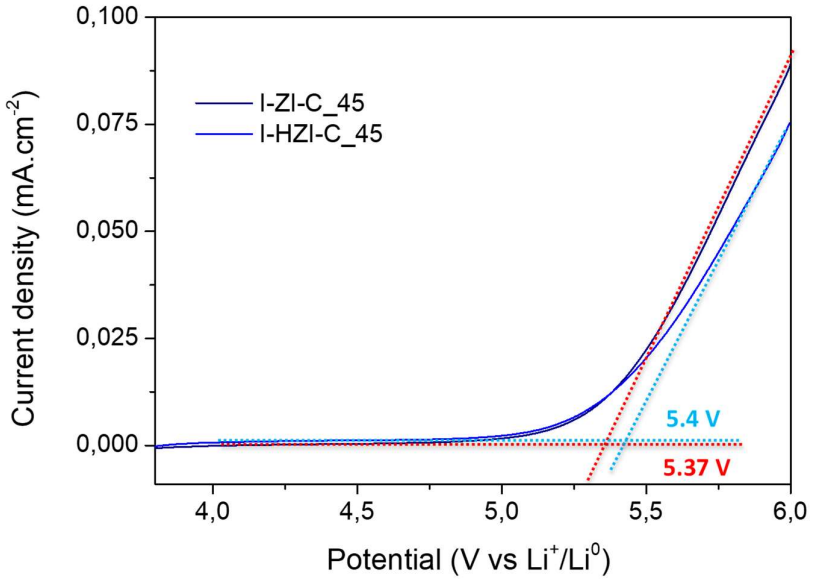

Figure 24: Oxidation stability towards Li metal for I-ZI-C_45 and HI-ZI-C_45 electrolytes at 60°C

To conclude, promising cycling was realized for the polymer s-IPN I-ZI-C_45 in Li symmetrical cells. High content of LiFSI helps to form a stable SEI. This latter can easily be regenerated over cycling thanks to the high concentration of salt. This property enables the cell to cycle at high current density, up to 1 mA.cm^{-2}. Use of a plasticizer (TEGDME) allows to reach acceptable ionic conductivity (9.10^{-5} S/cm) at mild temperature and improve the interfacial contact between the lithium and the electrolyte. The zwitterionic and cationic moieties helps to dissociate LiFSI, but the formation of large aggregates cannot be dismissed. Low transference number (t_{Li+}= 0,14) and diffusion coefficient (D_{Li+}= $4,27.10^{-13}$ cm²/s) further confirms this hypothesis. The use of higher LiFSI content to reach the polymer-in-salt regime can be interesting to enhance the cycling performance, by boosting Li ion transport. Hybrid s-IPN HI-ZI-C_45, with 10 wt.% LLZO, worsens the cycling efficiency. This was unexpected as the addition of the garnet particles can increase the transference number, by helping the dissociation of LiFSI salt. Nevertheless, the discrepancy of transport number between the polymer and LLZO phases favorizes uneven Li dissolution/deposition at the lithium surface. Beneficial effect of LLZO can be considered in the polymer-in-salt regime, which achieves sufficient transference number (around 0,5 and 0,6).

5.4. Conclusions

In this last chapter, hybrid and polymer s-IPN solid electrolytes were obtained by combining a PEG network, cationic and pseudo-zwitterionic copolymers, LiFSI salt and LLZO inorganic particles. For this purpose, a new pseudo-zwitterionic copolymer was synthesized. Like traditional polyzwitterions, a pseudo-zwitterion is a neutral polymer which owns equal positive and negative charges in its backbone. However, these charges are not borne by a unique pendant, but by two complexed adjacent monomer units. This polymer architecture was successfully obtained by the conventional radical copolymerization of a pseudo-zwitterionic monomer, previously formed by the coprecipitation of a cationic and anionic monomers in water. This technique is simple compared to the usual polyzwitterions synthesis and enable a variety of new zwitterionic structures to be synthesized in the future.

Ionic polymer blends were prepared by simply mixing cationic and pseudo-zwitterionic copolymers. The blends showed the aspect of gels. FTIR-ATR analysis show that strong ionic physical interactions occur between cationic and pseudo-zwitterionic copolymers. These ionic polymer blends were thought to be an ideal host for highly conductive polymer-in-salt systems. Then, high LiFSI content was added to these ionic polymer blends in order to form Li ion solid electrolytes. This salt was also chosen for its ability to form stable SEI layers on the lithium. Surprising, high concentration of salt (up to 45 wt.%) can dissolved in these electrolytes without compromising the ionic conductivity at room temperature. Besides, faster ionic conduction at high temperatures can be observed, up to $5{,}5.10^{-5}$ S/cm at 60°C. FTIR-ATR analysis proves that the cationic and pseudo-zwitterionic copolymers help the salt to dissociate.

The formation of a semi-interpenetrated network (s-IPN) allows to get self-standing membranes while keeping the flexibility and deformability of the electrolyte. This allows to use these electrolytes in our all-solid state lithium symmetric battery set-up at mild temperature. However, it was necessary to add small content of plasticizer (TEGDME) to achieve faster ionic conduction. This combination leads to an ionic conductivity close to 1.10^{-4} at 60°C, which is quite high for high salt concentrations. A hybrid composition with low content of LLZO (10 wt.%) was processed by spray coating. The addition of the inorganic particles fosters the ionic dissociation, by immobilizing anions through interactions with the garnet inorganic particles.

The polymer s-IPN provides excellent cycling capability, reaching a CCD of 1 $mA.cm^{-2}$. Intimate interfacial contact between the solid electrolyte and the lithium anode was realized upon the addition of the plasticizer. An extremely stable SEI, sufficient ionic conductivity and ion regulation thanks to the ionic polymer phase are the several reasons for this successful performance. Nevertheless, the HSE electrolyte showed bad cycling performance despite improved properties in term of ionic dissociation. The presence of large ionic aggregates, confirmed by the determination of the lithium transference number and the diffusion coefficient, induces large polarization between the polymer and the garnet phases. In all likelihood, this mismatch of Li ion transport number favorizes heterogeneous Li dissolution/deposition processes on the lithium metal.

This exploratory study sheds light on the importance of ionic interactions and polymer/salt/LLZO compositions on the cycling efficiency of hybrid polymer electrolytes. Further synthesis of pseudo-zwitterionic polymers with other co-monomer compositions and the investigation of their ionic physical interactions by DSC or rheological experiments will be

needed. Furthermore, the enhancement of the performance of these solid electrolytes might need the use of higher content of LiFSI to reach the polymer-in-salt regime.

5.5. References.

1. Islam, A. *et al.* Zwitterions for Organic / Perovskite Solar Cells , Light-Emitting Devices , and Lithium Ion Batteries : Recent Progress and Perspectives. *Adv. Energy Mater.* **9**, 1803354 (2019).

2. Suematsu, M. *et al.* Effect of zwitterions on electrochemical properties of oligoether-based electrolytes. *Electrochim. Acta* **175**, 209–213 (2015).

3. Li, Z. H. *et al.* Effect of zwitterionic salt on the electrochemical properties of a solid polymer electrolyte with high temperature stability for lithium ion batteries. *Electrochim. Acta* **56**, 804–809 (2010).

4. Byrne, N. *et al.* Effect of zwitterion on the lithium solid electrolyte interphase in ionic liquid electrolytes. *J. Power Sources* **184**, 288–296 (2008).

5. Shao, Q. & Jiang, S. Molecular Understanding and Design of Zwitterionic Materials. *Adv. Mater.* **27**, 15–26 (2015).

6. Guzmán, G., Nava, D. P., Vazquez-Arenas, J. & Cardoso, J. Design of a Zwitterion Polymer Electrolyte Based on Poly[poly (ethylene glycol) methacrylate]: The Effect of Sulfobetaine Group on Thermal Properties and Ionic Conduction. *Macromol. Symp.* **374**, 1–7 (2017).

7. Lu, F. *et al.* Zwitterionic impetus on single lithium-ion conduction in solid polymer electrolyte for all-solid-state lithium-ion batteries. *Chem. Eng. J.* **384**, 123237 (2020).

8. Li, G., Guan, X., Wang, A., Wang, C. & Luo, J. Cations and Anions Regulation through Zwitterionic Gel Electrolytes for Stable Li Metal Anodes. *Energy Storage Mater.* **24**, 574–578 (2019).

9. Erfani, A. *et al.* Interactions between biomolecules and zwitterionic moieties : a review. *Biomacromolecules* **21**, 2557–2573 (2020).

10. D'Angelo, A. J. & Panzer, M. J. Decoupling the Ionic Conductivity and Elastic Modulus of Gel Electrolytes: Fully Zwitterionic Copolymer Scaffolds in Lithium Salt/Ionic Liquid Solutions. *Adv. Energy Mater.* **8**, 1–13 (2018).

11. Rebollar, L. & Panzer, M. J. Zwitterionic Copolymer-Supported Ionogel Electrolytes: Impacts of Varying the Zwitterionic Group and Ionic Liquid Identities. *ChemElectroChem* **6**, 2482–2488 (2019).

12. Delgado, J. D. & Schleno, J. B. Static and Dynamic Solution Behavior of a Polyzwitterion Using a Hofmeister Salt Series. *Macromolecules* **50**, 4454–4464 (2017).

13. Petroff, M. G., Garcia, E. A., Herrera-alonso, M. & Bevan, M. A. Ionic Strength Dependent Interactions & Dimensions of Adsorbed Zwitterionic Copolymers. *Langmuir* **35**, 4976–4985 (2019).

14. Laschewsky, A. Structures and Synthesis of Zwitterionic Polymers. *Polymers (Basel).* **6**, 1544–1601 (2014).

15. Ohno, H. & Yoshizawa, M. Ion conductive characteristics of ionic liquids prepared by neutralization of alkylimidazoles. *Solid State Ionics* **155**, 303–309 (2002).

16. Farooq, S., Razzaq, H., Razzaque, S., Khan, B. A. & Qaisar, S. Structural and Physical Impacts of Nano fillers in Ionogels : A Comprehensive Overview. *Polym. Compos.* **40**,

11–23 (2019).

17. Yang, G., Song, Y., Wang, Q., Zhang, L. & Deng, L. Review of ionic liquids containing , polymer / inorganic hybrid electrolytes for lithium metal batteries. *Mater. Des.* **190**, 108563 (2020).

18. Wen, S. J. *et al.* FTIR characterization of PEO + LiN(CF3SO2)2 electrolytes. *J. Electroanal. Chem.* **408**, 113–118 (1996).

19. Wohde, F. *et al.* Li+ ion transport in ionic liquid-based electrolytes and the influence of sulfonate-based zwitterion additives. *Solid State Ionics* **284**, 37–44 (2016).

20. Wang, X. *et al.* Preparation and characterization of gel polymer electrolytes using poly(ionic liquids) and high lithium salt concentration ionic liquids. *J. Mater. Chem. A* **5**, 23844–23852 (2017).

21. Bhandary, R. & Schönhoff, M. Polymer effect on lithium ion dynamics in gel polymer electrolytes: Cationic versus acrylate polymer. *Electrochim. Acta* **174**, 753–761 (2015).

22. Kerner, M., Plylahan, N., Scheers, J. & Johansson, P. Thermal stability and decomposition of lithium bis(fluorosulfonyl)imide (LiFSI) salts. *RSC Adv.* **6**, 23327–23334 (2016).

23. Yoon, H., Best, A. S., Forsyth, M., MacFarlane, D. R. & Howlett, P. C. Physical properties of high Li-ion content N-propyl-N-methylpyrrolidinium bis(fluorosulfonyl)imide based ionic liquid electrolytes. *Physical Chemistry Chemical Physics* vol. 17 4656–4663 (2015).

24. Soberats, B., Yoshio, M., Ichikawa, T., Ohno, H. & Kato, T. Zwitterionic liquid crystals as 1D and 3D lithium ion transport media. *J. Mater. Chem. A* **3**, 11232–11238 (2015).

25. Qiao, X., Sun, P., Wu, A., Dong, B. & Zheng, L. Supramolecular Thermotropic Ionic Liquid Crystals Formed via Self-Assembled Zwitterionic Ionic Liquids. *Langmuir* **35**, 1598–1605 (2019).

26. Zhang, H. *et al.* Lithium bis(fluorosulfonyl)imide/poly(ethylene oxide) polymer electrolyte. *Electrochim. Acta* **133**, 529–538 (2014).

27. Pożyczka, K., Marzantowicz, M., Dygas, J. . & Krok, F. Ionic Conductivity And Transference Number of Poly(Ethylene Oxide):LiTFSI system. *Electrochim. Acta* **227**, 127–135 (2017).

28. Ma, Y. *et al.* The Measurement of a Complete Set of Transport Properties for a Concentrated Solid Polymer Electrolyte Solution. *J. Electrochem. Soc.* **142**, 1859–1868 (1995).

29. Porthault, H., Piana, G., Duffault, J. M. & Franger, S. Influence of ionic interactions on lithium diffusion properties in ionic liquid-based gel polymer electrolytes. *Electrochim. Acta* **354**, 136632 (2020).

30. Mehrotra, A., Ross, P. N. & Srinivasan, V. Quantifying Polarization Losses in an Organic Liquid Electrolyte / Single Ion Conductor Interface. *J. Electrochem. Soc.* **161**, A1681–A1690 (2014).

31. Angell, C. A., Liu, C. & Sanchez, E. Rubbery solid electrolytes with dominant cationic transport and high ambient conductivity. *Nature* **362**, 137–139 (1993).

32. Fan, R., Liu, C., He, K. & Cheng Ho-Sum, S. Versatile Strategy for Realizing Flexible

Room-Temperature All-Solid-State Battery through a Synergistic Combination of salt Affluent PEO and Li6.75La3Zr1.75T0.25O12 nanofibers. *ACS Appl. Mater. Interfaces* **12**, 7222–7231 (2020).

APPENDIX

A. Characterization methods for solid-state electrolyte

A.1. Structural characterization of polymer electrolytes: ^{1}H Nuclear Magnetic Resonance (NMR) and Attenuated Total Reflectance Fourier Infrared Spectroscopy (ATR-FTIR)

^{1}H NMR spectra were recorded on an Advance 500 spectrometer (Bruker). Chemical shifts are reported in ppm, using the signal related to the residual protons of the deuterated solvent used as standard.

ATR-FTIR measurements were performed on an ALPHA Spectrometer (Bruker). The spectra were recorded 32 times and compiled, with a resolution of 4 cm^{-1} in the ATR mode.

A.2. Determination of the molecular weight of polymer electrolytes: Size Exclusion Gel Permeation chromatography (SEC-GPC)

The molecular weights (M_n, M_w) and Poly Dispersity Index (PDI) of single ion random free copolymers were studied using a PL-GPC 50 gel permeation chromatograph (Aluent), coupled with an integrated IR detector, a TSK-GEL SuperAW4000 column (Tosoh) and SuperAW-L Guard column (Tosoh). 0.1 M LiCl solution in water/ACN mixture (4:1 v/v) was selected as an eluent with a flow rate of 0.5 mL/min at 25°C. The columns used can only detect molecular weights lower or equal to 2000 kg/mol.

A.3. Thermal characterization: Differential Scanning Calorimetry (DSC)

Thermal properties were analysed by DSC with a PerkinElmer 8000 DSC fitted with an Intracooler I. Approximately 5 mg of sample is used for this test. For no isothermal runs, a heating rate of 20°C/min in a 70 to 100 °C range was used. The samples, encapsulated in aluminum pans, were first heated to 100 °C to erase thermal history, and then, cooling and second heating scans were performed. The glass transition temperature T_g was determined at the midpoint of the heat enthalpy change during the transition to the glassy to rubbery state. The melting temperature T_m was calculated by integrating the area below the endothermic enthalpy peak.

The crystallinity degree of semi crystalline hybrid and pristine polymer electrolytes based on PEO blends was estimated as follows:

$$X_c = \frac{\Delta H_m}{f.\Delta H_{m0}}$$

Where ΔH_m is the measured melting enthalpy, ΔH_{m0} is the equilibrium melting enthalpy and f is the PEO weight fraction in the electrolyte. The value of ΔH_{m0}=214 J/g was used for PEO.

A.4. Gelation kinetics of UV polymerization: Photo-rheology

Photo-rheology study was performed on an AR-G2 (TA Instrument). Liquid monomer mixture was exposed to UV light, the irradiance set up a 58 $mW.cm^{-2}$. The liquid was compressed to get membranes with fixed thickness of 800 µm. The experiment was monitored with a frequency of 1 Hz and an oscillatory shear fixed at 12% strain.

A.5. Observation of LLZO dispersions in hybrid electrolytes: Environmental Scanning Electron Microscopy (ESEM) and Scanning Electron Microscopy (SEM)

ESEM was used to observe LLZO particles dispersion within plasticized crosslinked hybrid electrolyte (FEI QUANTA 500, ThermoFisher). This technique allows analysing crosslinked networks swollen with solvent. SEM was carried out to evaluate the homogeneity of LLZO particles in doctor bladed and spray-coated hybrid blends. In both cases, neat cross-sections of material were made outside the glovebox by immersing the materials into liquid N_2 bath. Before analysis, the samples were metalized to minimize the electron beam.

A.6. Mechanical characterization: Dynamical Mechanical Thermal Analysis (DMTA)

DMTA was conducted using an AR-G2 (TA Instrument) with oscillatory compression. Storage (G′) and the loss (G´´) moduli and the glass transition temperature T_g were recorded at fixed frequency (1 Hz), in the temperature range from -100°C to 80°C.

A.7. Understanding Li ion conduction in hybrid polymer electrolytes: Magic Angle Spinning (MAS) and Pulsed Field Gradient (PFG) NMR.

Solid NMR was used to better apprehend the ionic transport within hybrid plasticized crosslinked electrolytes. Measurements and calculations were undertaken by Dr: Haijin Zhou thanks to a collaboration with Deakin University, Australia.

^{7}Li and ^{19}F MAS NMR were performed on an Advance spectrometer with 4 mm Bruker HXY triple resonance probe (Bruker). The samples were spun at 6 kHz. Recycle delays were 200s and 10s for ^{7}Li and ^{19}F respectively. The ^{7}Li and ^{19}F NMR relaxation times (T_1) were measured on a 300 MHz Bruker Advance III spectrometer. These experiments were performed at various temperatures ranging from 25°C to 70°C using a Bruker 5 mm Diff50 pulsed field gradient (PFG) NMR probe. Diffusion coefficients were measured using the same NMR probe with the stimulated echo pulse sequence.

B. Description of electrochemical characterisation techniques

B.1. Determination of the ionic conductivity: Electrochemical Impedance Spectroscopy (EIS)

The ionic conductivity was determined at different temperatures by EIS. The measurement was carried out with an Autolab 302N potentiostat galvanostat (Metrohm AG) with a temperature controller (Microcell HC station). The temperatures were set between 25°C and 90°C. Electrolytes were sandwiched between two stainless steels electrodes. EIS was monitored using a frequency range of 0.1 Hz to 100 kHz with an amplitude comprised between 10-25 mV, depending on the electrolyte tested. Ionic conductivity measurements were done at least two times for each composition to assess the reproducibility of the obtained values. The ohmic resistance $R_{bulk,}$ determined by fitting the impedance spectrum by an equivalent circuit, was used to calculate the ionic conductivity thanks to the following equation:

$$\sigma = \frac{L}{A}\frac{1}{R_{bulk}}$$

Where L is the thickness of the electrolyte and A the area of the stainless electrode respectively. The activation energies were obtained by fitting the Arrhenius and VTF curves.

B.2. Electrochemical stabilization towards the lithium: Evolution of the resistances in Li symmetrical cells (RE).

Li symmetrical cells were assembled in an Argon filled glovebox and further tested using a VMP3 multichannel potentiostat (Biologic). Firstly, the Li foil was carefully mechanically scraped to remove the native layer (Li_2CO_3, Li_2O) on Li surface. Disks of 11 mm² diameter were pinched from the prepared Li foils and used as electrodes for the symmetrical cells. The cell was then assembled by sandwiching the electrolyte between two beforehand cleaned Li foils. Its stability towards the lithium was then evaluated by monitoring the evolution of the

resistances over time under open circuit voltage (OCV) conditions. This test was performed at 60°C.

B.3. Measurement of Li ions diffusion coefficients

Li salt diffusion coefficients were calculated according to the method proposed by Ma and co-workers. Li symmetrical cells were prepared as described previously and stabilized at 60°C to form the SEI. A constant current (0,1 mA.cm^{-2}) was then applied to the cell for a short time (1-2 min) in order to generate a salt concentration gradient. Once the current was stopped, the cell potential was monitored during the relaxation of the concentration profile. The curve log(V) in function of time was plotted and the linear curve was fitting to this following equation:

$$\mathbf{Slope} = -\frac{\pi . \mathbf{D_{Li+}}}{\mathbf{L}^2}$$

Where D_{Li+} is the Li^+ diffusion coefficient and L the thickness of the electrolyte. This measurement was done at least two time to confirm the values.

B.4. Determination of the transference number

Lithium transference numbers were determined using the method described by Bruce and Vincent, which couples EIS and chronoamperometry. Li symmetrical were assembled as explained in section B.2. The cells were stabilized at 60°C thanks to a temperature-controlled chamber, for a period determined previously by monitoring the resistances over time. Once the solid electrolyte interphase (SEI) between lithium metal and polymer remained steady, it was possible to launch cell polarization. The cells were polarized by applying a small perturbation (ΔV =25-40 mV) between 100 kHz and 1Hz, to evaluate the initial and the steady-state currents I_0 and I_{ss}. EIS was carried out with similar amplitude (25-40 mV) before and after cell polarization in order to determine the initial and final resistances of the SEI interphase R_0 and R_{SS}. These latter were precisely established by fitting the EIS spectra with Equivalent Circuit Model (ECM). The transference number t_{Li+} was then calculated as follows:

$$\mathbf{t_{Li+}} = \frac{\mathbf{I_{SS}}(\Delta \mathbf{V} - \mathbf{I_o}.\mathbf{R_i})}{\mathbf{I_0}(\Delta \mathbf{V} - \mathbf{I_{SS}}.\mathbf{R_{SS}})}$$

B.5. Electrochemical stability window (ESW): Cyclic voltammetry

Cyclic voltammetry was performed to analyse the anodic stability of solid electrolyte towards Li metal. The electrolyte was sandwich between the working electrode (stainless steel)

and a lithium foil as counter electrode. The scan was carried out between OCV and 6 V versus Li^+/Li at a constant rate of 1 mV/s.

B.6. Post-mortem characterization: Optical microscopy

Optical Microscope DMC4500 (Leica) was also used to analyse cycled electrolytes. The samples were cut with a scalpel and observed directly in the glovebox.

C. Properties of LLZO particles

C.1. Confirmation of cubic phase and purity of LLZO particles: X-Ray Diffraction (XRD)

XRD was carried out on LLZO particles to verify their crystalline structure and their purity, by using a MiniflexX600 X-ray diffractiomer (Rigaku). The XRD scans (step = 0.026°, 60 s per step) were collected from 10° to 70° at ambient temperature. The sample holder was protected from air contamination by a capsule which was closed beforehand in the glovebox. Figure 1 displays the XRD diffractogram of LLZO particles used for this project. Experimental peaks match closely the reference of the cubic $Li_5La_3Nb_2O_{12}$ (PDF 045-0109), which is known as the garnet crystalline structure. No peaks related to impurities (Li_2CO_3) were discerned in the XRD diffractogram, confirming the purity of the LLZO particles.

C.2. Inspection of air induced impurities on LLZO surface: Transmission Electron Microscopy (TEM)

To ascertain the purity of LLZO, especially in term of air contamination, TEM was employed to analyse the surface of the particles thanks to a 200kV TECNAI G2 20 TWIN. The formation of Li_2CO_3 in presence of moisture and CO_2 tends to recover the particles by a thin layer, observable in TEM. For this purpose, two batches of LLZO particles were observed and compared. The first one was stored in a glovebox (H_2O< 10 ppm, O_2<10 ppm) in a protective metal case. The second was intentionally exposed to the ambient atmosphere for a week. Before TEM observation, LLZO particles were coated by a resin, which was thinly cut thanks to a ultramicrotome. Figure 2 exhibits TEM pictures of air protected and air contaminated particles. Exposed LLZO presents thin layer around its surface, indicated by white arrows in the image. On the opposite, stored LLZO has a smooth surface, with no apparent reactive

layer. It was concluded that the inorganic particles were preserved from air contamination and could be used as received.

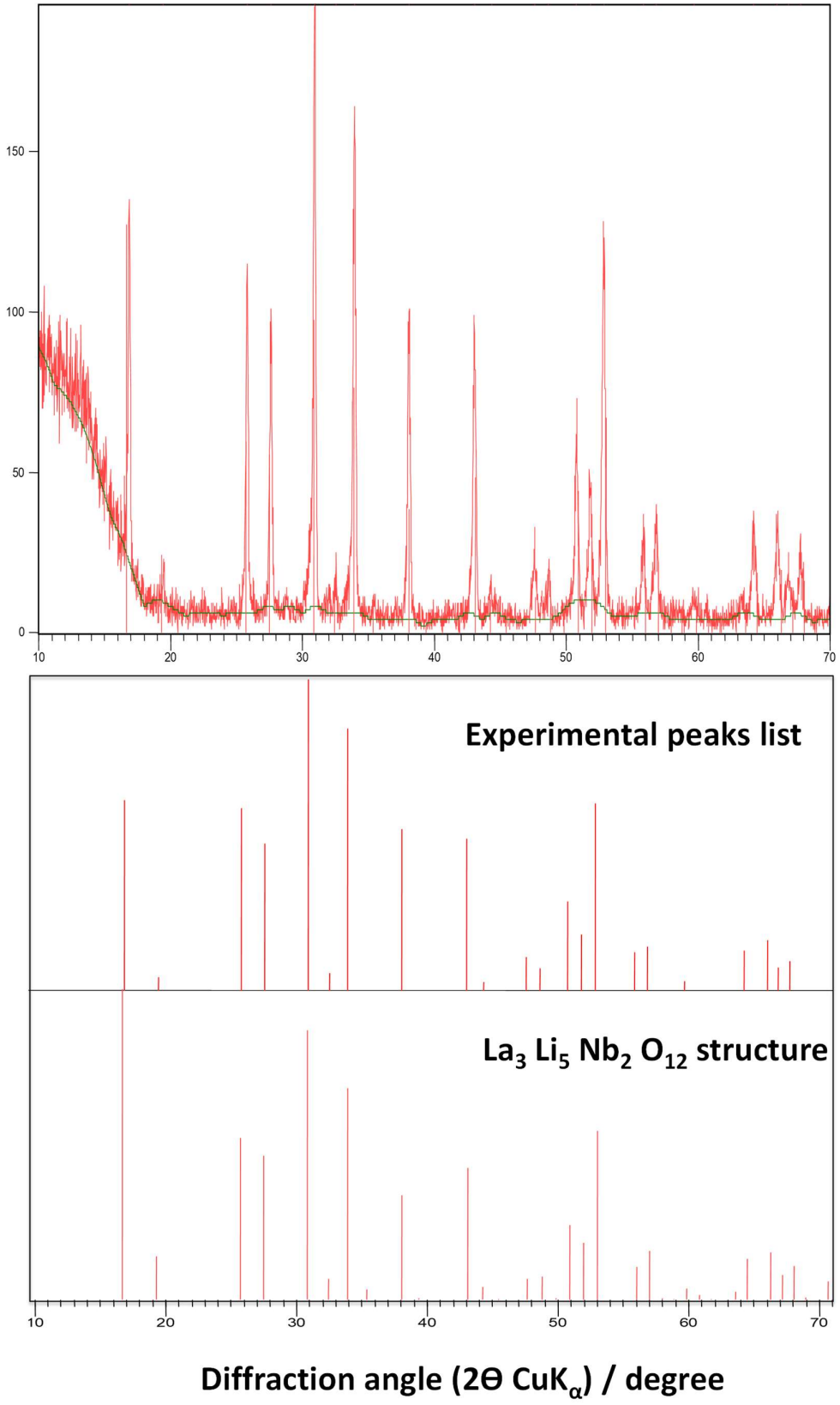

Figure 1: XRD diffractogram of LLZO particles as received (Top part), Comparison of experimental peaks with the cubic phase crystalline structure (Bottom part).

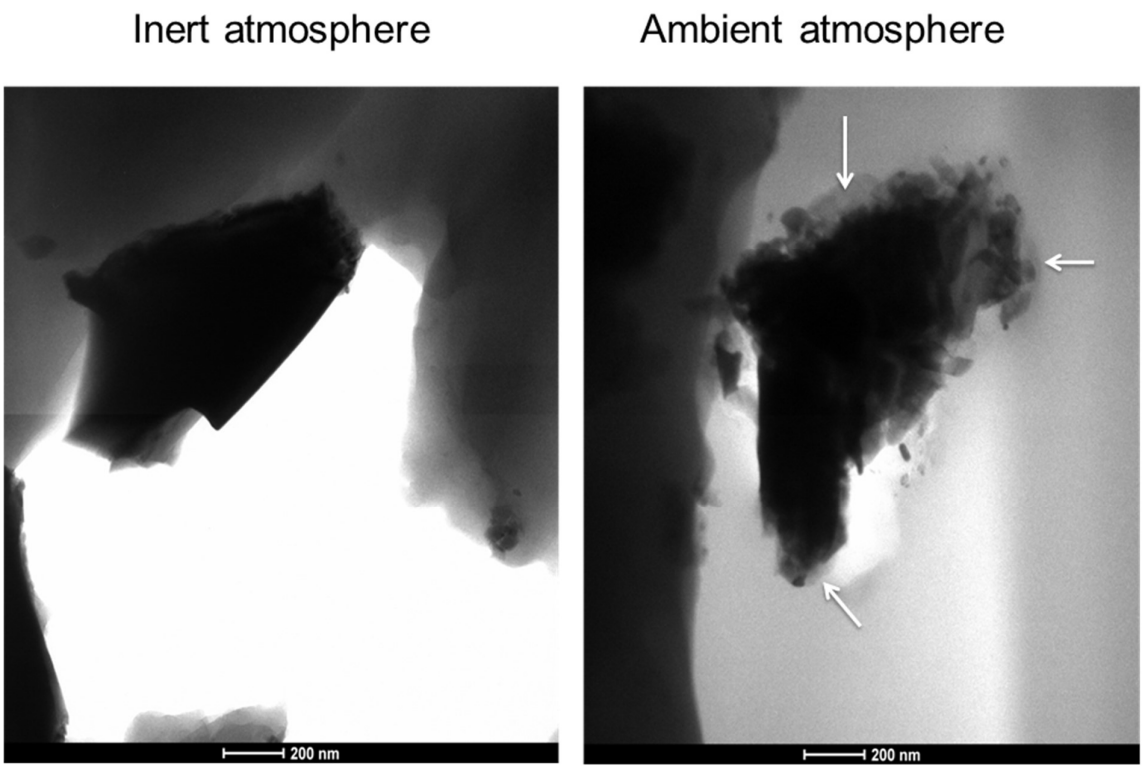

Figure 2: Comparison of TEM images of pure and air contaminated LLZO particles. White arrows show an interphase layer on the particle surface, likely to be Li_2CO_3 impurities.

D. Characterization of cationic and pseudo-zwitterionic monomers (Chapter 5)

D.1. ^{1}H NMR of cationic monomer NTFSI

Figure 1 shows the ^{1}H spectrum of NTFSI monomer after ionic exchange of chloride anions in water.

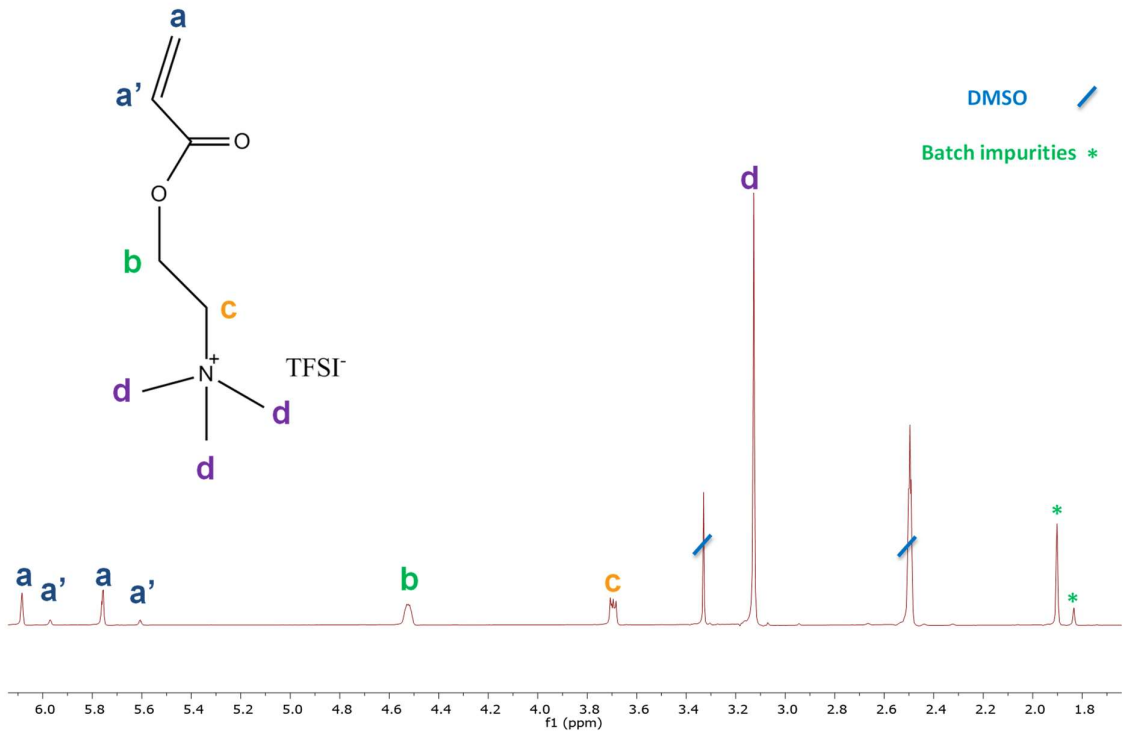

Figure 1: ^{1}H NMR spectrum of NTFSI monomer recorded in d_6-DMSO.

D.2. ^{1}H NMR of pseudo-zwitterionic monomer ZI

Figure 2 shows the ^{1}H spectrum of ZI monomer after complexation of tethered bis(trifluoromethanesulfonyl)imide $TFSI^-$ and triethylammonium $N^+(CH_3)_3$ from LiMTFSI and NTFSI monomers in water.

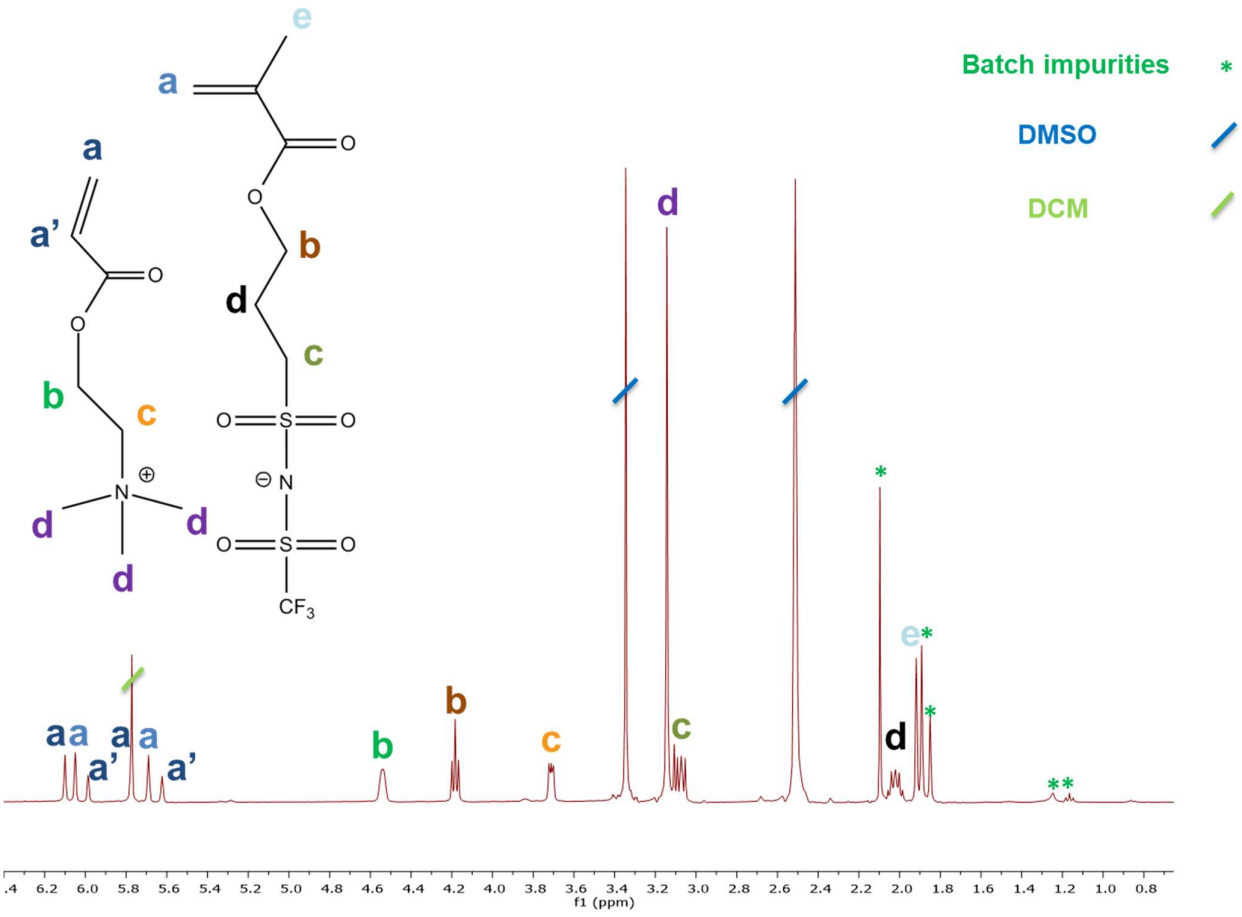

Figure 2: ^{1}H NMR spectrum of ZI monomer recorded in d_6-DMSO.

CHAPTER 6.

Conclusions

In this PhD, hybrid and polymer solid electrolytes based on ionic polymers, poly(ethylene glycol) units and LLZO particles were successfully synthesized and implemented in solid state batteries composed of a Li metal anode. Within the thesis, three new solid electrolytes are presented such as: the lithium single-ion hybrid gel solid electrolytes (Chapter 3); the hybrid solid electrolytes based on the blending of PEO, lithium single-ion copolymer and LLZO particles (Chapter 4); and the hybrid pseudo zwitterionic semi-IPN solid electrolytes (Chapter 5). All these different polymer electrolytes showed distinct mechanical and electrochemical properties, despite their chemical similarities. This work highlights the versatility of polymer chemistry and material design for solid electrolytes of lithium metal batteries.

In **Chapter 2**, the method based on galvanostatic cycling with increased current densities and electrochemical impedance spectroscopy (EIS) was described. This test enables to determine the critical current density (CCD), which is a key factor for practical application of the solid electrolytes developed in this PhD thesis. In addition, it was demonstrated that the study of voltage profiles gives important information on the Li stripping/plating processes. This technique was employed to analyse the cycling performance of the different hybrid and polymer electrolytes developed in this PhD.

In **Chapter 3**, lithium single ion hybrid gel electrolytes were prepared by fast UV photopolymerization. Homogeneous LLZO dispersion in the polymer matrix was easily achieved by simple magnetic stirring. High loading of inorganic particles (up to 40 wt.%) can be achieved without observing agglomerates or sediments. These hybrid solid electrolytes show promising properties as potential Li anolytes thanks to its high ionic conductivity, high transference number and good mechanical stability. Solid NMR was employed to better understand the role of LLZO particles on the ionic conduction in both single and dual ion polymer matrices. This study showed that the presence of the inorganic particles was beneficial for both matrices, as the Li motion increases and the anions are immobilized by physical interactions with the LLZO particles. Besides, an additional ionic environment for fluoride anions was noticed in single ion gels. According to similar examples from the literature, it was concluded that the tethered anionic moieties from LiMTFSI monomer were able to adsorb on LLZO surface. This interaction explains the excellent dispersion of LLZO within the polymer matrix and the improvement of Li^+ mobility within these electrolytes, which increases the ionic conductivity. The affinity between LiMTFSI moieties and LLZO particles can be extremely beneficial to develop future innovative hybrid polymer electrolytes. The high ionic conductivity and near single ion conduction allow to achieve high critical current density (CCD=1 $mA.cm^{-2}$ at 60°C) for both the polymer and the hybrid electrolyte. The polymer cycling performance was

further enhanced by in situ polymerization and the use of FEC additive. As consequence, the CCD increases to 2 $mA.cm^{-2}$. On the other hand, the hybrid electrolyte showed worsened cycling performance as dendrites formation was observed above the CCD. The water traces from the propylene carbonate plasticizer look to be at the origin of the poor electrochemical stability of the hybrid towards the lithium. Nevertheless, its cycling performance was encouraging, knowing the limited CCD of garnet particles (0,3 $mA.cm^{-2}$).

In **Chapter 4**, hybrid and polymer blend solid electrolytes based on lithium single ion copolymers, PEO and LLZO particles were presented. For this purpose, we carried out first the synthesis of new poly($LiMTFSI_x$-co-$PEGM_{1-x}$) random copolymers by free radical copolymerization and studied the optimum composition for obtaining the highest ionic conductivity. Then, high molecular weight PEO was mixed with these copolymers to improve its ionic conductivity at ambient and mild temperatures while maintaining a high transference number. The blend formulation (PEO content) were thoroughly analysed by EIS, DSC and ATR-FTIR. Blends containing low PEO amount ($\leq$ 30 wt.%) show the highest ionic conductivity (up to 10^{-6} S/cm at 25°C) but suffer from poor mechanical stability. This study showed that PEO crystallinity is strongly inhibited by the concentration of LiMTFSI. However, the high content of salt leads to sluggish ionic conductivity. On the other hand, high PEGM composition plasticizes the blend, without affecting PEO's crystallinity. To further improve the ionic conductivity and the mechanical stability of the blend, UV crosslinking of the PEO was carried out. The hybrid electrolytes were successfully prepared by spray-coating of a solution of the three components (copolymer, PEO and LLZO). Spray coating gives a uniform dispersion of inorganic particles within the polymer matrix and thin hybrid films (< 200 µm). pH detection and FTIR-ATR analysis was carried during the preparation of the hybrid electrolytes to verify the contamination of LLZO particles by water traces. Extremely dried HSE films were successfully obtained by simple wet method. The use of LLZO particles enables to enhance the ionic dissociation within the polymer matrix, which boosts the Li ion conduction. ATR-FTIR proved that the inorganic particles can interact with free and tethered anionic moieties. These solid electrolytes were tested in lithium symmetrical cells to conclude about their potential use as anolyte in Li metal batteries. To form a stable SEI, salt additive was added to the hybrid and polymer electrolytes. This modification leads to decreased transport number but doubles the CCD. Nevertheless, inefficient ionic conductivity limits the cycling performance. Acceptable CCD was achieved for the polymer and the hybrid (0,5 $mA.cm^{-2}$ at 60°C). Dendrites tend to form above the CCD. The poor interfacial contact between the electrolyte and the Li likely causes uneven Li stripping/plating. Concerning the hybrid, it presents improved mechanical and electrochemical properties, such as Li ion transport and oxidative stability. However, the addition of particles does not help the electrolyte to have a better interfacial contact with the electrodes. Then, no enhancement in term of cyclability has been observed for the hybrid blend. Major improvement in term of cyclability can be achieved by using a plasticizer (glyme), which can both increase the ionic conductivity and the anode wetting. A better design of the SEI (dual salt additives) can also be highly beneficial.

Finally, **Chapter 5** described the preparation of hybrid and polymer semi-interpenetrating networks (s-IPN) by combining a PEG network, cationic and pseudo-zwitterionic copolymers, LiFSI salt and LLZO inorganic particles. For this purpose, a new

pseudo-zwitterionic copolymer was synthesized. Unlike traditional polyzwitterions, a pseudo-polyzwitterion is a neutral polymer which owns two complexed adjacent monomer units, each one bearing independently positive and negative charges. This polymer architecture was successfully obtained by coprecipitation of an anionic and cationic monomers, which were afterwards polymerized. This technique is simple compared to the usual polyzwitterions synthesis and enable a variety of new zwitterionic copolymer structures. Ionic polymer blends were prepared by simply mixing cationic and pseudo-zwitterionic copolymers. FTIR-ATR analysis shows that strong physical interactions occur between these two copolymers. These ionic polymer blends present interesting mechanical properties (stickiness, deformability) thanks to the formation of a physical network. Besides, they are promising candidate as polymer host for highly conductive polymer-in-salt systems. To prove this, high LiFSI content was added to these ionic polymer blends. This salt was also chosen for its ability to form stable SEI layers on the lithium. Surprising, high concentration of salt (up to 45 wt.%) can dissolved in these electrolytes without compromising the ionic conductivity at room temperature. FTIR-ATR analysis proves that the cationic and pseudo-zwitterionic copolymers help the salt to dissociate. The addition of LLZO particles is also highly beneficial in terms of ionic dissociation. The inorganic particles can interact with LiFSI salt, enhancing the ionic conductivity and the transference number. The formation of a semi-interpenetrated network (s-IPN) allows to get self-standing membranes while keeping the flexibility and deformability of the electrolyte. This allows to use these electrolytes in our all-solid state battery set-up at mild temperature. However, it was necessary to add small content of plasticizer to achieve faster ionic conduction. Distinct cycling performances were obtained for the polymer and hybrid s-IPNs. The polymer s-IPN provides excellent cycling capability, reaching a CCD of 1 $mA.cm^{-2}$. The SEI is highly stable and can adapt the large volume change of the Li metal, thanks to the high content of LiFSI salt. On the other hand, the cycling performance is aggravated in presence of LLZO particles. The CCD is reduced to 0,4 $mA.cm^{-2}$. Nevertheless, no dendrites were formed. This poor cyclability can be explained by the large mismatch of transference number between the polymer and the inorganic phase. A way to improve the hybrid cycling performance is maybe to use higher salt content to reach the polymer-in-salt regime, where intermediate transport number (0,45-0,5) can be obtained.

Despite their weaknesses, the solid electrolytes developed in this PhD thesis displays interesting features to be coupled with Li metal. Their successful implementation in a true solid-state battery set up further confirms their potential as solid electrolyte. Besides, low-cost reactants, facile synthesis and scalable films processes for the developed polymers make them desirable for industrial battery applications. However, better SEI design and characterization are mandatory to optimize these materials. The hybrid electrolytes present distinct results in term of cyclability. Their common feature is that LLZO particles does not improve the cycling performance of the polymer matrix. The unique effect of LLZO is to interact with the anionic species, whether immobilized or free. Therefore, the addition of the particles can be advantageous at the condition to deeply understand their interactions with the salt or the ionic polymer used. Unfortunately, solid knowledge is still lacking in this study. Then, it is extremely challenging to conclude about the reason of the low performance of the HSEs. Nonetheless, two points can be retained from this thesis. Firstly, the wetting method (use of a solvent to mix the different components) may not be adequate for hybrid polymers based on LLZO. As explicated previously, the high reactivity of LLZO with water traces can be avoided

by using solid state processes. Even with dried solvents, the risk of contamination cannot be null. Then, improved cyclability can be optimistically achieved by optimizing the hybrid synthesis. Secondly, the use of ionic polymers or unreacted ionic liquid monomer during the mixing step with the particles can have a great impact on the final properties of the hybrid. HSIPE-x hybrid electrolyte (Chapter 3) outperforms the other developed hybrids thanks to enhanced interaction with unreacted LiMTFSI monomer. The functionalization of LLZO particles with ionic liquid monomers can be an interesting research trail to upgrade hybrid polymer electrolytes.

Resumen

El siglo XXI, a pesar de su avance científico y desarrollo tecnológico, aún enfrenta grandes desafíos en términos de desregulación climática, sostenibilidad y seguridad energética. El calentamiento global del planeta está siendo causado por la acumulación de gases de efecto invernadero liberados por las actividades humanas. El dióxido de carbono (CO_2) es el principal responsable. El transporte por carretera es uno de los emisores de CO_2 más importantes y es pronosticado que puede liberar el doble para el año 2050. Entonces, es urgente pasar rápidamente a automóviles de bajo o cero emisiones de carbono, que funcionen con motores eléctricos. Las baterías parecen ser la tecnología más madura para esta aplicación, especialmente basada en la química de iones de litio. Sin embargo, sus limitaciones en cuanto al alcance, vida útil, seguridad y costo restringen actualmente su uso en vehículos eléctricos.

Una batería recargable está compuesta por un electrodo positivo (cátodo) y un electrodo negativo (ánodo) separados por un electrolito. El electrolito asegura la movilidad iónica entre los dos electrodos. Es un conductor iónico, generalmente un solvente orgánico con una sal de litio. Una vez que los electrodos están conectados externamente, el ánodo genera espontáneamente un flujo de electrones y de iones positivos que equilibran la carga en el electrolito, los cuales fluyen hacia el cátodo. Este mecanismo se llama descarga, cuando la oxidación ocurre en el lado del ánodo (pérdida de electrones) y la reducción ocurre en el lado del cátodo (ganancia de electrones). Una vez finalizadas las reacciones, se detiene el flujo de electrones (estado descargado). Como estas reacciones son reversibles, es posible invertir el flujo de corriente desde el cátodo al ánodo utilizando una fuente de energía externa: esta es la carga. Luego, las baterías recargables se pueden usar varias veces para producir electricidad al cargarlas nuevamente después de su uso.

El uso de baterías de iones de litio para aplicaciones de vehículos eléctricos todavía está limitado debido al a su baja energía específica de 350 $Wh.kg^{-1}$. Una solución prometedora para mejorar la energía específica es reemplazar el ánodo de grafito por un ánodo de metal litio. El metal de litio posee una capacidad específica extremadamente alta y tiene el potencial electroquímico más bajo. Al acoplarse con un cátodo de alto voltaje, este tipo de batería puede cumplir con los requisitos futuros de las baterías de vehículos eléctricos en términos de voltaje y capacidades de electrodos. Desafortunadamente, los electrolitos líquidos que se usan comúnmente en las baterías de iones de litio son extremadamente inestables frente al metal de litio. El proceso de ciclo heterogéneo y las interfases inestables entre el electrolito y el electrodo conducen a la formación y crecimiento de filamentos de Li comúnmente conocidos como dendritas. Este fenómeno impredecible es extremadamente dañino ya que puede generar cortocircuitos, pérdida de capacidad y problemas de seguridad de la batería.

Además, los electrolitos líquidos presentan muchas debilidades en términos de seguridad, ya que son altamente inflamables y volátiles. La fuga térmica de la batería puede ser inducida fácilmente por la presencia de dendritas, una sobrecarga o aplastamiento de la celda en caso de un accidente de coche, por ejemplo. Este proceso térmico desencadena reacciones electroquímicas, que son exotérmicas y, lamentablemente, pueden estar fuera de control. Por eso, un sobrecalentamiento de la batería puede provocar un incendio y / o una explosión.

Las baterías sólidas, en las que el electrolito líquido se reemplaza por un conductor iónico sólido, podrían alimentar automóviles eléctricos. De hecho, las baterías sólidas tienen energías específicas más altas que las baterías convencionales. Los electrolitos sólidos pueden ser una solución prometedora para abordar estos problemas de seguridad, ya que no son volátiles y pueden ser utilizados a una temperatura superior. Además, los electrolitos sólidos tienen mejor resistencia a la propagación de dendritas. Esta propiedad permitiría usar el metal de litio como ánodo. A pesar de estas ventajas, todavía los electrolitos solidos presentan limitaciones para poderse integrar en una batería sólida. De hecho, no respetan las siguientes especificaciones:

- Alta conductividad iónica
- Alto número de transporte
- Contacto intimo con los electrodos
- Interfase química inestable (SEI)
- Poca protección contra las dendritas

Los electrolitos solidos se pueden clasificar en dos familias químicas principales: conductores sólidos inorgánicos y poliméricos. Los electrolitos inorgánicos pueden ser materiales cerámicos o vidriosos. Poseen características interesantes como conducción de iones litio única y rápida, mayor estabilidad térmica y electroquímica (generalmente hasta 5V frente a Li^+/Li). Además, presentan excelentes propiedades mecánicas que se cree que dificultan el crecimiento de las dendritas. Desafortunadamente, su pobre contacto interfacial y su mala estabilidad electroquímica dificulta su uso en baterías de estado sólido. Por otro lado, los electrolitos poliméricos están compuestos por una sal disuelta en una fase polimérica, donde los iones metálicos se coordinan con los grupos polares de la matriz. Generalmente, los electrolitos de polímero demuestran una buena interfaz con los electrodos gracias a su flexibilidad y pueden procesarse fácilmente. En comparación con los conductores inorgánicos, son candidatos de bajo costo para baterías de estado sólido. Sin embargo, importantes inconvenientes impiden que se utilicen con fines industriales. En primer lugar, baja conductividad iónica a temperatura ambiente y número de transporte de litio (generalmente por debajo de 10^{-6} S/cm y 0,2). Los investigadores han logrado en los últimos años mejorar la conductividad iónica hasta 10^{-5}-10^{-4} S/cm eligiendo estructuras poliméricas amorfas entrecruzadas, mezclas o copolímeros en lugar de polímeros lineales. Además, estos polímeros se pueden mejorar aún más con aditivos que pueden aumentar su conductividad iónica como plastificantes, adicción de partículas inorgánicas etc. El número de transporte se puede mejorar gracias al diseño de polímeros iónicos, como los electrolitos de polímero aniónico conductores de litio ion único, donde el grupo aniónico está anclado covalentemente al esqueleto del polímero. Estos polímeros iónicos ganaron un interés considerable ya que la conducción iónica solo es soportada exclusivamente por iones Li; su número de transferencia está cerca de la unidad. Esta característica es extremadamente atractiva ya que la polarización de las células puede impedirse. Por consiguiente, estos polímeros se consideran candidatos potenciales para la protección de dendritas en baterías de metal de litio.

Los electrolitos híbridos, generalmente compuestos por una matriz de polímero y partículas inorgánicas conductoras, exhiben una sinergia de propiedades tales como superior conducción iónica, mejor resistencia mecánica y mayor estabilidad electroquímica con el litio. Se han reforzado una variedad de matrices poliméricas (Poli(óxido de etileno) (PEO), Poli(fluoruro de vinilideno) (PVDF), policarbonatos (PPC)) con partículas conductoras iónicas inorgánicas como NASICON (LAGP) o garnets (LLZO). Entre estos híbridos, los electrolitos

basados en PEO y el conductor LLZO han mostrado propiedades interesantes. La baja transición vítrea y la capacidad para coordinarse con las sales de litio convierten el PEO en una el polímero de referencia. Además, las partículas LLZO disminuyen la cristalinidad del polímero, mejoran la disociación iónica en el material y generan una mejor interfase con el litio. Por lo tanto, los híbridos basados en PEO-LLZO muestran una conductividad iónica y una estabilidad electroquímica al litio superiores que otros electrolitos híbridos.

Aparte de la conductividad iónica, otras propiedades electroquímicas como la estabilidad electroquímica, el número de transferencia y la eficiencia culómbica a diversas densidades de corriente siguen siendo insatisfactorias, principalmente debido a las limitaciones de la matriz de PEO. Para optimizar aún más electrolitos híbridos sólidos, los investigadores optaron por utilizar PEO modificado o parientes como matriz polimérica. La primera solución consiste en mejorar las propiedades del PEO mediante modificación química, como la reticulación UV. La reticulación mejora la estabilidad mecánica del PEO, lo que permite calentar la celda a temperaturas moderadas para aumentar la conductividad iónica. Además, la inmovilización de las cadenas de PEO reticuladas limita su descomposición en la superficie del metal Li, lo que hace que el SEI sea más estable. Finalmente, se puede agregar un mayor contenido de plastificante en la composición híbrida sin afectar su integridad mecánica. El otro enfoque es usar como matriz polimérica parientes de PEO tales como acrilato o metacrilato de poli (etilenglicol) metiléter que polimerizan fácilmente mediante polimerización radicalaria. Estos polímeros son amorfos con una temperatura baja de transición vítrea y tienden a ser líquidos. Luego, a menudo se copolimerizan o se usan en mezclas para obtener electrolitos sólidos a temperatura ambiente. Además de los ejemplos anteriores, el uso de polímeros iónicos de iones únicos o polímeros zwiteriónicos puede ser interesante para aumentar el número de transporte y la disociación iónica en estos híbridos.

El objetivo principal de este proyecto de investigación es estudiar nuevos electrolitos poliméricos híbridos e iónicos para baterías de estado sólido de metal de litio. Elegimos la combinación de polímeros iónicos que incluyen el motivo químico más exitoso (óxido de etileno) como matrices potenciales de nanopartículas inorgánicas del garnet LLZO para obtener nuevos electrolitos sólidos híbridos. Los principales objetivos han sido evaluar y comparar cada híbrido para futuras aplicaciones en baterías de estado sólido de metal de litio. Para ello se han estudiado durante la tesis nuevos polímeros a base de poli(etilenglicol) metil éter metacrilato y monómeros de litio 1-[3-(methacryloyloxy)-propylsulfonyl]-1-(trifluoromethylsulfonyl)imide (LiMTFSI). El procesado húmedo, es decir, la mezcla del polímero y la fase inorgánica en un medio líquido se ha elegido para dispersar LLZO. Este método es simple, escalable y adaptado a una variedad de polímeros. Como objetivo final, esta tesis se centró en la prevención de las dendritas de litio en configuración de batería sólidas que utilizan ánodos de litio metal. Los híbridos y los electrolitos poliméricos relacionados se compararon para llegar a una conclusión sobre el efecto de las partículas LLZO en la eficiencia y la ciclabilidad de las baterías. Para este propósito, se realizaron estudios galvanostáticos de celdas simétricas de Li para analizar los procesos de stripping/plating del litio.

En el tercer capítulo, se investigaron electrolitos híbridos y poliméricos reticulados, de conducción de iones casi única y plastificados con un solvente orgánico y partículas inorgánicas de LLZO. El objetivo es investigar un nuevo híbrido en el que tanto la matriz de polímero como sus cargas inorgánicas son conductores de iones litio únicos. Proponemos la fotopolimerización UV como método rápido y sencillo para obtener este tipo de electrolito

sólido. Los mecanismos de transporte iónico para explicar el efecto beneficioso de las partículas inorgánicas LLZO fueron analizados gracias a la RMN sólida. Estos electrolitos también se compararon con electrolitos híbridos de iones duales, donde tanto el litio como los aniones son móviles, para comprender mejor el papel de las partículas LLZO en la conducción iónica. El movimiento de iones de litio aumentó gracias a la mejor disociación iónica, inducida por las interacciones físicas entre las fracciones aniónicas y LLZO. La alta conductividad iónica, la conducción de iones única y el buen contacto interfacial permiten lograr densidad de corriente crítica (CCD) alta tanto para electrolitos poliméricos como híbridos. El rendimiento del electrolito sólido en la batería se mejoró aún más mediante la polimerización in situ y el uso de aditivos fluorados que mejoren la SEI. Por otro lado, el electrolito híbrido mostró un peor rendimiento ya que se observó la formación de dendritas por encima del CCD.

En el cuarto capítulo, se estudiaron electrolitos sólidos híbridos y poliméricos a base de mezclas entre nuevos copolímeros de iones únicos de litio, PEO y de partículas de LLZO. Se realizó en primer lugar la síntesis de nuevos copolímeros al azar poli($LiMTFSI_x$-co-$PEGM_{1-x}$) mediante copolimerización radicalaria y se estudió la composición óptima para obtener la mayor conductividad iónica. Luego, se mezcló PEO de alto peso molecular con estos copolímeros para mejorar su conductividad iónica a temperatura ambiente mientras se mantenía un alto número de transferencia. La composición y la conductividad iónica de esta mezcla ternaria con LLZO se optimizaron e investigaron en detalle. Las mezclas que contienen una cantidad baja de PEO (≤ 30% en peso) muestran la mejor conductividad iónica (hasta 10^{-6} S / cm a 25°C) pero adolecen de una mala estabilidad mecánica. La cristalinidad de PEO está fuertemente inhibida por la concentración de monómero líquido iónico LiMTFSI. Para mejorar aún más la conductividad iónica y la estabilidad mecánica de la mezcla, se realizó la reticulación del PEO. Además, el uso de partículas LLZO permite de mejorar la disociación iónica, lo que aumenta la conducción de iones de litio. Los electrolitos sólidos obtenidos se evaluaron finalmente en celdas simétricas de litio. Para formar una interfase química estable, se añadió como aditivo una sal (LiFSI) a los electrolitos híbridos y poliméricos. Electrolitos sólidos híbridos y poliméricos lograron una baja CCD a causa de una baja conductividad iónica y de un contacto deficiente entre el electrolito y el litio. El uso futuro de un plastificante podría resolver estos defectos y mejorar la ciclabilidad de estos electrolitos sólidos

En el quinto capítulo, se examinaron electrolitos sólidos híbridos y poliméricos basados en redes semi-interpenetrantes mediante la combinación de una red de poli(etilenglicol), copolímeros catiónicos y pseudo-zwiteriónicos, sal LiFSI y partículas inorgánicas LLZO. En primer lugar, se sintetizó un nuevo copolímero pseudo-zwiteriónico. A diferencia de los polizwitteriones un pseudo-polizwitterión es un polímero neutro que posee dos unidades monoméricas iónicas adyacentes, cada una con cargas positivas y negativas independientes. Esta arquitectura polimérica se obtuvo con éxito mediante la complejación de un monómero aniónico y otro catiónico, que posteriormente se polimerizaron. Esta técnica es simple en comparación con la síntesis habitual de los polizwitteriones y permite una variedad de nuevas estructuras de este tipo de polímeros. Se prepararon mezclas de polímeros iónicos simplemente mezclando copolímeros catiónicos y pseudo-zwiteriónicos. Se observó que se producen fuertes interacciones físicas entre estos dos copolímeros y se traduce en el aspecto macroscópico de los polímeros. Estas mezclas de polímeros iónicos presentan interesantes propiedades mecánicas (pegajosidad, deformabilidad) gracias a la formación de una red física de interacciones iónicas. Posteriormente, se añadió un alto contenido de sal LiFSI a estas mezclas de polímeros iónicos para formar electrolitos sólidos de iones de litio. Esta sal también

se eligió por su capacidad para formar una interfase estable el litio. La presencia de fracciones catiónicas y bipolares en la estructura del polímero permite añadir un alto contenido de sal sin comprometer la conductividad iónica. La adición de partículas LLZO es muy beneficiosa en términos de disociación iónica, mejorando la conducción iónica y el número de transporte del litio. Las partículas inorgánicas pueden interactuar con la sal LiFSI, mejorando la conductividad iónica y el número de transferencia. La formación de una red semi-interpenetrada de poli(etilenglicol) permite obtener filmes solidos con flexibilidad y deformabilidad. Esto permite utilizar estos electrolitos en nuestra configuración de batería de estado sólido a temperatura moderada. Sin embargo, fue necesario agregar un pequeño contenido de plastificante para lograr una mayor conducción iónica en los electrolitos sólidos. El electrolito polímerico logró una excelente ciclabilidad gracias una interfase muy estable con el litio. Por otro lado, la ciclabilidad en presencia de partículas de LLZO. Esta mala ciclabilidad puede explicarse por el gran desajuste del número de transferencia entre el polímero y la fase inorgánica.

A pesar de sus debilidades, esta familia de electrolitos sólidos presenta interesantes características para combinarse con el metal Li. Su implementación exitosa en una verdadera batería de estado sólido confirma aún más su potencial como electrolito sólido. Además, los reactivos de bajo costo, la fácil síntesis y procesado como filmes los hacen materiales interesantes para aplicación como electrolitos sólidos en baterías de litio metal. Sin embargo, un mejor diseño y caracterización de la interfase entre el electrolito y el litio son obligatorios para optimizar en el futuro estos materiales. Sin embargo, los electrolitos híbridos investigados presentan diferentes resultados en términos de ciclabilidad. Su característica común es que las partículas LLZO no mejoran el rendimiento en comparación con los electrolitos poliméricos. El efecto único de LLZO es interactuar con las especies aniónicas, ya sea inmovilizadas o libres.

List of acronyms

EESS Electrochemical energy storage systems

GHG Green Houses Gas

EV Electrical Vehicle

BEV Battery Electrical Vehicle

ICE Internal Combustion Vehicle

HEV Hybrid Electrical Vehicle

PHEV Plug-in Electrical Vehicle

LiB Li ion Battery

CE Coulombic efficiency

SSE Solid state electrolyte

ASSB All solid-state batteries

LMB Lithium Metal Battery

TN Transference number

SEI Solid Electrolyte Interphase

EW Electrochemical window

ISE Inorganic Solid Electrolyte

SPE Solid polymer electrolyte

PEO Poly(ethylene oxide)

EO Ethylene oxide

HSE Hybrid Solid Electrolyte

SIPE Single ion conducting polymer electrolyte

EIS Electrochemical impedance spectroscopy

VTF Vogel-Tamman-Fulcher

NMR Nuclear magnetic resonance

MAS NMR Magic Angle Spinning Nuclear magnetic resonance

PFG NMR Pulse-Field Gradient Nuclear magnetic resonance

LiTFSI Lithium trifuoromethylsulfonylimide

LiFSI Lithium bis(fluorosulfonyl)imide

FTIR-ATR Fourier Transform Infrared-Attenuated total reflection

DSC Differential scanning calorimetry

DMTA Dynamical Mechanical Thermal Analysis

SEM Scanning Electron Microscopy

ESEM Environmental Scanning Electron Microscopy

EIS Electrochemical Impedance Spectroscopy

ECM Equivalent Circuit Model

CPE Constant Phase Element

Mn Number average molecular weight

$\mathbf{T_g}$ Glass transition temperature

$\mathbf{T_m}$ Melting temperature

TEM Transmission Electron Microscopy

XRD X-Ray Diffraction

GEIS Galvanostatic cycling coupled with EIS

CCD Critical Current Density

SEC-GPC Size Exclusion Gel Permeation chromatography

PEGM Poly (ethylene glycol) methyl ether methacrylate

PEGDM Poly(ethylene glycol) dimethacrylate

LiMTFSI Lithium1-[3-(methacryloyloxy)-propylsulfonyl]-1(trifluoromethylsulfonyl)imide

NTFSI Acryloyloxyethyltrimethylammoniumbis(trifluoromethanesulfonyl)imide

ZI Pseudo zwitterionic monomer formed by the complexation of LiMTFSI and NTFSI

IL Ionic liquid

PIL Poly(ionic liquids)

LLZO Lithium lanthanum zirconium oxide

NASICON Sodium (Na) Super Ionic CONductor

LATP Lithium Aluminium Titanium Phosphate

DCM Dichloromethane

MeOH Methanol

Et_2O Diethyl ether

THF Tetrahydrofuran

DMF Dimethylformide

PC Propylene Carbonate

FEC Fluoroethylene Carbonate

TEGDME Tetraethylene Glycol Dimethyl Ether

DMSO Deuterated DimethylSulfoxide

AIBN Azobis(2-methylpropionitrile)

DAROCUR 2-Hydroxy-2-methylpropiophenone

BAPO Phenylbis(2,4,6-trimethylbenzoyl)phosphine oxide

BZ Benzophenone

UV Ultraviolet

HSIPE-x Hybrid Single ion Polymer Electrolyte with x= LLZO in wt.%

Poly(LiMTFSI$_x$-co-PEGM1$_{-x}$) Random copolymer based on LiMTFSI and PEGM with x= LiMTFSI in mol.%

Li$_{0.2}$BL Blend serie based on high molecular weight PEO and poly(LiMTFSI$_{0.2}$-co-PEGM0$_{.8}$)

Li$_{0.5}$BL Blend serie based on high molecular weight PEO and poly(LiMTFSI$_{0.5}$-co-PEGM0$_{.5}$)

Li$_1$BL Blend based on high molecular weight PEO and homopolymer poly(LiMTFSI)

CLi$_{0.2}$BL Crosslinked blend based on PEO (30 wt.) and poly(LiMTFSI$_{0.2}$-co-PEGM$_{0.8}$) (70 wt.%)

CLi$_{0.5}$BL Crosslinked blend based on PEO (30 wt.) and poly(LiMTFSI$_{0.5}$-co-PEGM$_{0.5}$) (70 wt.%)

HLi$_{0.5}$BL-x Blend based on PEO (30 wt.), poly(LiMTFSI$_{0.5}$-co-PEGM$_{0.5}$) (70 wt.%) and LLZO particles with x=LLZO in wt.%

HCLi$_{0.5}$BL-x Crosslinked blend based on PEO (30 wt.), poly(LiMTFSI$_{0.5}$-co-PEGM$_{0.5}$) (70 wt.%) and LLZO particles with x=LLZO in wt.%

Poly(NTFSI$_{0.2}$-co-PEGM$_{0.8}$) (C) Random Copolymer based on NTFSI and PEGM with x= 20 mol.% NTFSI

Poly(ZI$_{0.2}$-co-PEGM$_{0.8}$)(ZI) Random Copolymer based on ZI and PEGM with x= 20 mol.% ZI

Poly(LiMTFSI$_{0.2}$-co-PEGM$_{0.8}$) (A) Random copolymer based on PEGM and LiMTFSI with x= 20 mol.% LiMTFSI

ZI-C Ionic polymer blend obtained by mixing of 50wt.% pseudo-zwitterionic and 50wt.% cationic copolymers Z and C

ZI-A Ionic polymer blend obtained by mixing of 50wt.% pseudo-zwitterionic and 50wt.% cationic copolymers Z and A

ZI-C_x Ionic polymer blend obtained by mixing of 50wt.% pseudo-zwitterionic and 50wt.% cationic copolymers Z and A, with x= LiFSI in wt.%

s-IPN semi-InterPenetrated Network

I-ZI-C_45 Polymer s-IPN formed by combination of poly(ethylene) glycol network, cationic and pseudo-zwitterionic copolymers and 45 wt.% of LiFSI salt

HI-ZI-C_45 Hybrid s-IPN formed by combination of poly(ethylene) glycol network, cationic and pseudo-zwitterionic copolymers, 45 wt.% of LiFSI salt and 10 wt.% of LLZO particles